

- I. INFRARED SPECTRA OF MONOMERIC AND POLYMERIC HCL
AND DCL IN SOLID KRYPTON AND XENON

- II. INFRARED SPECTRA OF NH₂ AND ND₂ PRODUCED BY
PHOTOLYSIS AND X-RADIOLYSIS OF AMMONIA IN SOLID
KRYPTON

- III. ULTRAVIOLET SPECTRA OF CH PRODUCED BY X-RADIOLYSIS
OF METHANE IN SOLID ARGON

Thesis by
Leon Frank Keyser

In Partial Fulfillment of the Requirements
For the Degree of
Doctor of Philosophy

California Institute of Technology
Pasadena, California

1965

(Submitted May 4, 1965)

ACKNOWLEDGMENTS

I wish to express my gratitude to Professor G. W. Robinson for his advice and encouragement in the course of this work.

The construction of the variable temperature dewar and the experiments with HCl were carried out in collaboration with Joel Kwok; his cooperation is greatly appreciated.

Financial support from a National Science Foundation Graduate Fellowship (1959-1963) and from the California Institute of Technology is gratefully acknowledged.

- I. Infrared Spectra of Monomeric and Polymeric HCl and DCl in Solid Krypton and Xenon
- II. Infrared Spectra of NH₂ and ND₂ Produced by Photolysis and X-Radiolysis of Ammonia in Solid Krypton
- III. Ultraviolet Spectra of CH Produced by X-Radiolysis of Methane in Solid Argon

By Leon Frank Keyser

ABSTRACT

PART I

The construction and operation of a low temperature infrared cell is described; the cell is capable of maintaining temperatures between 7 and 50°K while in the light beam of a Beckman IR-7 spectrophotometer.

Infrared spectra of HCl and DCl at 0.2 to 2% concentrations in solid krypton and xenon are reported. Fine structure in the region of the (1-0) vibrational transitions of HCl and DCl is assigned to monomeric and polymeric species of HCl and DCl.

The monomer lines are assigned to vibration-rotation transitions of HCl and DCl. In krypton the R(0) transition of HCl occurs at 2872.7, R(1) at 2887, P(1) at 2837.4, and Q(0) at 2852.8 cm⁻¹. The R(0) transition of DCl in krypton occurs at 2078.9, R(1) at 2089, P(1) at 2058, and Q(0) at 2067.5 cm⁻¹. In xenon the R(0) transition of HCl occurs at 2858.2, R(1) at 2872, P(1) at 2825.5, and Q(0) at 2837.8 cm⁻¹. The R(0) transition of DCl in xenon occurs at 2069,

R(1) at 2075, P(1) at 2047 and Q(0) at 2058 cm^{-1} .

Besides a J-independent band origin shift with respect to the gas phase frequencies of -31 cm^{-1} in krypton and -44 cm^{-1} in xenon, the rotational levels of HCl exhibit J-dependent perturbations of 5 to 10 cm^{-1} . The band origin shift of DCl is -23 cm^{-1} in krypton and -33 cm^{-1} in xenon; the J-dependent perturbations of the DCl rotational levels lie between 1 and 3 cm^{-1} . Hindered rotation and libration of HCl and DCl in the rare gas crystals are not suitable descriptions of the J-dependent perturbations. A model based on the interaction of the rotational motion with the localized translational motion of HCl and DCl at substitutional sites in the rare gas crystals is used to interpret the J-dependent perturbations. The translational frequencies of HCl and DCl and the strength of the translation-rotation interaction are treated as parameters. The values of the translational frequencies which give the best fit to the observed rotational spacings are 36 cm^{-1} in xenon, 57 cm^{-1} in krypton, and 31 cm^{-1} in argon. The strength of the translation-rotation interaction as measured by the distance between the center of mass and the center of electrical symmetry in the molecule is 0.13 \AA for HCl and 0.096 \AA for DCl.

A mechanism for the induction of a Q branch in the vibration-rotation spectra of monomeric HCl and DCl in the solid rare gases is discussed.

The vibrational spectra of polymeric HCl and DCl are discussed in terms of dimeric and trimeric aggregates.

PART II

The photolysis of ammonia in solid krypton with 1849 Å light or with X radiation gives rise to new absorption maxima at 1521, 1114, 1289, and 1280 cm^{-1} in the infrared. The line at 1521 cm^{-1} is assigned to the previously unobserved bending mode of the NH_2 radical. Experiments with isotopic ammonia show that the bending mode of ND_2 occurs at 1106 cm^{-1} in solid krypton.

PART III

The CH radical is produced by X-radiolysis of methane in solid argon and krypton. The radiolysis mechanism is discussed in terms of energy transfer from the rare gas lattice to methane.

TABLE OF CONTENTS

PART	PAGE
I. INFRARED SPECTRA OF MONOMERIC AND POLYMERIC HCL AND DCL IN SOLID KRYPTON AND XENON	1
Introduction	2
Experimental	4
Results	16
Discussion	30
Hindered rotation	30
Libration	36
Translation-rotation interaction	36
Induced Q branch	62
Polymers	76
APPENDIX I. Derivation of the Hamiltonian operator for the interaction of translational and rotational motions	83
APPENDIX II. Symmetry properties of the translation-rotation Hamiltonian	91
References	93
II. INFRARED SPECTRA OF NH ₂ AND ND ₂ PRODUCED BY PHOTOLYSIS AND X-RADIOLYSIS OF AMMONIA IN SOLID KRYPTON	95
Introduction	96
Experimental	98

PART	PAGE
Results	102
Infrared spectrum of ammonia in solid	
krypton	102
Photolysis of ammonia with 1849 Å	
radiation	102
X-Ray photolysis of ammonia	110
Infrared spectrum of deuterated ammonia	
in solid krypton	113
X-Ray photolysis of deuterated ammonia	113
Discussion	123
The 1114 cm^{-1} line	125
The 1280 and the 1289 cm^{-1} lines	126
The 1521 cm^{-1} line	127
Isotopic substitution	128
Conclusion	129
References	132
III. ULTRAVIOLET SPECTRA OF CH PRODUCED BY	
X-RADIOLYSIS OF METHANE IN SOLID ARGON	134
Introduction	135
Experimental	136
Results	138
Discussion	146
The CH bands	146
CH ₃ and CH ₂	150

PART	PAGE
Photolysis mechanism	150
References	158
PROPOSITIONS	160

PART I

INFRARED SPECTRA OF MONOMERIC AND POLYMERIC
HCL AND DCL
IN SOLID KRYPTON AND XENON

INTRODUCTION

Recently much interest has developed in the study of rotational motions of small molecules in solids. Molecular hydrogen is a well-known example of nearly free rotation in both liquid and solid phases (1). Other molecules show signs of rotation when they are present at low concentrations in inert solids such as the rare gases.

Infrared spectra of H_2O and D_2O in solid rare gas matrices indicate that these molecules are undergoing nearly free rotation (2). Comparison of the rotational spacings in the matrix with the corresponding spacings in the gas phase shows that the rotational motion of D_2O is perturbed less than that of H_2O . If the environmental (band origin) shift, which is approximately the same for all the rotational lines in a given vibration-rotation band, is taken into account, the frequencies of most of the rotational lines observed in the spectrum of matrix isolated water agree within 2 to 3 cm^{-1} with the values calculated from the gas phase rotational constants. In a few instances, however, two lines instead of one are observed at a calculated frequency position; one occurs on either side of the calculated value. Redington and Milligan (2) have suggested that these splittings may be caused by a resonance interaction of a rotational level of water with a localized translational lattice mode. An approximation to such a lattice mode involves the oscillation (translation) of the matrix isolated molecule as a whole about the center of the substitutional site which it occupies in the solid. As will be seen below, the interaction of rotation with this quasi-translational motion is important in

understanding the vibration-rotation spectrum of HCl and DCl in the solid rare gases.

Evidence for the hindered rotation of CH₄ at 0.2% concentrations in rare gas crystals has been reported by Cabana, Savitsky, and Hornig (3). The fine structure observed in the ν_3 and ν_4 vibrational transitions indicates that the barrier to rotation about the fourfold crystal axes is approximately 60 cm⁻¹ in argon, krypton, and xenon. As expected for a hindered rotor, the rotation of CD₄ in the same solids appears more highly perturbed. Other systems which show signs of rotation in the solid include NH₃ in krypton (4), HCl and DCl in argon (5), and NH₂ in argon (6).

Previous studies in these laboratories (7) have shown that quasi-rotational motion can account for most of the bandwidths and structure observed in the vibration-rotation spectra of the hydrogen halides in liquid xenon. Extrapolating from these earlier studies one might expect that HCl and DCl rotate in solid krypton and xenon; evidence will be presented to show that perturbed rotation of monomeric HCl and DCl does indeed occur in these solids. Hindered rotation, libration, and the interaction of the rotational motion with the localized translational motion of HCl and DCl at a substitutional site in a rare gas crystal will be considered as possible explanations of the rotational perturbations. A mechanism for the induction of a Q branch in the vibration-rotation spectra of monomeric HCl and DCl in the solid rare gases will also be discussed. Finally, the vibrational spectra of polymeric species of HCl and DCl will be discussed in terms of dimeric and trimeric aggregates.

EXPERIMENTAL

The infrared cell used in these experiments is capable of maintaining temperatures between 7 and 50°K when liquid helium is used as a coolant. The system is portable and can be placed in the sample compartments of the Beckman IR-7 and the Perkin-Elmer Model 21 infrared spectrophotometers. Cross sections of the cell are shown in Figures 1 and 2.

Liquid helium is stored in a conventional metal dewar (C) to which is attached a thin-walled, stainless steel conduction cylinder (N). Temperature control in the 7 to 50°K range is achieved by varying the pressure of helium gas in the cylinder, which acts as a variable thermal conductor between the liquid helium reservoir (C, K) and the cold window (R). When the cylinder is evacuated, the thermal conductivity is limited by the stainless steel walls, and the temperature of the cold window reaches its highest values because of radiative heating from the surrounding heat shields at 77°K. Addition of helium gas to the cylinder increases the effective thermal conductivity of the steel cylinder and thereby reduces the cold window temperature. The conduction cylinder is 3.8 cm in diameter and 10 cm long with a wall thickness of 0.25 mm. The bottom plate of the cylinder is in thermal contact with a copper flange in which a cesium bromide cold window (R) is mounted. Thermal contact between the parts is maintained by means of indium wire gaskets.

The helium gas inlet (A) and outlet (J) of the conduction cylinder are not connected to the main pumping system (Q) used to

Figure 1. Cross section of variable temperature infrared cell.

- A. Helium gas inlet (copper)
- B. Liquid nitrogen dewar
- C. Liquid helium dewar
- D. Pressure gauge: -1 to 2 atmospheres
- E. Valve
- F. To vacuum pump
- G. This flange used to rotate the dewars, heat shielding, and cold window with respect to the housing
- H. Rubber O-ring
- I. Teflon gasket
- J. Helium gas outlet (stainless steel)
- K. Extension of liquid helium dewar
- L. Outer heat shield at 77°K
- M. Inner heat shield at 77°K
- N. Conduction cylinder (stainless steel)
- O. Housing
- P. Middle heat shield with windows
- Q. To gate valve and pumping system
- R. Cold window
- S. Carbon resistor
- T. Stainless steel strip
- U. Worm gear assembly
- V. Nylon insulator
- W. Drive shaft

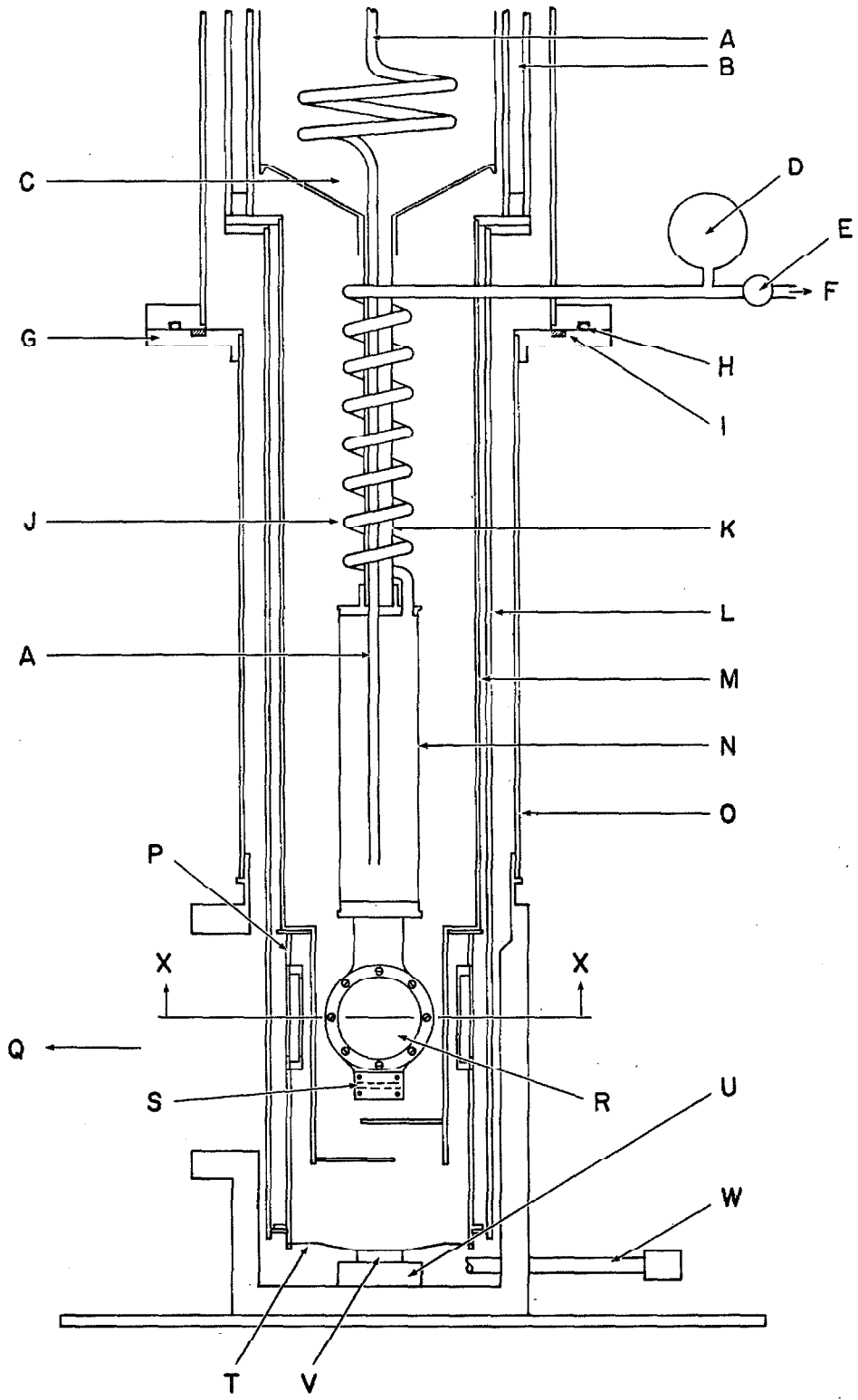


FIGURE 1

Figure 2. Cross section of variable temperature infrared cell
(section X-X of Fig. 1) showing heat shielding and sample
inlet system.

- AA. Teflon gaskets
- BB. To inlet valve and sample supply
- CC. Stop
- DD. Sample inlet tube with 1 mm orifice
- EE. Pressure screw
- L. Outer heat shield
- M. Inner heat shield
- P. Middle heat shield with windows
- Q. To gate valve and pumping system
- R. Cold window
- Y. Housing windows

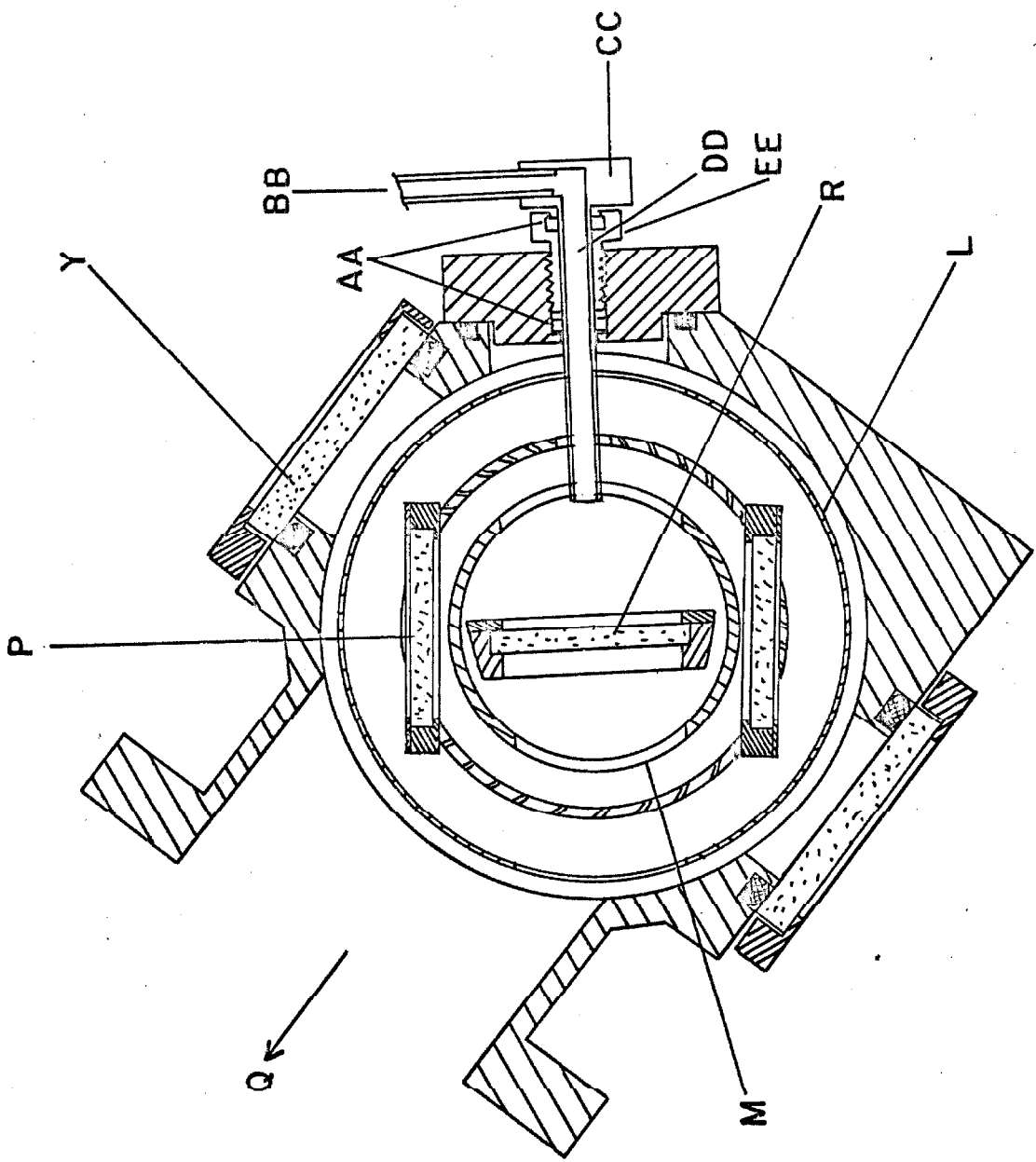


Fig. 2a. Alignment for deposition.

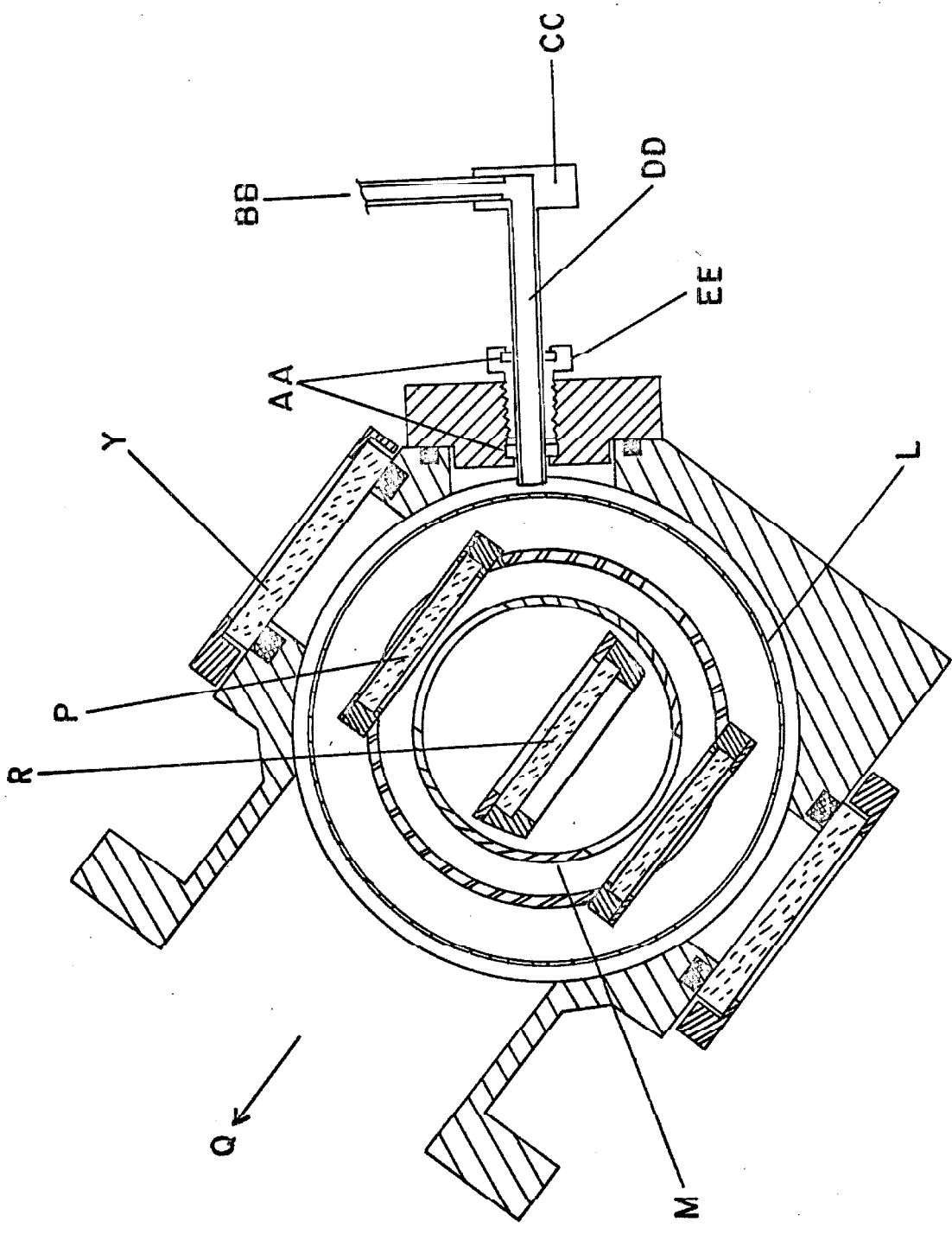


Fig. 2b. Alignment for recording spectrum.

evacuate the infrared cell and the helium and nitrogen dewars. The helium gas line is attached to a separate rough vacuum system for the purpose of controlling the pressure in the conduction cylinder. To prevent excessive heat leakage into the liquid helium, the copper tube (A) is soldered to a stainless steel tube (not shown) that passes out of the liquid helium dewar to a flowmeter and a helium gas supply. The helical configuration of the stainless steel outlet tube allows for thermal contraction when the dewar is cooled to 4.2°K.

Radiation heating is minimized by triply heat shielding the cold window, as shown in Figures 1 and 2. The middle heat shield (P) contains windows which for good thermal contact bear against indium metal gaskets. These cooled windows protect the 4.2°K sample window from direct exposure to high temperature radiation sources even while spectra are being taken. This heat shield can be rotated out of the path of the incoming gases and thus itself kept clear of unwanted, infrared-absorbing deposits. Since the middle heat shield merely rests on flanges between the inner heat shield (M) and the outer one (L), it is in poor thermal contact with the liquid nitrogen reservoir. However, the inner and outer heat shields act to cool the middle one by radiative cooling. A stainless steel strip (T), which fits into slots at the base of the middle heat shield, is under spring tension and acts to keep the heat shield squarely in position. The drive shaft (W) permits the stainless steel strip and thereby the middle heat shield to be rotated when the dewar is cooled down and evacuated.

An Allen-Bradley one watt, 250 ohm carbon resistor is used to measure the temperature in the 4 to 50°K range. The insulating cover was carefully sandblasted off and a coating of G. E. resin No. 7031 was applied for electrical insulation. The resistor was then wrapped in indium metal wire and squeezed into the cavity (S) provided for it below the cold window.

Figure 3 shows the cold window temperature as a function of helium pressure in the conduction cylinder when the cell is not in the light beam of the Beckman IR-7. In the light beam the minimum and maximum temperatures are 7 and 50°K. The cold window temperature is seen to be most sensitive to helium pressures below 25 mm Hg.

A given temperature between 7 and 50°K can be held indefinitely by setting the helium pressure in the cylinder to the appropriate value. Temperature increases can be achieved rapidly by evacuating the cylinder. After the temperature has risen to a desired value, the pressure is adjusted so that equilibrium is attained. Temperature changes between 7 and 40°K can be carried out in 30 minutes. Equally fast decreases in temperature can be achieved by admitting helium gas rapidly to the cylinder. After the cold window has cooled to the new temperature, the pressure is adjusted to attain equilibrium. Admission of small amounts of helium or evacuation of the cylinder for short periods of time can be used to make small adjustments in the temperature.

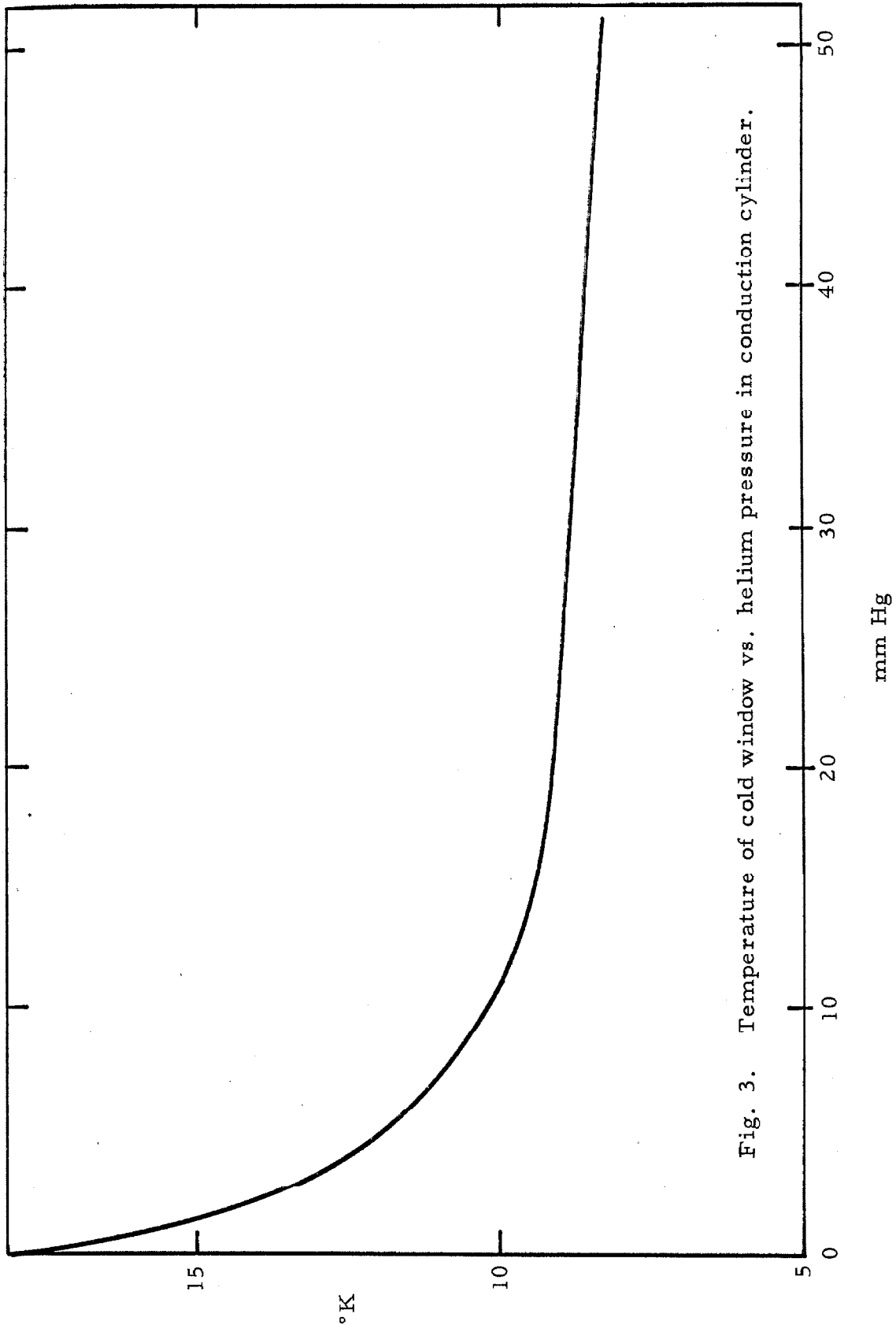


Fig. 3. Temperature of cold window vs. helium pressure in conduction cylinder.

The liquid helium boil-off rate depends upon which windows and which heat shields are used and whether the dewar is in the Beckman IR-7 light path or not. Table I summarizes the effect of various window and heat shield combinations on the helium boil-off rate. When a cesium bromide cold window is used at (R) and barium fluoride windows are used in the middle heat shield (P) and housing at (Y), the boil-off rate is 190 ml/hr. in the light path. Under these same conditions, but without the middle heat shield, the boil-off rate increases to 320 ml/hr.

During sample deposition, the cold window is set normal to the sample inlet tube (see Fig. 2a) by turning the dewar on flange (G); this results in uniform distribution of the deposit over the cold window surface. Orienting the middle heat shield and inlet tube as shown in Figure 2a, prevents deposition on the windows of this heat shield. After the deposition is complete the cold windows and heat shields are realigned to record the spectrum (see Fig. 2b).

The deposition rate of the sample mixture must be sufficiently slow to prevent heating of the cold window to the point where a lot of diffusion occurs, since diffusion within the solid deposit leads to polymer formation. Rates about 1cc/min at STP meet this requirement and were used in these experiments. The temperature of the cold window during deposition is kept close to 16°K for krypton mixtures and 20°K for xenon.

Prior to deposition, the gas samples were mixed by distilling them several times between liquid nitrogen traps or by keeping them

Table I. Effect of windows and heat shields on the helium boil-off rate.

Cell In or Out of Spectrometer Light Path	Housing Window	Middle Heat Shield Window	Cold Window	Helium Boil Off Rate (ml/hr)
Out	CsBr	CsBr	CsBr	200
In	CsBr	CsBr	CsBr	330
Out	BaF ₂	BaF ₂	CsBr	175
In	BaF ₂	BaF ₂	CsBr	190
Out	BaF ₂	Shield not present	CsBr	270
In	BaF ₂	" "	CsBr	320

together for 12 to 18 hours in a vacuum system. Both methods gave reproducible results as long as the same rate of deposition was employed. More elaborate methods of mixing, such as a teflon paddle wheel turned by a magnetic stirrer, were used but gave results no different than those obtained by the simpler mixing techniques.

The HCl with a stated purity of 99% was obtained from The Matheson Co. The DCl, having a 99% minimum isotopic purity was supplied by Merck, Sharp, and Dohme, Ltd. of Canada. The krypton and xenon were Linde MSC grade. All the gases were used without further purification.

The spectra were recorded on a Beckman IR-7 infrared spectrophotometer. The resolution was 1 to 2 cm^{-1} with an accuracy of 0.5 to 1 cm^{-1} . The spectrometer was calibrated using the gas phase spectra of HCl and DCl.

RESULTS

Representative spectra of HCl and DCl in krypton and xenon are shown in Figures 4 to 7. The assignment of the absorption features to monomer or polymer species is based mainly on experiments with HCl and DCl in krypton. The same assignments for HCl and DCl in xenon can then be made because of the close similarity in the spectra. Figure 8 shows the results of varying the concentration of HCl in krypton. The effect of annealing the sample is shown in Figure 9. The low frequency lines grow in intensity as the concentration of HCl or DCl is increased and as the sample is annealed. They are assigned to dimers and polymers. The high frequency lines are observed even at low concentrations, for example, 0.2% HCl in krypton (see Fig. 8a) where, from a statistical point of view, 97% of the HCl is expected to be isolated (8). Moreover, the intensities of the high frequency lines decrease after the sample has been warmed and recooled. They are assigned to monomeric HCl and DCl. Table II lists the observed frequencies for HCl and DCl in krypton and xenon and their assignments.

The monomer lines show reversible intensity variations when the sample is warmed and recooled to its original temperature. This behavior is illustrated by Figure 10. These reversible intensity variations of the monomer lines with temperature are in addition to the irreversible decrease in intensity of these same lines when the sample is warmed and recooled. The reversible intensity variations are characteristic of Boltzmann population and depopulation of low

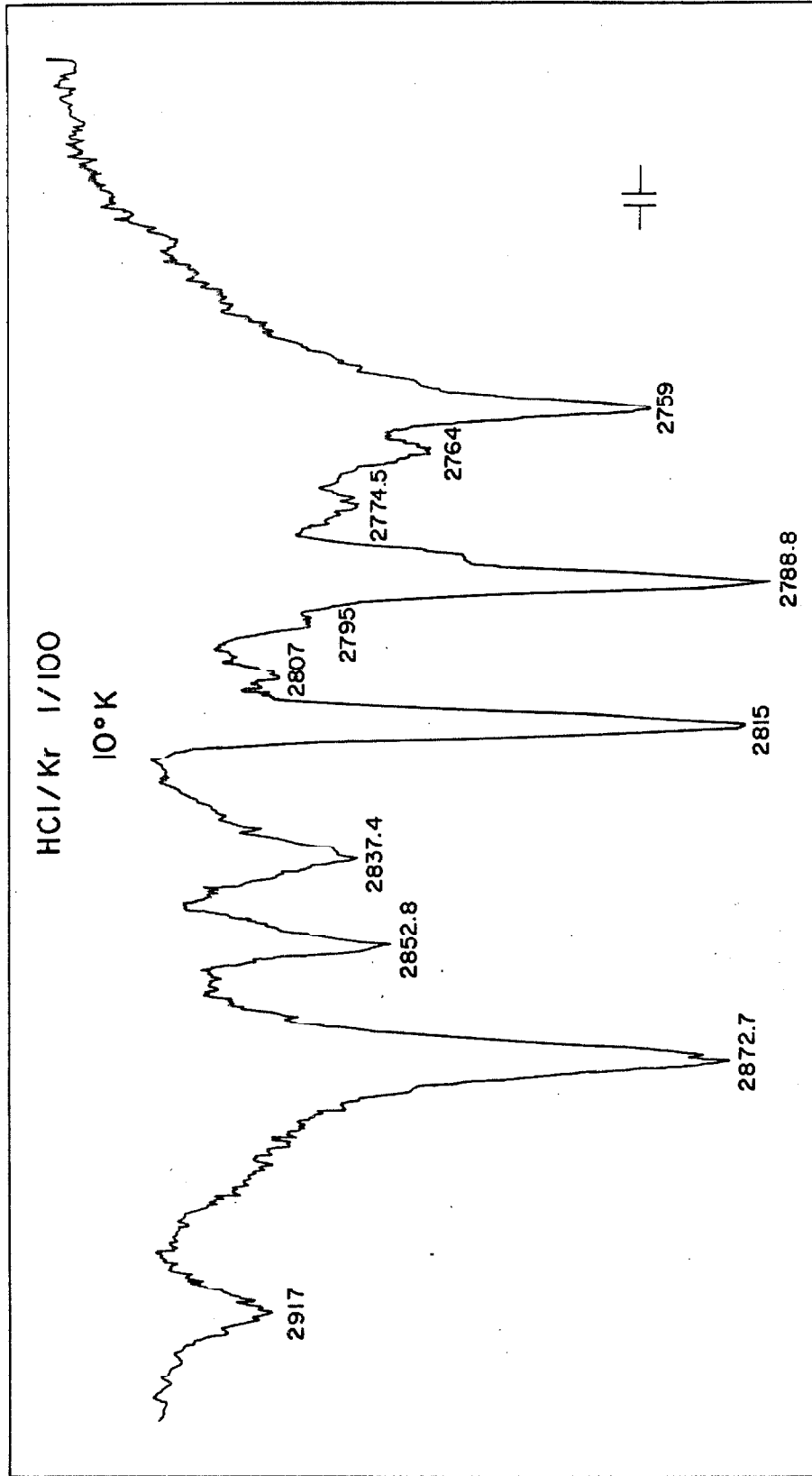
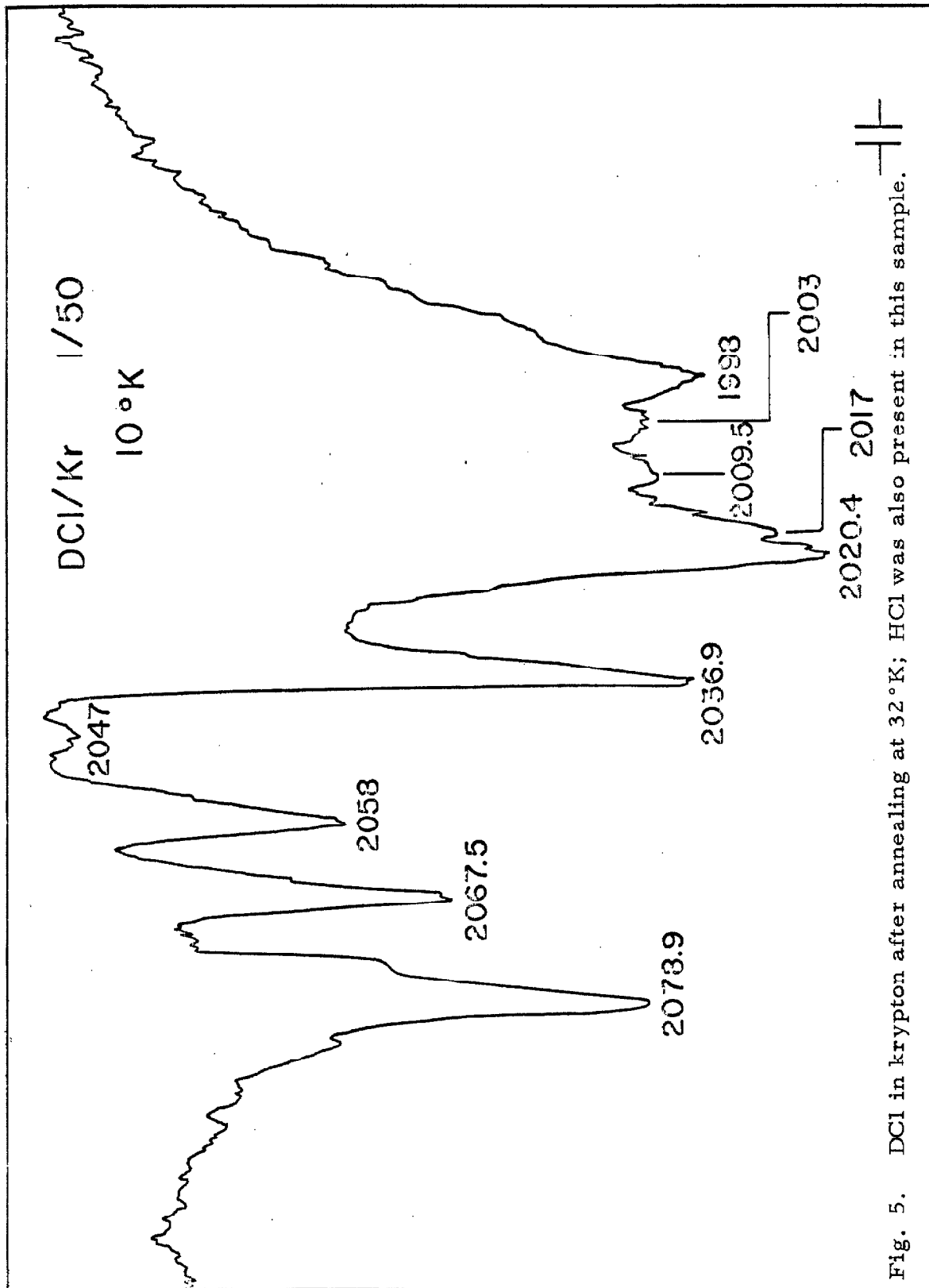


Fig. 4. HCl in krypton after annealing at 26°K.



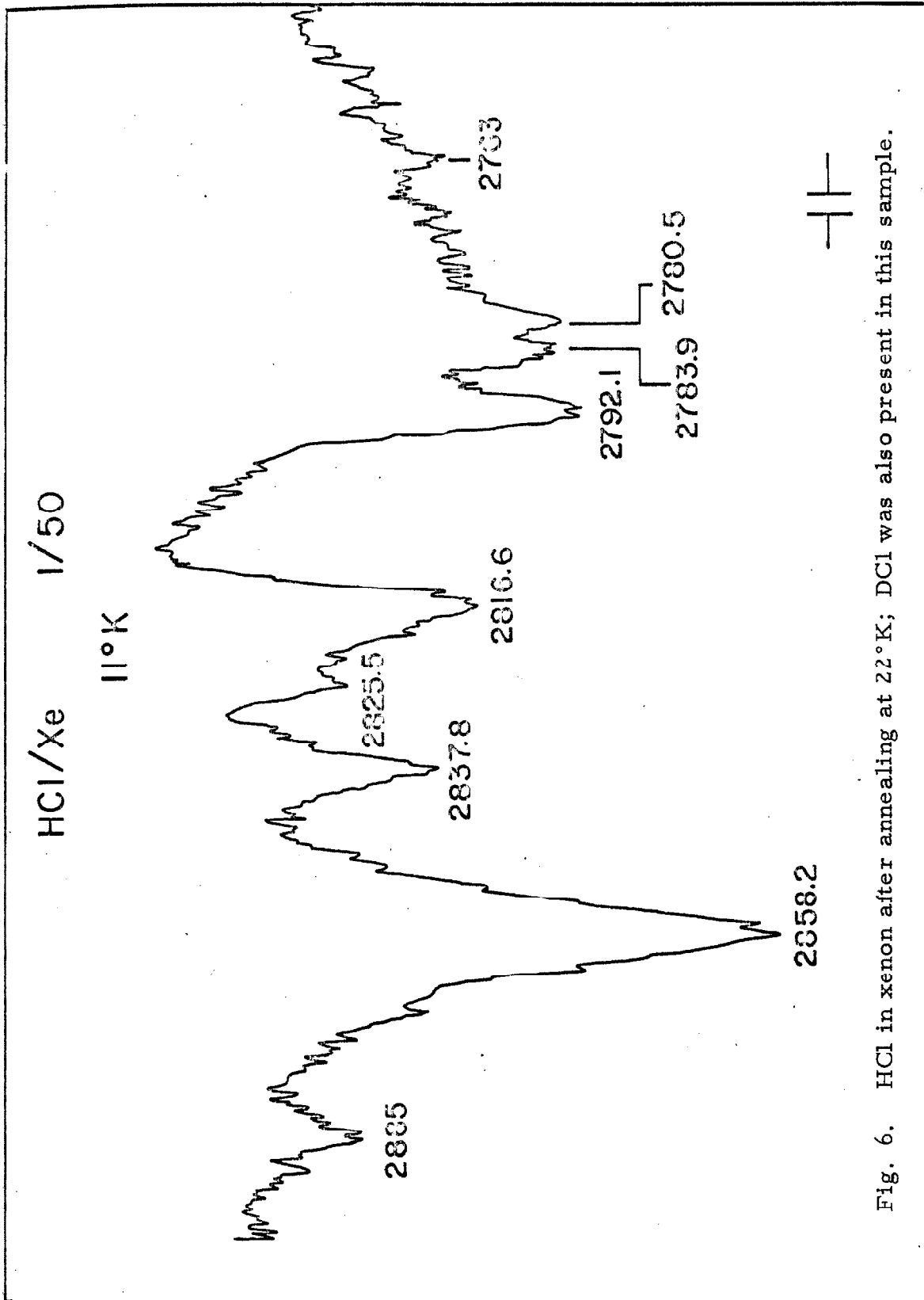


Fig. 6. HCl in xenon after annealing at 22°K; DCl was also present in this sample.

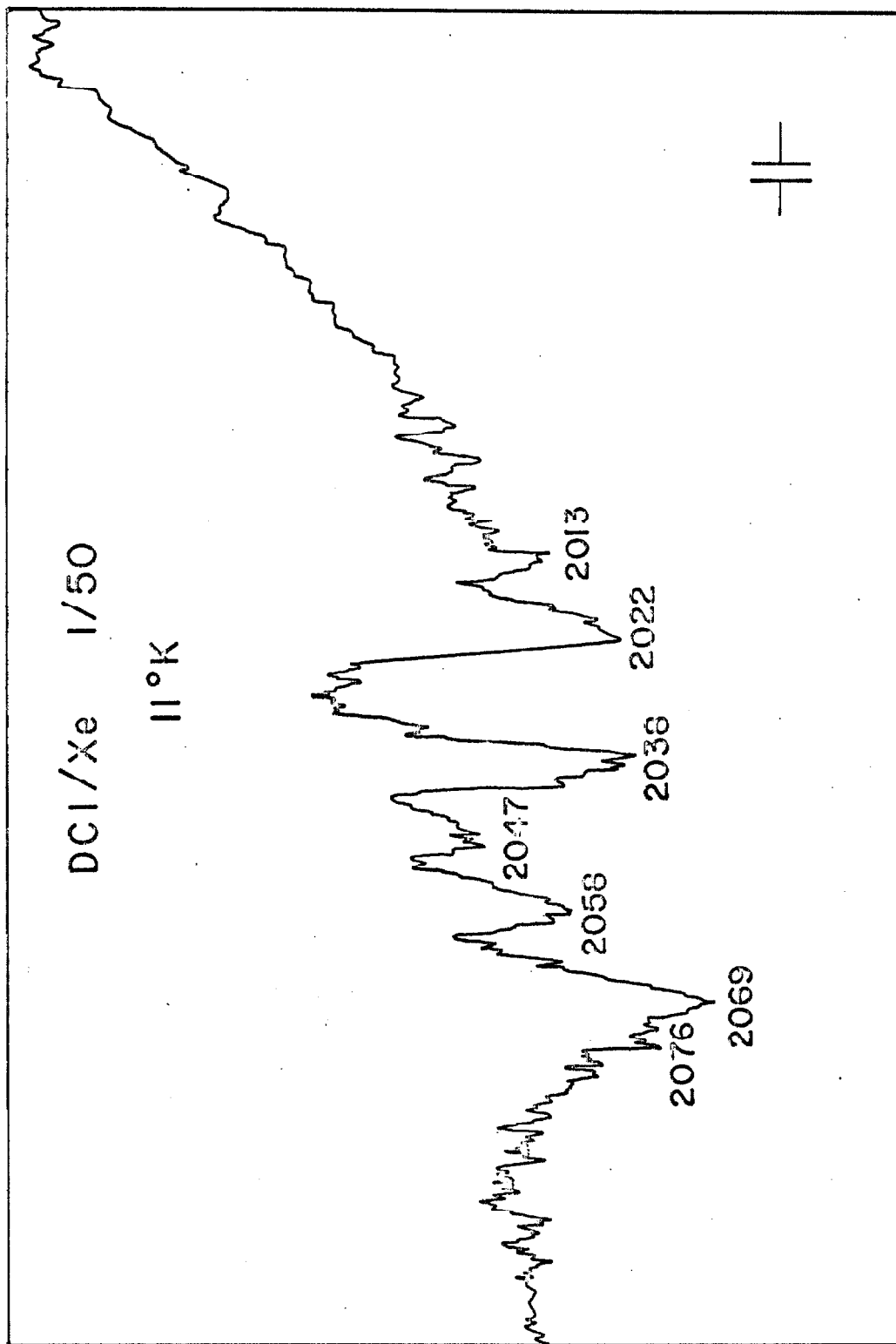


Fig. 7. DCI in xenon; HCl was also present in this sample.

Figure 8. Effect of varying the concentration of HCl in krypton:
a) 0.2% HCl/Kr, b) 1.0%, c) 2.0%; the spectra were
taken at 10°K.

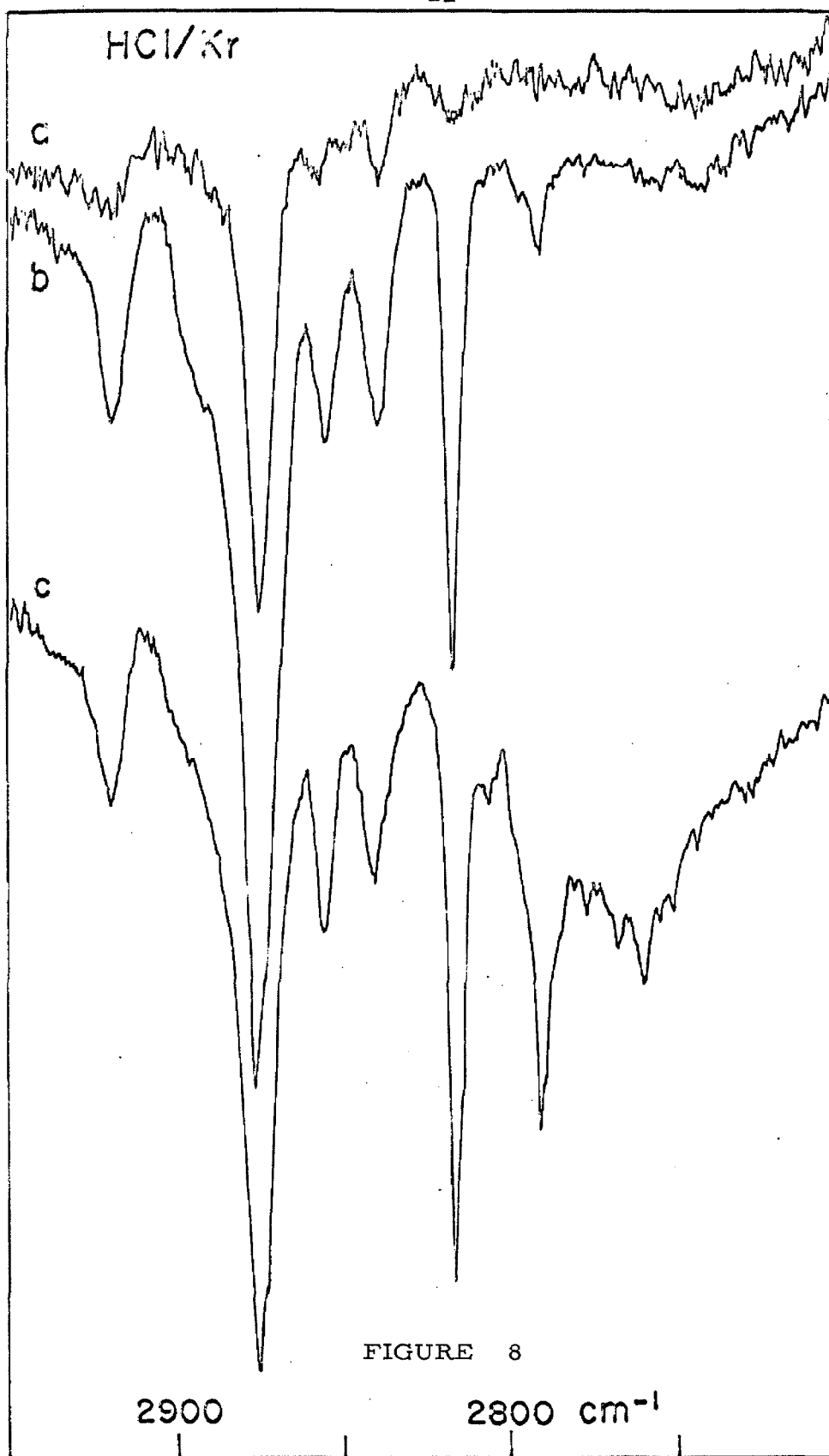


Figure 9. Effect of annealing a 1.0% HCl in krypton sample: a) original sample, b) after annealing at 19°K, c) after annealing at 27°K; the spectra were taken at 12°K.

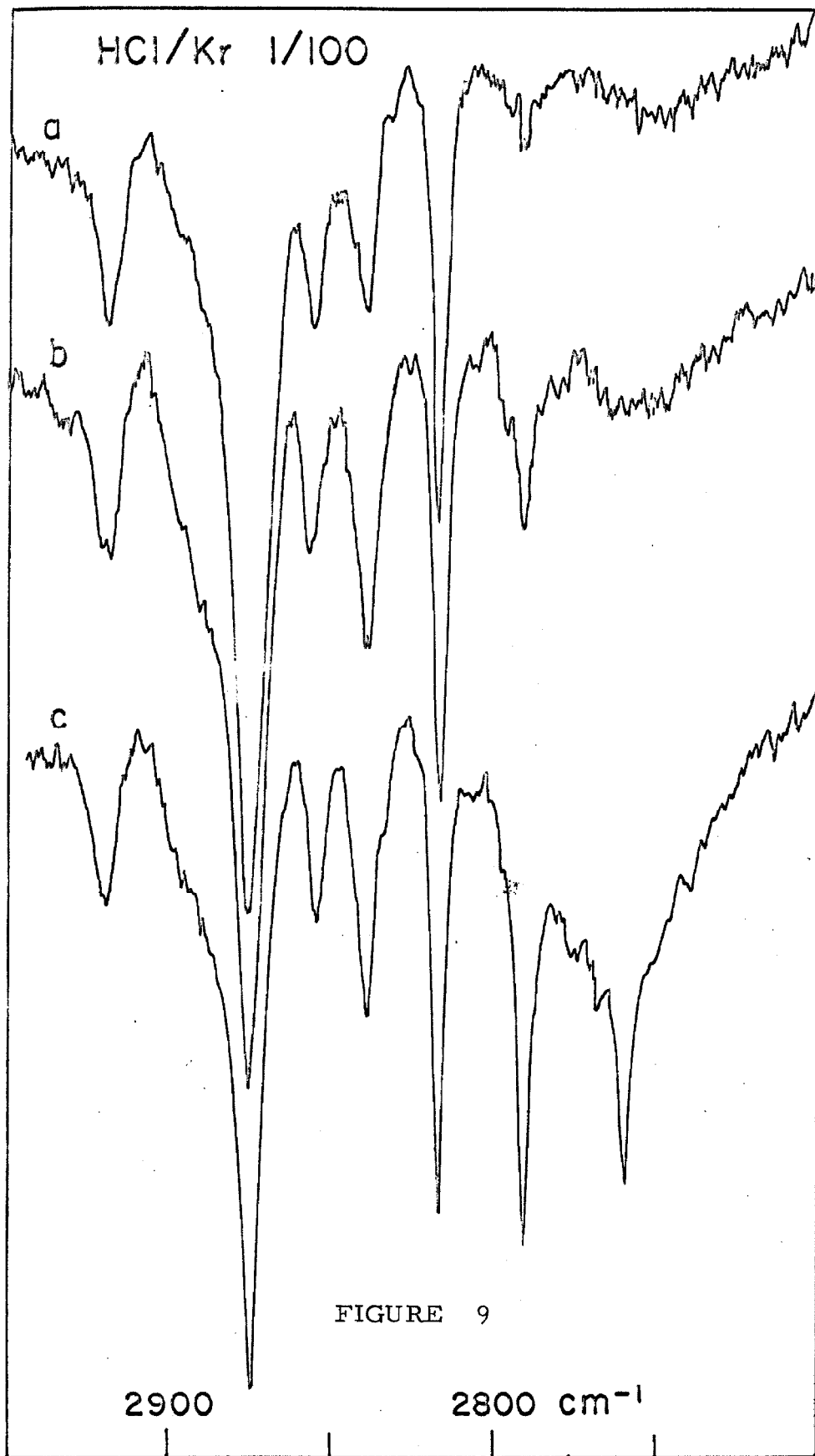


Table II. Absorption frequencies of HCl and DCl in krypton and xenon

HCl			
Krypton		Xenon	
ν (cm ⁻¹)	Assignment ^a	ν (cm ⁻¹)	Assignment ^a
2759 ± 1	P	2763	P
2764 ± 1	P	2780.5 ± 0.5	P
2774.5 ± 0.5	P	2783.9 ± 0.6	P
2780.2 ± 0.5 ^b	P	2792.1 ± 0.5	P
2788.8 ± 0.5	P	2816.6 ± 0.5	P
2795 ± 1	P	2825.5 ± 1	M
2807 ± 1	P	2837.8 ± 0.7	M
2815 ± 1	P	2858.2 ± 0.6	M
2837.4 ± 0.5	M	2872 ± 3 ^c	M
2852.8 ± 0.5	M	2885 ± 1	M
2872.7 ± 0.5	M		
2887 ± 4 ^c	M		
2917 ± 1	M		

Table II (continued)

DCI

Krypton		Xenon	
ν (cm ⁻¹)	Assignment ^a	ν (cm ⁻¹)	Assignment ^a
1998	P	2004 ± 4	P
2003	P	2013 ± 1	P
2009.5 ± 0.7	P	2022 ± 1	P
2020.4 ± 0.5	P	2038 ± 1	P
2036.9 ± 0.7	P	2047 ± 1	M
2047 ± 1	?	2058 ± 1	M
2058 ± 1	M	2069 ± 1	M
2067.5 ± 0.7	M	2075 ± 3	M
2078.9 ± 0.7	M		
2089 ± 3			

^aM = monomer; P = polymer.

^bThis line appears only if DCI is present.

^cThis shoulder observed only when sample is warmed to 20°K or above.

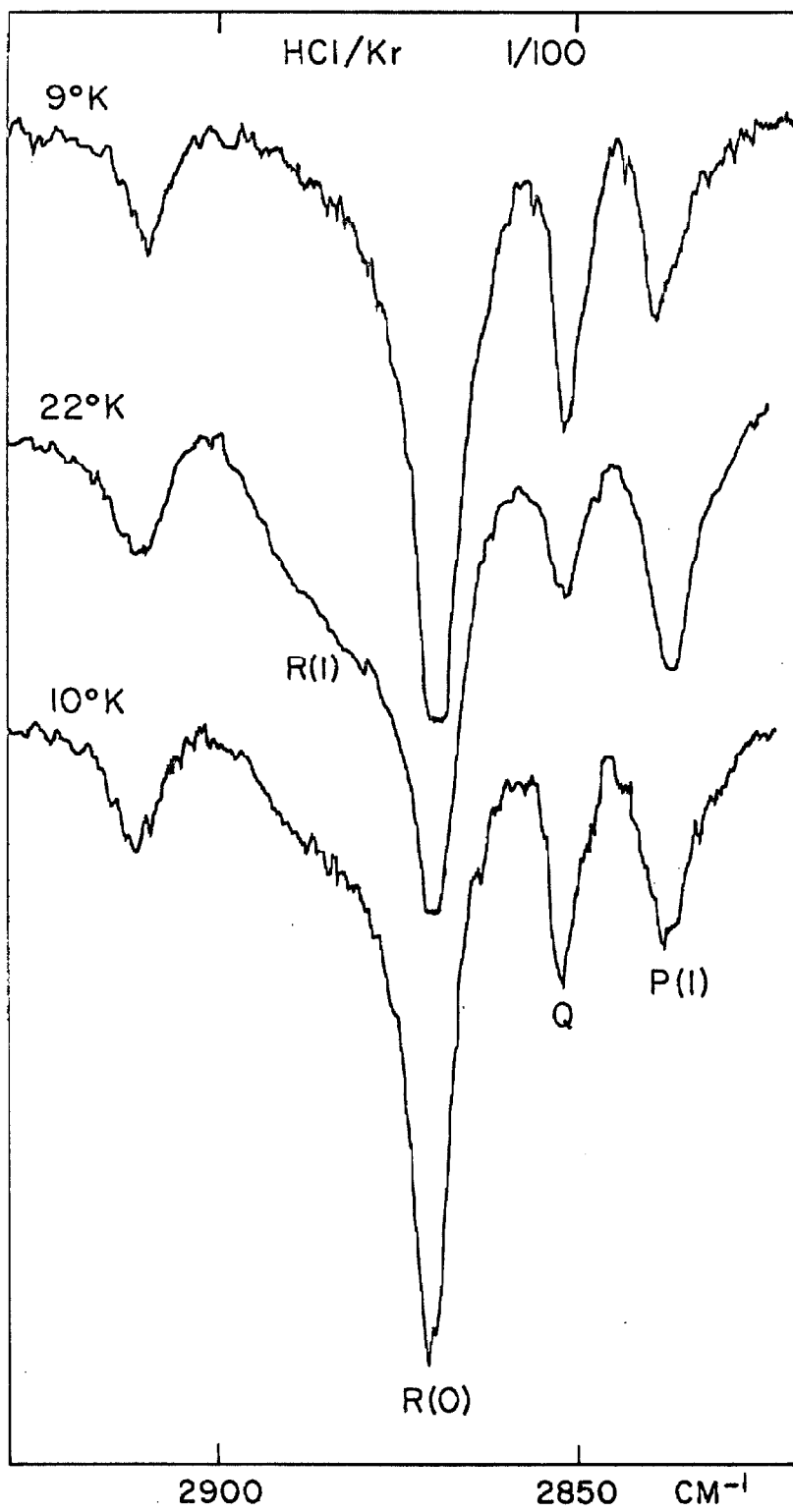


Fig. 10. Effect of temperature on intensity of HCl monomer lines.

lying energy states which correspond to quantized motion of HCl and DCl in the rare gas crystals. The observed intensity variations and relative positions of the individual lines in the spectra of monomeric HCl and DCl in krypton and xenon agree with the intensity variations and relative positions of the R(0), P(1), and R(1) vibration-rotation transitions in the gas phase spectra of HCl and DCl; however, the frequency separations between the lines in the solid are not the same as the corresponding frequency separations in the gas phase spectra. Thus the monomer lines of HCl and DCl in solid krypton and xenon are assigned to perturbed vibration-rotation transitions. Schoen et al. (5) have already made similar assignments for the fine structure observed in the infrared spectra of HCl and DCl in solid argon. The vibration-rotation assignments for HCl and DCl in solid argon, krypton, and xenon are summarized in Table III.

Compared to the gas phase values, the rotational levels in the solid exhibit a J-dependent shift; this is shown in the last two columns of Table III. The effect is much more pronounced for HCl than for DCl. In addition to this J-dependent shift, the vibration-rotation band origin is shifted to lower frequencies; and the Q branch, absent in the gas phase, is observed in the solid rare gases.

Table III. Vibration-rotation assignments.

		HCl						
		Q(0)						
	R(1)	R(0)	P(1)	Obs.	Calc. ^a	R(0) - P(1)	R(1) - P(1)	
Gas ^b	2925.9	2906.3	2865.1	-	2885.7	41.15	60.80	
Argon ^c	2896	2888.1	2853.6	-	2870.8	34.5	42.4	
Krypton	2887	2872.7	2837.4	2852.8	2855.0	35.3	49.6	
Xenon	2872	2858.2	2825.5	2837.8	2841.8	32.7	46.5	

		DCI						
		Q(0)						
	R(1)	R(0)	P(1)	Obs.	Calc. ^a	R(0) - P(1)	R(1) - P(1)	
Gas ^b	2111.95	2101.6	2080.3	-	2091.0	21.35	31.68	
Argon ^c	-	2090.0	2069	-	2080	21	-	
Krypton	2089	2078.9	2058	2067.5	2068	20.9	31	
Xenon	2075	2069	2047	2058	2058	22	28	

^aQ(0) calc. = [R(0) + P(1)]/2.

^bReference 9.

^cReference 5.

DISCUSSION

Hindered Rotation

The J-dependent perturbation on the vibration-rotation transitions will be discussed first in terms of a hindered rotator model. It is assumed that HCl is located at a substitutional site of the rare gas lattice; because of the small size of the interstitial sites, it is unlikely that they are important (see Table IV). A barrier to rotation arises because of interactions of the HCl with the surrounding nearest neighbor rare gas atoms. Recently, Flygare (10) has discussed the origin of a barrier of octahedral symmetry in terms of attractive interactions. This is the appropriate symmetry for a substitutional site in a face-centered cubic crystal (11). Some time ago Devonshire (13) solved the problem of a linear molecule rotating in a field of octahedral symmetry. The energy levels obtained by him as a function of barrier height are shown in Figure 11. Both energy and barrier height are expressed in units of the rotational constant B, which is 10.4 cm^{-1} for HCl and 5.39 cm^{-1} for DCl in the gas phase. The positive values of the barrier correspond to repulsive interactions between the HCl and the nearest neighbor rare gas atoms; i. e., potential energy maxima occur when HCl is aligned along the nearest neighbor directions. The negative barriers arise if the HCl is in a potential energy minimum when oriented along nearest neighbor directions.

Table IV. Nearest neighbor distances (Å).

Substitutional site		Interstitial site	
Crystal	Octahedral	Octahedral	Tetrahedral
Argon	3.75	2.65	2.30
Krypton	4.02	2.84	2.46
Xenon	4.31	3.05	2.64
HCl	3.67		

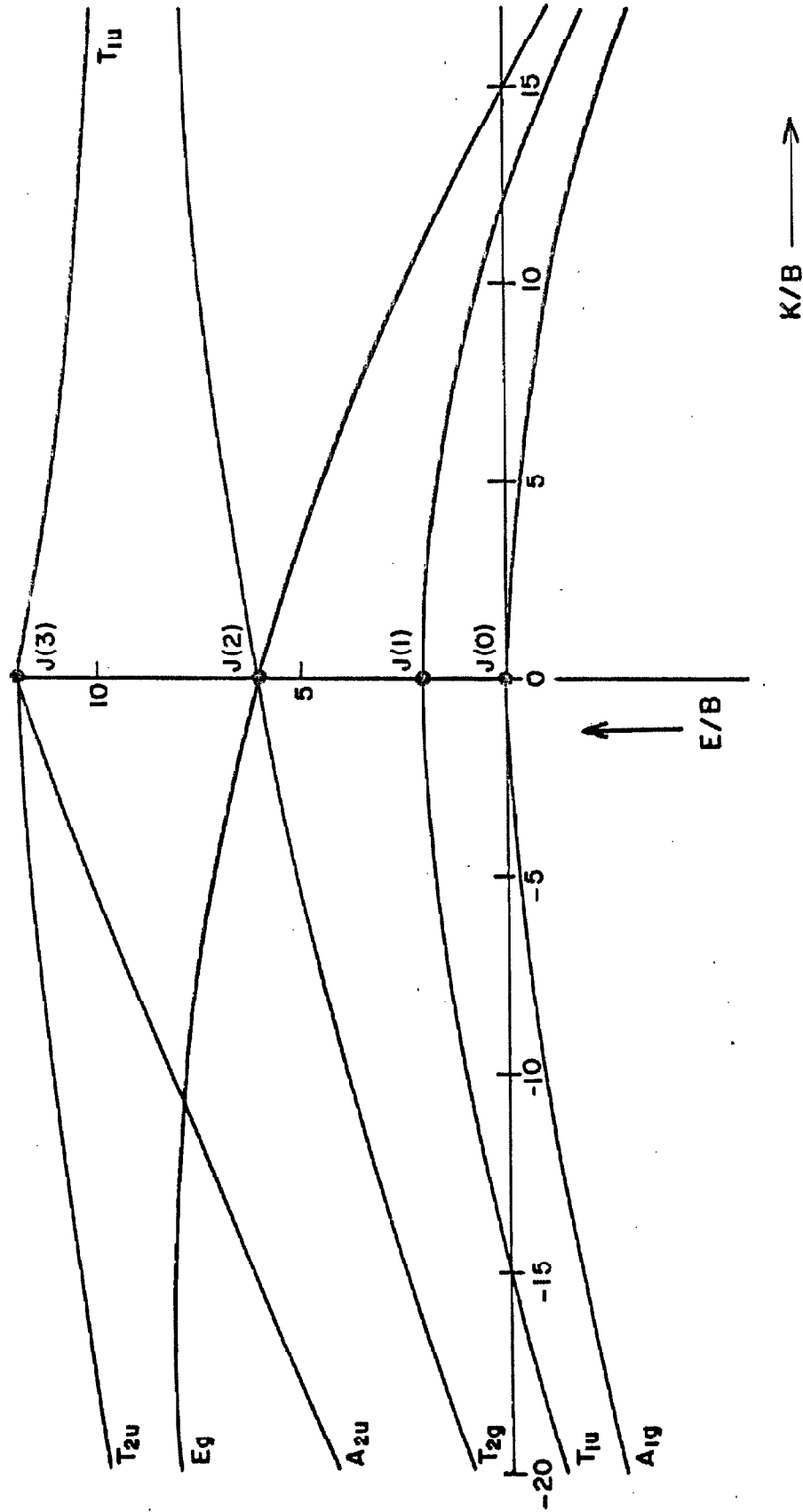


Fig. 11. Energy levels vs. barrier height.

The levels in Figure 11 are labeled according to the irreducible representations of the octahedral symmetry group. The dipole selection rules allow transitions from A_{1g} to T_{1u} ; from the T_{1u} level, transitions are allowed to A_{1g} , T_{2g} , E_g , and T_{1g} levels. We thus should expect to observe lines corresponding to the $R(0)$ ($A_{1g} \rightarrow T_{1u}$) and $P(1)$ ($T_{1u} \rightarrow A_{1g}$) transitions of the gas phase spectrum and two lines corresponding to the split $R(1)$ transition ($T_{1u} \rightarrow T_{2g}$ and $T_{1u} \rightarrow E_g$).

Lines corresponding to the $R(0)$ and $P(1)$ transitions indeed exist, but only one broad absorption in the $R(1)$ region on the high frequency side of $R(0)$ is observed. It grows in intensity as the temperature is increased (see Fig. 10). Since the splitting of the $R(1)$ line is very sensitive to the barrier height, the observation of only one line in the $R(1)$ region sets an upper limit to the barrier height. For a barrier no higher than ± 3 , for example, the two components of the $R(1)$ transition in HCl would be split by only about 10 cm^{-1} . Such a splitting would not be resolvable due to the increased linewidths at the elevated temperatures where these transitions can be seen. If such a low barrier were really the case, however, the calculated values of the perturbations on the $R(0) - P(1)$ rotational spacings would be in the range of tenths of cm^{-1} compared to observed values of 5 to 10 cm^{-1} . Thus the low barrier obtained from the lack of splitting in the $R(1)$ transition is highly inconsistent with rotational energy shifts in HCl.

Because of line broadening the upper component of the R(1) transition ($T_{1u} \rightarrow E_g$ for negative barriers or $T_{1u} \rightarrow T_{2g}$ for positive barriers) may not have been observed; therefore, the shoulder on the high frequency side of the R(0) line may be due solely to the low frequency component of the R(1) transition ($T_{1u} \rightarrow T_{2g}$ for negative barriers or $T_{1u} \rightarrow E_g$ for positive barriers). If this is the case, the observed rotational spacings of HCl may be fit reasonably well by a suitable choice of barrier height for each rare gas solid; in argon the barrier heights in units of B are -16.5 or +8; in krypton, -8 or +5; in xenon, -13 or +6. The negative values give a slightly better fit.

Since it arises from electronic interactions, the barrier (in units of B) is expected to be about twice as large for DCl as for HCl. Using the values obtained above for HCl, the appropriate barriers for DCl are -33 or +16 in argon, -16 or +10 in krypton, and -26 or +12 in xenon. For a barrier height of -16 in krypton, the calculated R(0) - P(1) and R(1) - P(1) spacings of the DCl rotational levels are 18 and 22 cm^{-1} respectively; these should be compared with the observed spacings of 21 and 31 cm^{-1} (see Table III). The difference between the calculated and the observed DCl rotational spacings is larger in argon and xenon; thus even for moderately high barriers, the rotational perturbations calculated on the basis of hindered rotation are not in agreement with the observed perturbations in HCl and DCl.

It has tacitly been assumed in the discussion above that the rotational constants of HCl and DCl are the same in a solid rare gas environment as they are in the gas phase. The rotational constants

are expected to decrease at least 1% in going from the gas phase to the solid rare gases; this is based on the observed 1% decrease in the vibrational frequency and the inverse relationship between frequency and bond length (Badger's rule). A 1% change in B will not significantly alter the barrier heights and the resulting perturbations due to hindered rotation discussed above. If for some reason a much larger decrease in B , say 10%, should occur in the solid and the hindered rotator model is used to account for any additional perturbations on the rotational energy levels, the barriers which give the best fit for HCl are -8 or $+5.5$ in argon, -3 or $+2$ in krypton, and -6 or $+4$ in xenon. For DCl the barriers will again be twice as large in units of B and the calculated perturbations on the $R(0) - P(1)$ and $R(1) - P(1)$ spacings of DCl are 18 and 24 cm^{-1} respectively in krypton. The agreement with the observed values (see Table III) still is not good.

The above discussion of the hindered rotator model may be summarized by noting that low values of the barrier (less than $|3|$) are not adequate to account for the 5 to 10 cm^{-1} perturbations on the $R(0) - P(1)$ rotational spacings of HCl. If the high frequency component of the split $R(1)$ transition was not observed because of line broadening in the solid, moderate values of the barrier account for the perturbations to the HCl rotational spacings; but the calculated perturbations on the DCl rotational levels are much larger than the observed perturbations. Hindered rotation alone is obviously not an adequate description of HCl and DCl in the solid rare gases.

Libration

In the limit of high barrier heights, the rotational motion is reduced to relatively small librations about an equilibrium orientation. This problem has been discussed by Hexter and Dows (14) and by Ewing (15). Their analysis is based on a quadratic potential for the librational motion. The selection rules so obtained are $\Delta N = 0, \pm 1, \pm 2, \dots$ in the order of decreasing probability. Here N denotes the librational quantum number. The $\Delta N = 0$ transition is expected to be much more intense than the $\Delta N = \pm 1$ transitions. On this basis we would have to assign the 2872.7 cm^{-1} line of HCl in krypton to the $\Delta N = 0$ transition, the 2887 cm^{-1} line to $\Delta N = +1$, and the 2852.8 cm^{-1} line to $\Delta N = -1$. At the low temperatures of these experiments, the $\Delta N = 0$ and $\Delta N = +1$ transitions originate almost entirely from the $N = 0$ librational level; when the sample is warmed, the corresponding absorption lines should decrease in intensity due to depopulation of the $N = 0$ level. Similarly, the $\Delta N = -1$ transition originates from the $N = 1$ librational level and the corresponding absorption line should increase in intensity when the sample is warmed. The observed intensity behavior of the lines assigned to the $\Delta N = \pm 1$ transitions is just opposite to what is expected (see Fig. 10); thus the librational model is not applicable to HCl and DCl in the solid rare gases.

Translation-Rotation Interaction

The J -dependent perturbations next will be discussed in terms

of interaction between the quasi-translational and the rotational motions. The quasi-translational motion is supposed equivalent to a localized lattice mode involving mainly motions of the HCl or DCl molecule. However, in the case of the argon matrix such a description may not be very appropriate because of the mass similarity of guest and host. This point is brought up again later in the paper. Friedmann and Kimel (16) have already discussed the J-dependent shifts in the vibration-rotation spectrum of HCl and DCl in argon in terms of this type of interaction. Using Lennard-Jones parameters to describe the interactions of HCl with argon, they calculated a value for the translational frequency; then using perturbation theory with the strength of the translation-rotation interaction as a parameter, they were able to obtain good agreement with experiment. This treatment is not generally applicable because the perturbation theory breaks down for near resonance between the translational and rotational levels and also because of the loss of the local lattice mode description for the translation. Because of the uncertainties in the calculated translational frequencies, we have chosen to regard both the translational frequency and the strength of the translation-rotation interaction as parameters. The Hamiltonian matrix is expressed as a function of these two parameters and an exact diagonalization is carried out.

The HCl or DCl molecule is assumed to translate and rotate about a substitutional site in the rare gas lattice. The classical kinetic energy of a rigid, translating, rotating molecule is given by

$$\begin{aligned}
2T = & \dot{\underline{R}}^2 \sum_i m_i + \sum_i m_i (\underline{\omega} \times \underline{r}_i) \cdot (\underline{\omega} \times \underline{r}_i) \\
& + 2\dot{\underline{R}} \cdot \underline{\omega} \times \sum_i m_i \underline{r}_i ; \quad (1)
\end{aligned}$$

where \underline{R} is the position of the translating coordinate system in the space fixed XYZ frame (see Fig. 12), $\underline{\omega}$ is the angular velocity of the coordinate system which rotates with the molecule, and \underline{r}_i is the position of the i^{th} atom in the rotating system (17).

Usually the origin of the translating coordinate system is chosen at the center of mass of the rotating molecule, in which case the third term in the kinetic energy of equation 1 is zero. For this choice of origin, the potential energy describing the interaction of the molecule with its environment is most simply expressed in terms of the position of the center of mass and the orientation of the molecule. However, in general the centers of mass of isotopic molecules are located at slightly different positions with respect to the electrons and nuclei of the molecules; this causes the potential energy function when expressed in terms of the positions of the centers of mass to be slightly different for the isotopic molecules. This is a distinct disadvantage of such a choice of coordinate system.

In order that the potential energy have the same form for HCl rare gas interactions as for DCl rare gas interactions, it must be expressed in terms of the position of the center of interaction of HCl and DCl (18, 19). The center of interaction can be thought of as the center of electrical symmetry of the molecule, and in general its

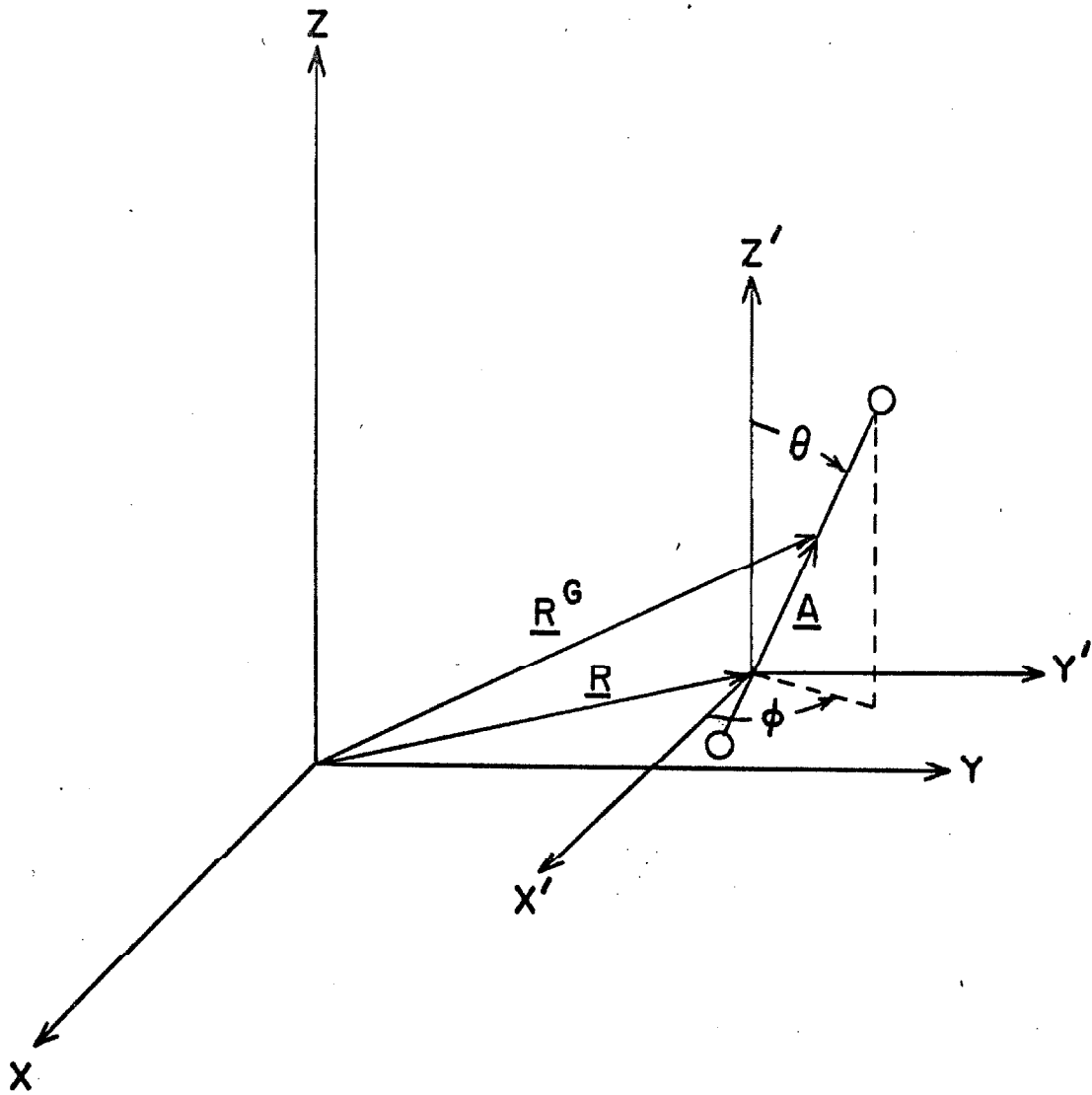


Fig. 12. Coordinate systems.

Space Fixed XYZ

Translating $X'Y'Z'$

position cannot be specified other than to say that it must lie on all symmetry elements present in the molecule. The relation between the center of mass and the center of interaction can be written as

$$\underline{R}^G = \underline{R} + A \underline{l} \quad (2a)$$

$$\underline{r}_i^G = \underline{r}_i - A \underline{l} \quad (2b)$$

where A is the distance between the center of mass and the center of interaction; \underline{l} for linear molecules is a unit vector along the molecular axis. \underline{R}^G is the position of the center of mass and \underline{R} is the position of the center of interaction in the space fixed coordinate system XYZ (see Fig. 12). The positions of the i^{th} atom in the rotating coordinate system with respect to the center of mass and the center of interaction are given by \underline{r}_i^G and \underline{r}_i respectively.

It is convenient to choose the origin of the translating coordinate system at the center of interaction, because in this case the same potential energy function can be used for HCl and DCl. For this choice of origin, the translational and rotational motions are no longer separable; that is, the third term of equation 1 is nonzero. The resulting Hamiltonian operator is given in equation 3, where X , Y , and Z are the coordinates of the center of interaction in the space fixed system, θ and ϕ are the angular coordinates of the linear molecule with respect to the translating coordinate system, M is the mass of the whole molecule, and I is its moment of inertia with respect to the center of mass. The derivation of equation 3 from the classical energy expressions is given in Appendix I.

$$\begin{aligned}
\hat{H} = & \frac{-\hbar^2}{2M} \left[\frac{\partial^2}{\partial X^2} + \frac{\partial^2}{\partial Y^2} + \frac{\partial^2}{\partial Z^2} \right] - \frac{\hbar^2}{2I} \left[\frac{1}{\sin \theta} \frac{\partial}{\partial \theta} \left(\sin \theta \frac{\partial}{\partial \theta} \right) + \frac{1}{\sin^2 \theta} \frac{\partial^2}{\partial \phi^2} \right] + V \\
& - \frac{\hbar^2 A}{2I} \left[\sin \theta \frac{\partial}{\partial Z} \frac{\partial}{\partial \theta} + \frac{1}{\sin \theta} \frac{\partial}{\partial Z} \frac{\partial}{\partial \theta} (\sin^2 \theta) - \cos \theta \cos \phi \frac{\partial}{\partial X} \frac{\partial}{\partial \theta} \right. \\
& - \frac{\cos \phi}{\sin \theta} \frac{\partial}{\partial X} \frac{\partial}{\partial \theta} (\sin \theta \cos \theta) + \frac{\sin \phi}{\sin \theta} \frac{\partial}{\partial X} \frac{\partial}{\partial \phi} + \frac{1}{\sin \theta} \frac{\partial}{\partial X} \frac{\partial}{\partial \phi} (\sin \phi) \\
& - \cos \theta \sin \phi \frac{\partial}{\partial Y} \frac{\partial}{\partial \theta} - \frac{\sin \phi}{\sin \theta} \frac{\partial}{\partial Y} \frac{\partial}{\partial \theta} (\sin \theta \cos \theta) - \frac{\cos \phi}{\sin \theta} \frac{\partial}{\partial Y} \frac{\partial}{\partial \phi} \\
& \left. - \frac{1}{\sin \theta} \frac{\partial}{\partial Y} \frac{\partial}{\partial \phi} (\cos \phi) \right] \\
& - \frac{\hbar^2 A^2}{2I} \left[(1 - \sin^2 \theta \cos^2 \phi) \frac{\partial^2}{\partial X^2} + (1 - \sin^2 \theta \sin^2 \phi) \frac{\partial^2}{\partial Y^2} + \sin^2 \theta \frac{\partial^2}{\partial Z^2} \right. \\
& \left. - 2 \sin^2 \theta \sin \phi \cos \phi \frac{\partial}{\partial X} \frac{\partial}{\partial Y} - 2 \sin \theta \cos \theta \cos \phi \frac{\partial}{\partial X} \frac{\partial}{\partial Z} - 2 \sin \theta \cos \theta \sin \phi \frac{\partial}{\partial Y} \frac{\partial}{\partial Z} \right]
\end{aligned}$$

(3)

If we assume for the purposes of this calculation that the barrier for hindered rotation of HCl in the rare gas crystal is low, we may ignore terms in the potential energy depending on the orientation of HCl. We shall also neglect the interaction of the translational motion with the lattice vibrations; i. e., we assume a rigid lattice. The potential energy in equation 3 may then be approximated by $kR^2/2$. Then it is seen that the problem in the absence of translation-rotation interaction ($A = 0$) reduces to that of a three dimensional harmonic oscillator plus a rigid rotator. The terms in A can therefore be considered perturbation terms which modify the zero-order wave functions and energies.

The zero-order wave functions are products of the three dimensional harmonic oscillator and rigid rotor wave functions.

$$\begin{aligned} \Psi^0(X, Y, Z, \theta, \phi) = & N \exp(-\gamma R^2/2) H_{n_X}(\gamma^{1/2}X) H_{n_Y}(\gamma^{1/2}Y) \cdot \\ & \cdot H_{n_Z}(\gamma^{1/2}Z) P_J^M(\cos \theta) \begin{cases} \sin M \phi \\ \cos M \phi \end{cases} \end{aligned} \quad (4)$$

where $\gamma = M\xi/2I$. The zero-order energies in units of the rotational constant B are therefore

$$E^0(n_X, n_Y, n_Z, J) = (n_X + n_Y + n_Z)\xi + J(J + 1) \quad (5)$$

where n_X , n_Y , and n_Z are the harmonic oscillator quantum numbers, J is the rotational quantum number, and

$$\xi = (k/M)^{1/2} / 2\pi cB \quad (6)$$

is the translational frequency. The zero point of energy has been taken at $3\xi/2$.

Zero-order levels included in the calculation are shown in Figure 13 where the translational quantum number is defined by

$$T = (n_X + n_Y + n_Z) . \quad (7)$$

The numbers in parentheses in Figure 13 give the degeneracies of the zero-order levels; the lower energy levels have also been labeled according to the irreducible representations of the D_{2h} point group (see discussion below). The $(T = 0, J = 3)$, $(T = 3, J = 0)$, $(T = 3, J = 1)$, and $(T = 3, J = 2)$ levels were not included in the calculation because they do not interact directly with the pure rotational levels $(T = 0, J)$.

The Hamiltonian in equation 3 is invariant under the symmetry operations of the D_{2h} group when the operations are carried out simultaneously in the space fixed and the translating coordinate systems. For example, the Hamiltonian is invariant with respect to an inversion carried out in the XYZ and X'Y'Z' systems. The symmetry properties are discussed in more detail in Appendix II. The Hamiltonian matrix can therefore be factored according to the irreducible representations of the D_{2h} group; the zero-order wave functions belonging to each factor are shown in Table V. The B_{2u} and B_{3u} factors are identical; the same is true of the B_{2g} and B_{3g} factors and only one of each pair need be considered. The A_u factor contains no pure rotational levels and will not be considered any further. The factors which remain are

Figure 13. Zero-order translational and rotational levels included in the calculation. T is the translational quantum number, J is the rotational quantum number. The numbers in parentheses indicate the degeneracies of the zero-order levels. In the figure the translational frequency ξ has been taken to be 3.5.










	T J		D _{2h} Symmetry Species
	1, 3	(21)	
	2, 2	(30)	
	1, 2	(15)	
	2, 1	(18)	
	2, 0	(6)	3 A _g , B _{1g} , B _{2g} , B _{3g}
	0, 2	(5)	2 A _g , B _{1g} , B _{2g} , B _{3g}
	1, 1	(9)	3 A _g , 2 B _{1g} , 2 B _{2g} , 2 B _{3g}
	1, 0	(3)	B _{1u} , B _{2u} , B _{3u}
	0, 1	(3)	B _{1u} , B _{2u} , B _{3u}
	0, 0	(1)	A _g

Fig. 13. Zero-order levels.

Table V. Symmetry of the zero-order functions.

n_X	n_Y	n_Z	P_0^0	$P_1^1 \sin \phi$	P_1^0	$P_1^1 \cos \phi$	$P_2^2 \sin 2\phi$	$P_2^1 \sin \phi$	P_2^0	$P_2^1 \cos \phi$	$P_2^2 \cos 2\phi$
0	0	0	A _g	B _{2u}	B _{1u}	B _{3u}	B _{1g}	B _{3g}	A _g	B _{2g}	A _g
1	0	0	B _{3u}	B _{1g}	B _{2g}	A _g	B _{2u}	A _u	B _{3u}	B _{1u}	B _{3u}
0	1	0	B _{2u}	A _g	B _{3g}	B _{1g}	B _{3u}	B _{1u}	B _{2u}	A _u	B _{2u}
0	0	1	B _{1u}	B _{3g}	A _g	B _{2g}	A _u	B _{2u}	B _{1u}	B _{3u}	B _{1u}
2	0	0	A _g	B _{2u}	B _{1u}	B _{3u}	B _{1g}	B _{3g}	A _g	E _{2g}	A _g
0	2	0	A _g	B _{2u}	B _{1u}	B _{3u}	B _{1g}	B _{3g}	A _g	E _{2g}	A _g
0	0	2	A _g	B _{2u}	B _{1u}	B _{3u}	B _{1g}	B _{3g}	A _g	E _{2g}	A _g
1	1	0	B _{1g}	B _{3u}	A _u	B _{2u}	A _g	B _{2g}	B _{1g}	E _{3g}	B _{1g}
1	0	1	B _{2g}	A _u	B _{3u}	B _{1u}	B _{3g}	B _{1g}	B _{2g}	A _g	B _{2g}
0	1	1	B _{3g}	B _{1u}	B _{2u}	A _u	B _{2g}	A _g	B _{3g}	E _{1g}	B _{3g}

Table V (continued)

n_X	n_Y	n_Z	$P_3^1 \sin 3\phi$	$P_3^2 \sin 2\phi$	$P_3^1 \sin \phi$	P_3^0	$P_3^1 \cos \phi$	$P_3^2 \cos 2\phi$	$P_3^3 \cos 3\phi$
1	0	0	B_{1g}	B_{3g}	B_{1g}	B_{2g}	A_g	B_{2g}	A_g
0	1	0	A_g	B_{2g}	A_g	B_{3g}	B_{1g}	B_{3g}	B_{1g}
0	0	1	B_{3g}	B_{1g}	B_{3g}	A_g	B_{2g}	A_g	B_{2g}

A_g , B_{1g} , B_{2g} , B_{1u} , and B_{2u} . An IBM 7094 computer was used to diagonalize these matrices for various values of the two parameters ξ and A .

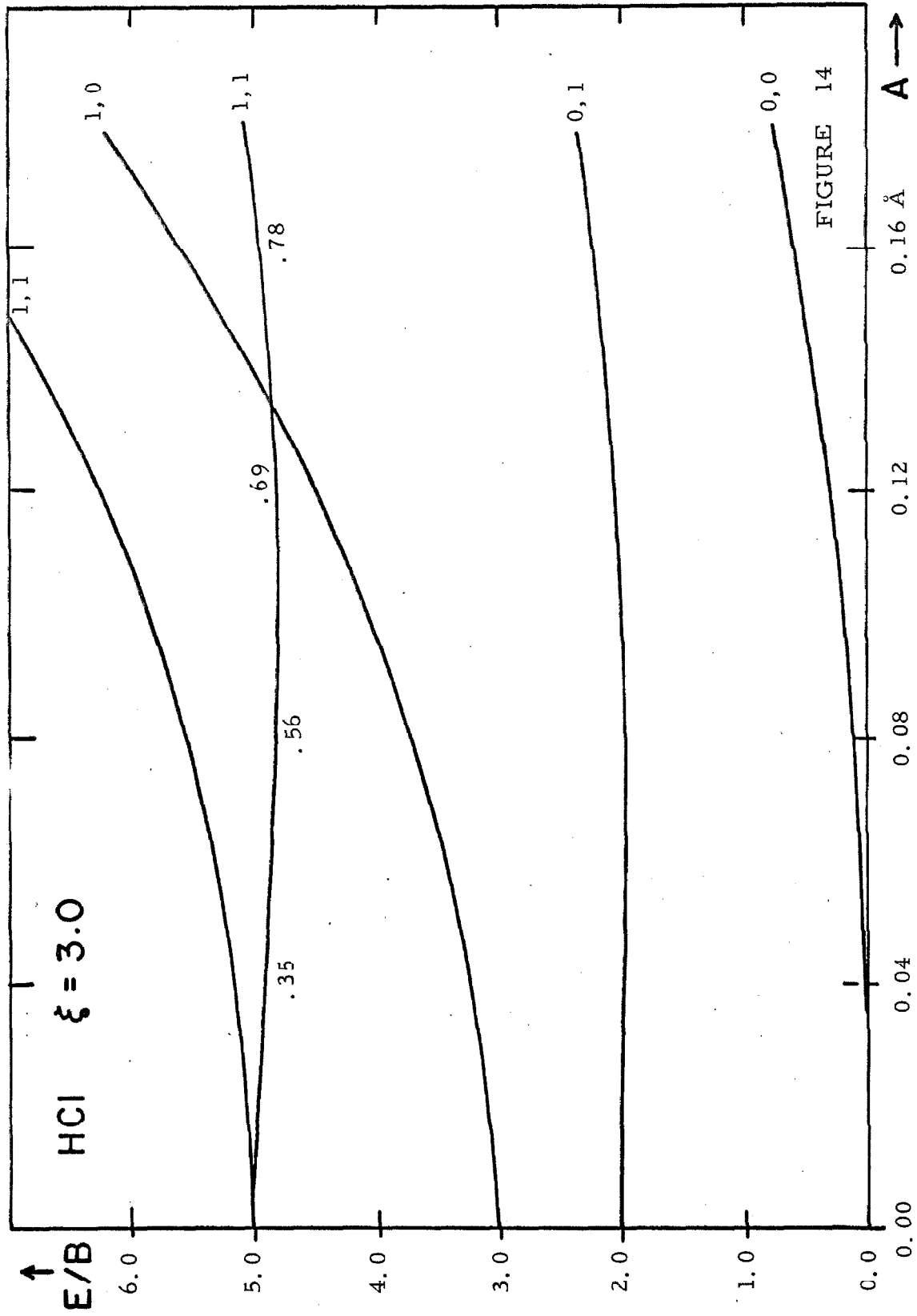
The results of the calculation for HCl are shown in Figures 14 to 22; representative results for DCl are shown in Figures 23 to 25. Instead of single lines used in the figures for clarity, the energy levels should be shown as narrow energy bands. The band formation arises from the superposition of levels from separate symmetry factors, in each of which the translation-rotation interaction is slightly different. For large values of A (about 0.2 \AA) the maximum band width is 1 to 1.5 cm^{-1} .

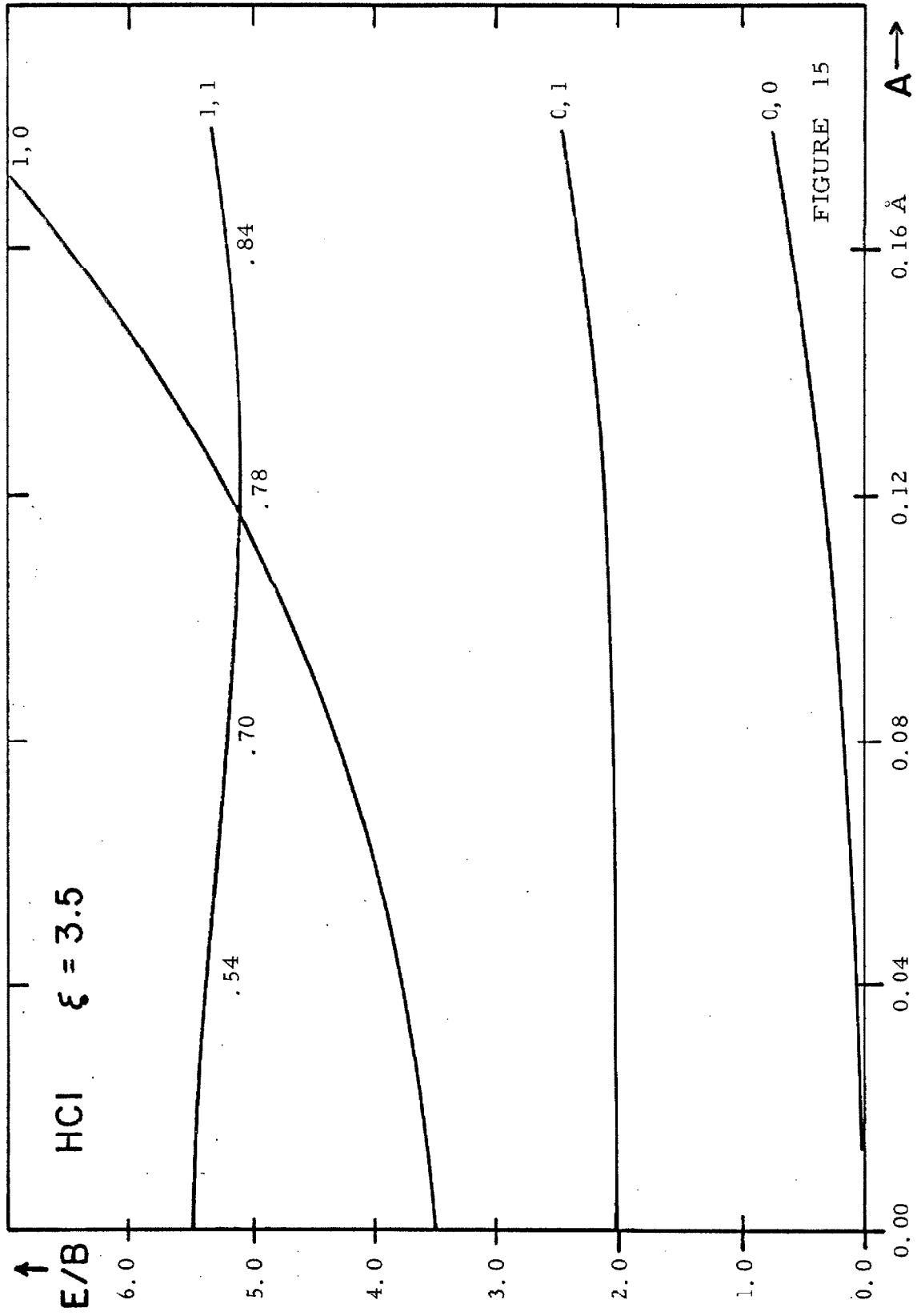
There are four independent parameters available which may be adjusted to get the best fit of the data. The translational frequencies of HCl in each of the rare gases are independent. However, the translational frequency of DCl in a given rare gas matrix is related to that of HCl in the same matrix by the factor $(B_{\text{HCl}}/B_{\text{DCl}})(M_{\text{HCl}}/M_{\text{DCl}})^{1/2}$. The mass difference is small and has been neglected in fitting the data. The parameter A is a molecular quantity and must be the same for HCl in all the rare gases. The value of A for DCl is related to that of HCl by

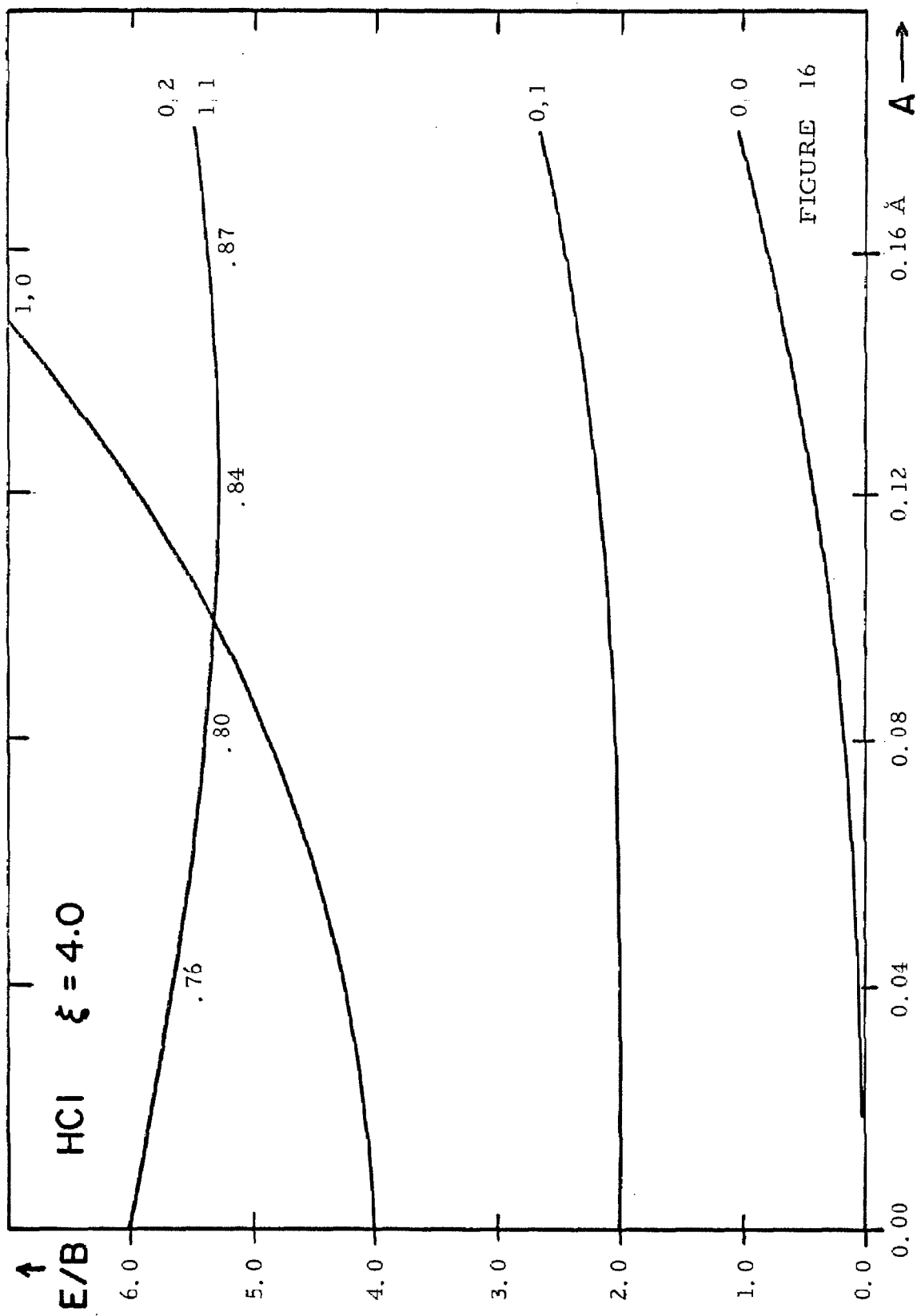
$$A_{\text{DCl}} = A_{\text{HCl}} \pm 0.034 \text{ \AA} \quad (8)$$

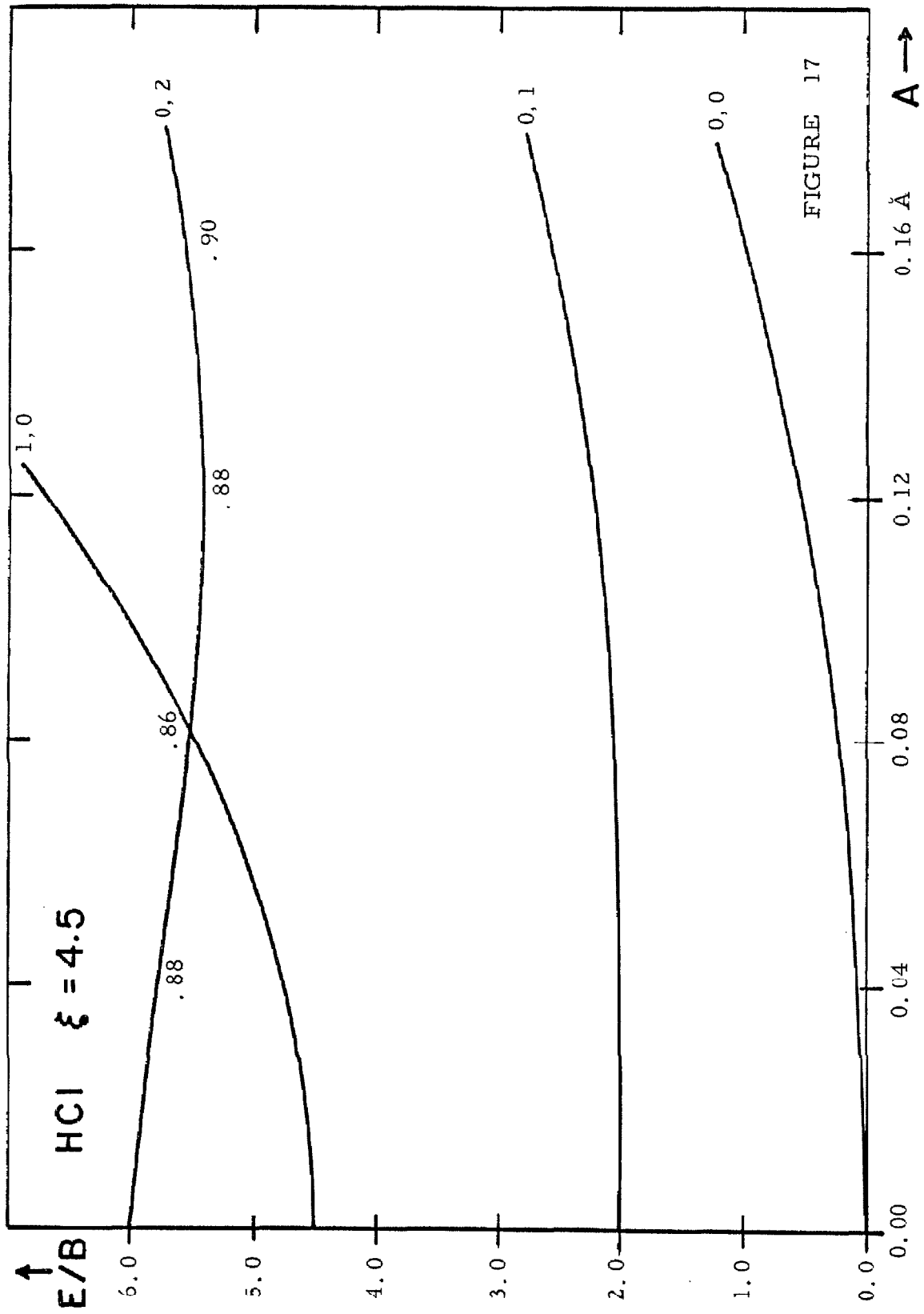
where 0.034 \AA is the change in the position of the center of mass in HCl and DCl. The plus sign is applicable if the center of interaction lies on the same side of the center of mass as the chlorine atom, the

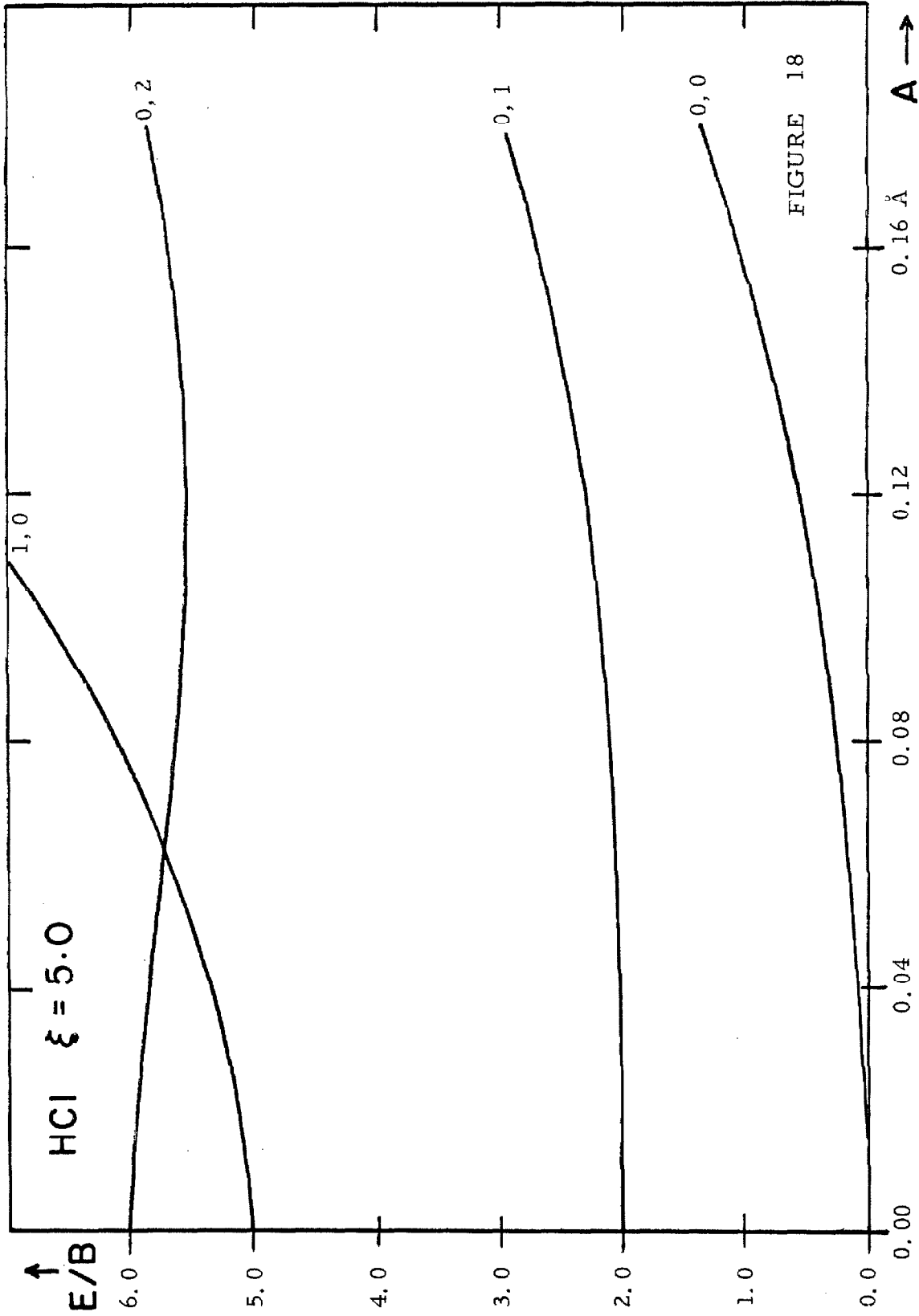
Figures 14 to 25. Translation-rotation energy levels of HCl and DCI vs. A ; ξ is the translation frequency in units of B ; A is the separation between the center of mass and the center of interaction. The numbers to the right of the perturbed levels indicate the zero-order levels (T, J) to which the perturbed levels correlate in the absence of translation-rotation interaction. The numbers above or below some of the perturbed levels give the coefficient of the $(T = 0, J = 2)$ zero-order wave function in the corresponding perturbed eigenfunction.

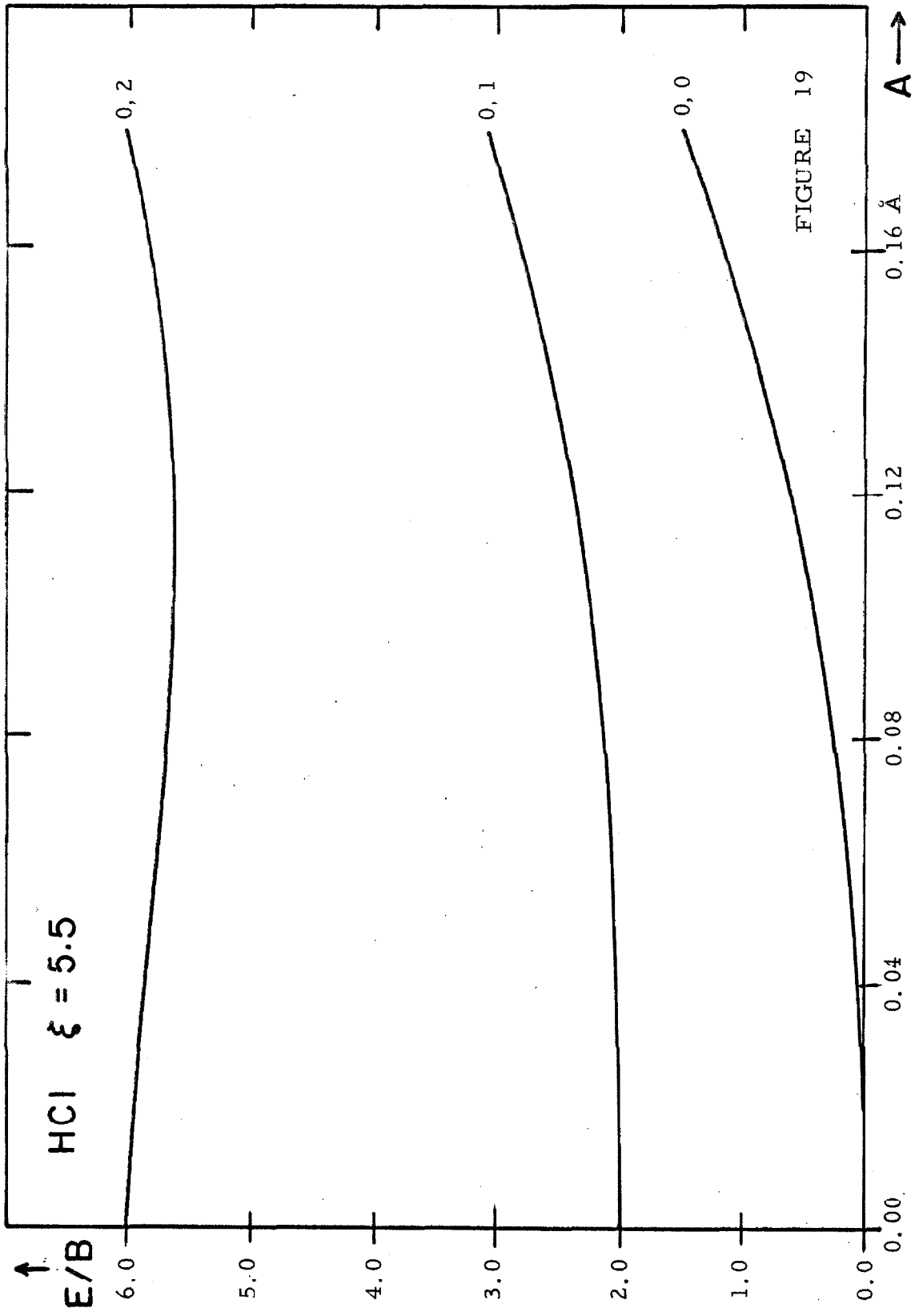


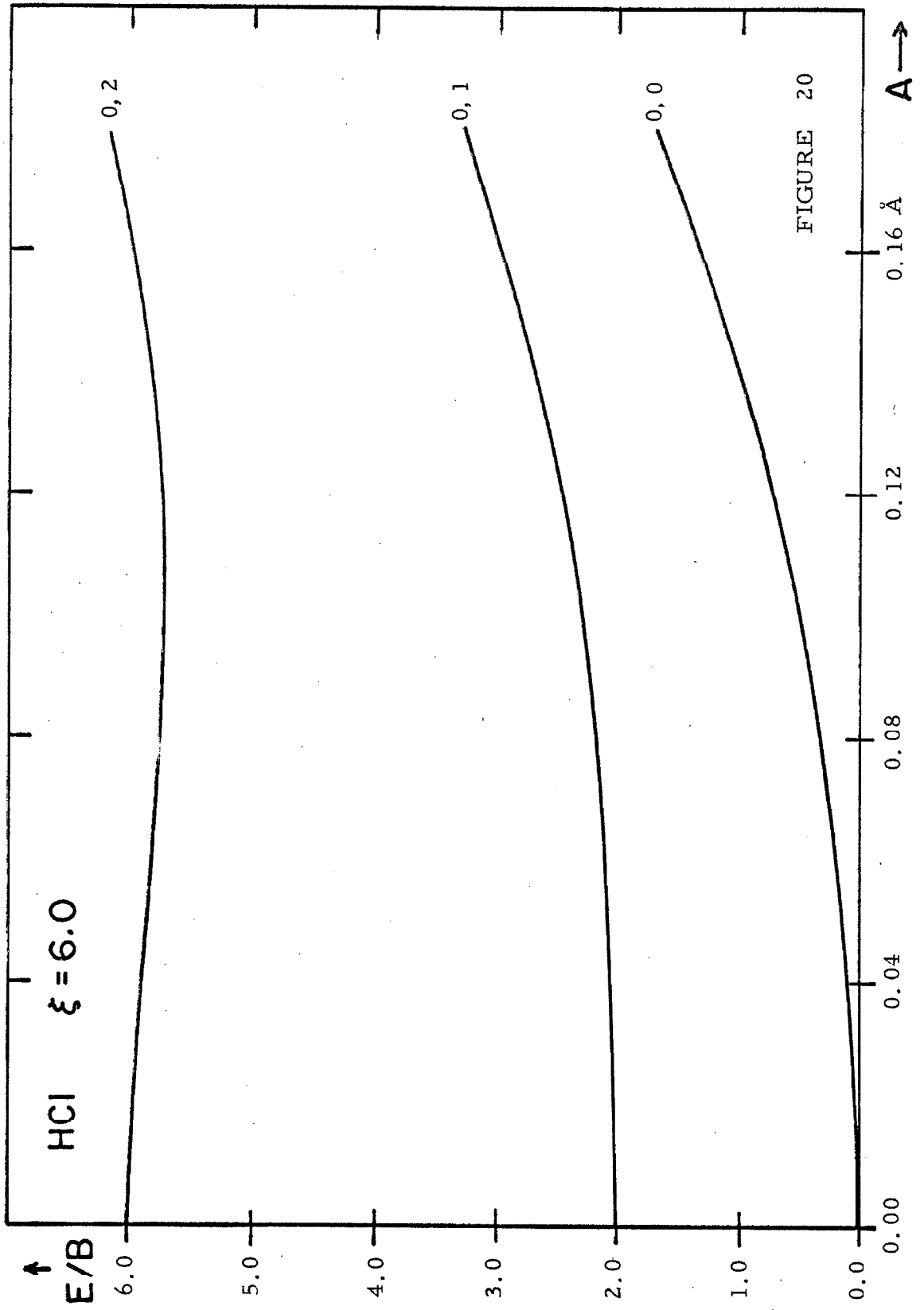


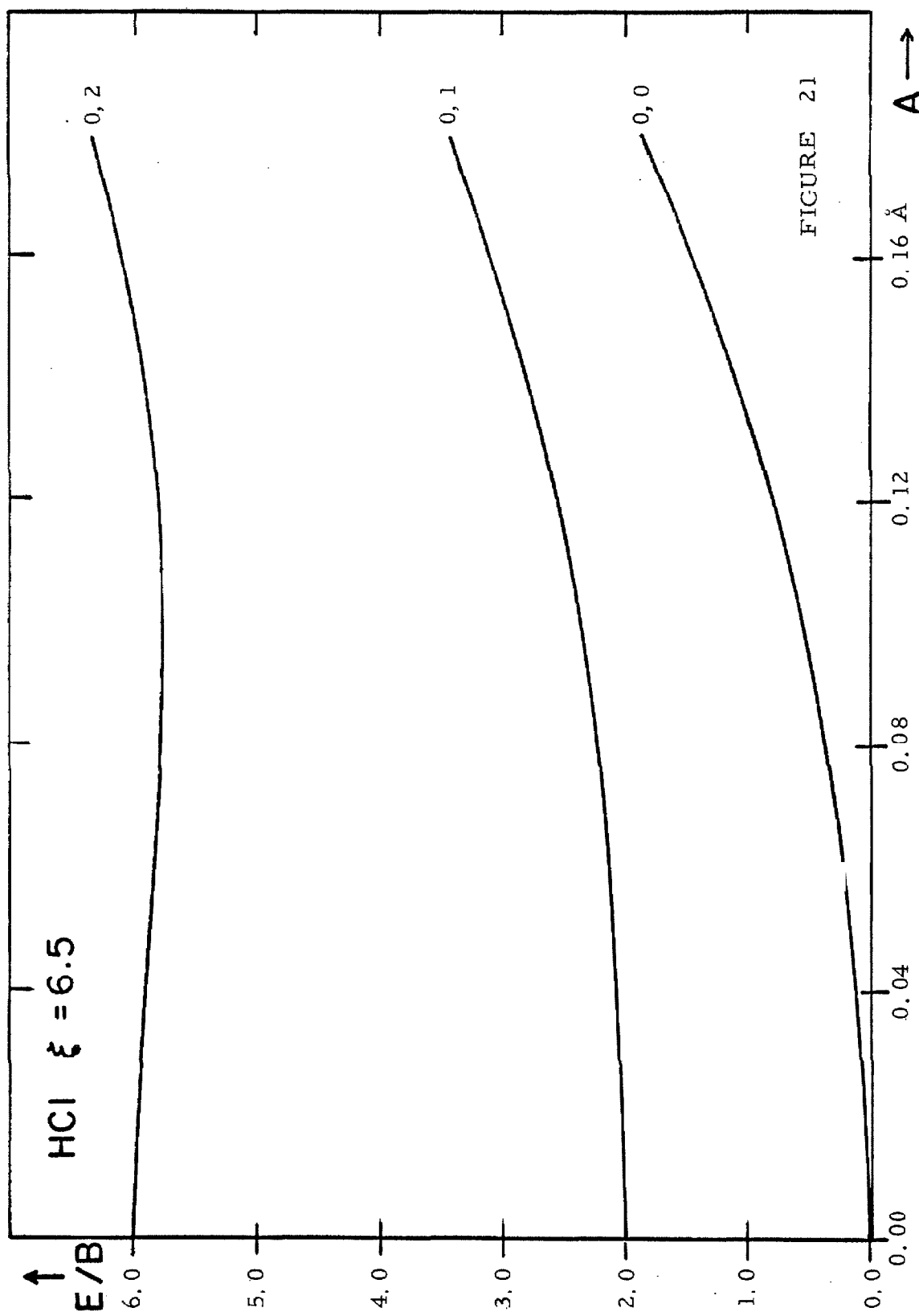












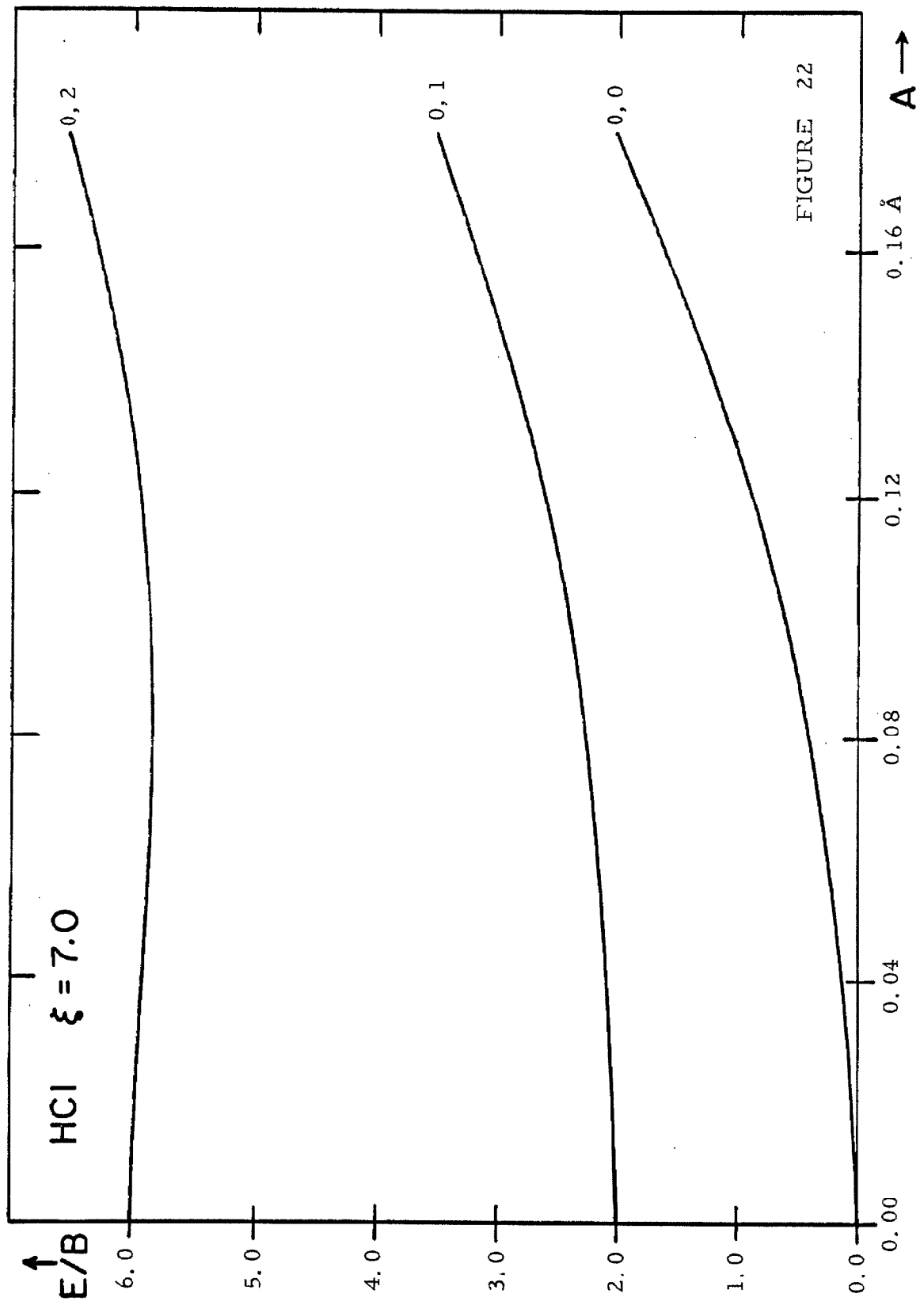
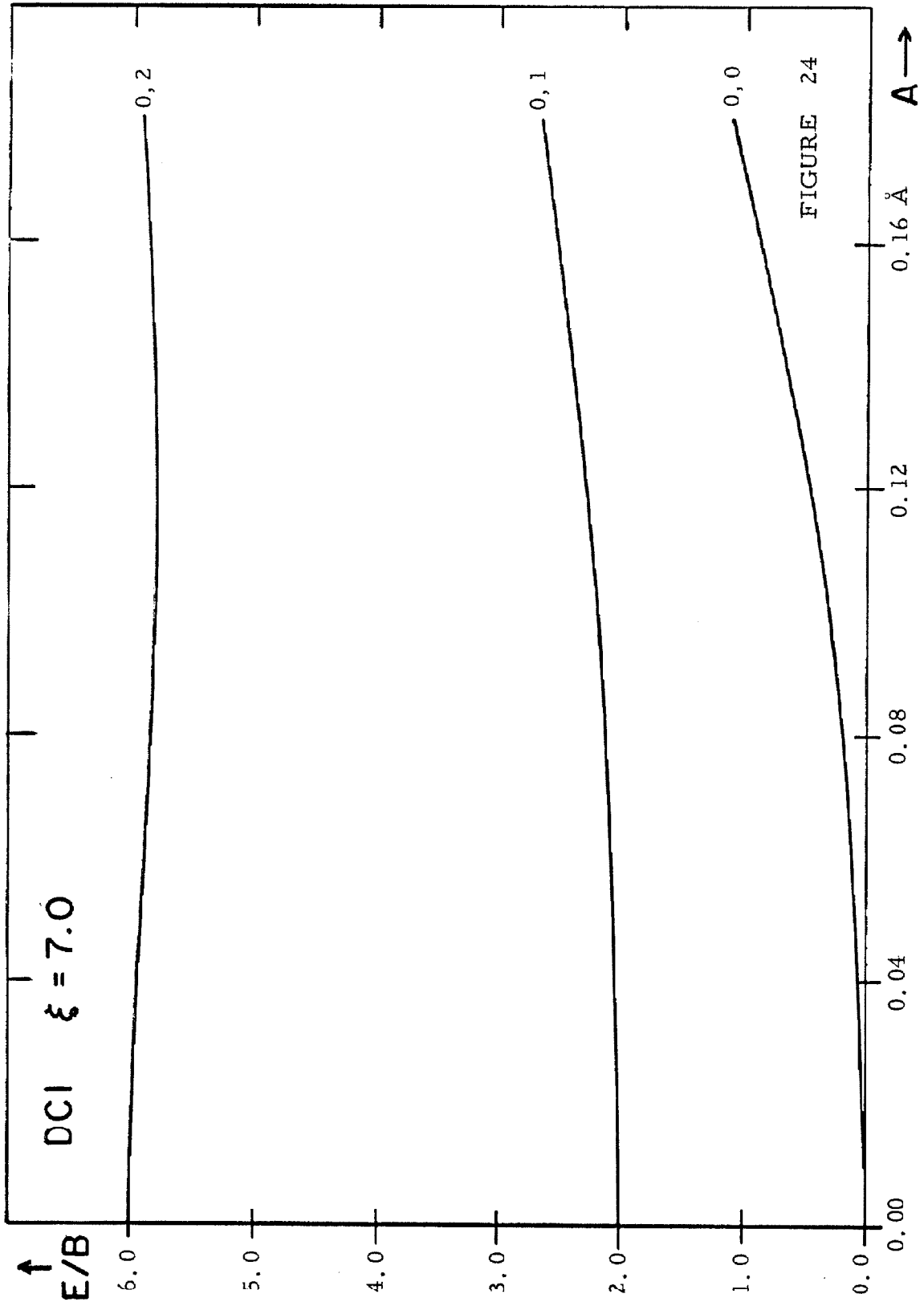
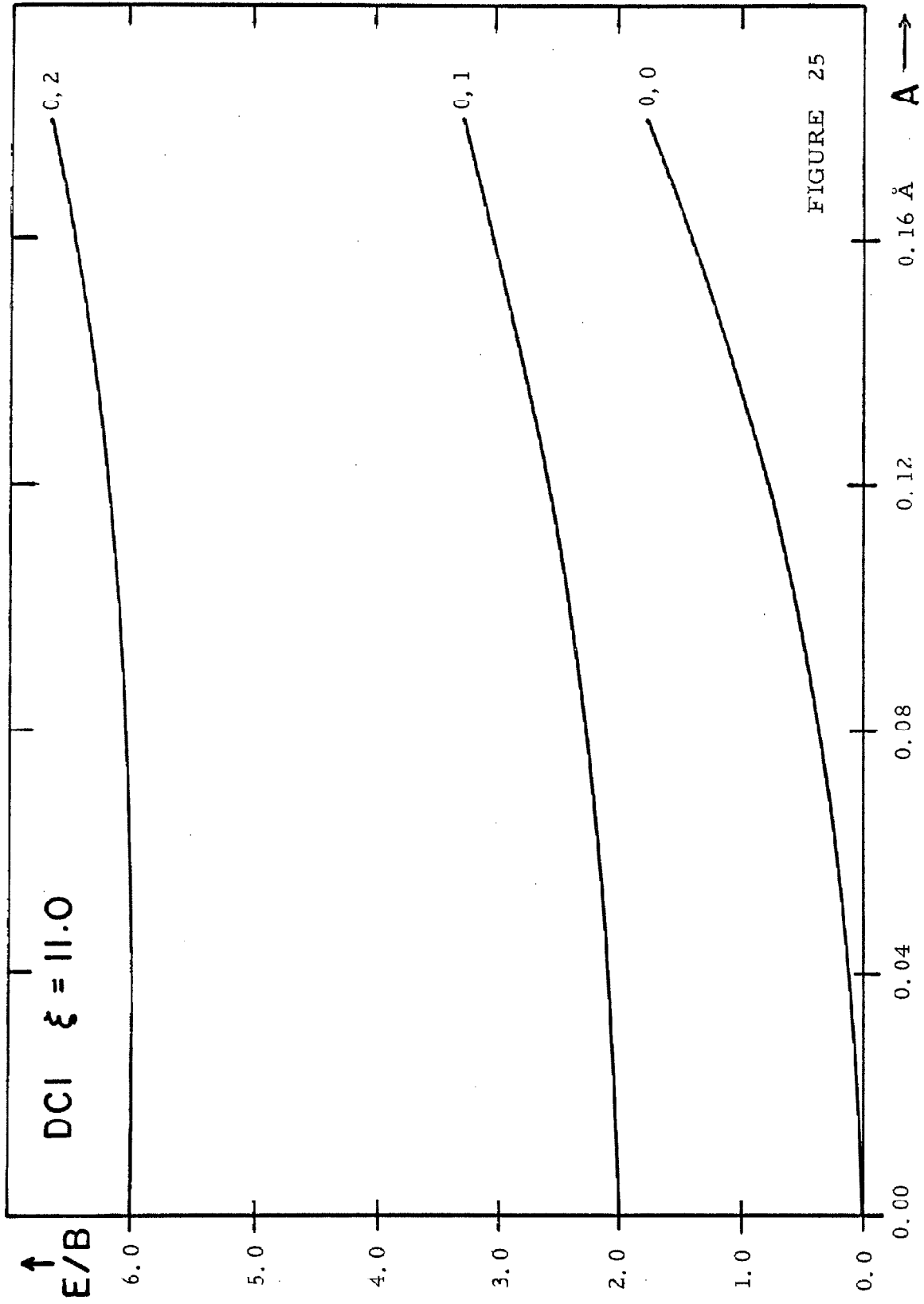


FIGURE 22





minus sign if the center of interaction lies on the hydrogen side of the center of mass.

With the above restrictions the parameters ξ_{Ar} , ξ_{Kr} , ξ_{Xe} , and A were used to attempt a fit of the observed rotational spacings of HCl and DCl in the solid rare gases. The results are shown in Table VI. The values of the parameters given in Table VI result in the best agreement with experiment; however, the calculated spacings do not change appreciably if ξ_{Kr} lies between 5.5 and 7.0, ξ_{Xe} between 3.5 and 4.0, and A_{HCl} between 0.10 and 0.13 Å (A_{DCl} between 0.066 and 0.096 Å). The calculation correctly shows that the perturbation on the DCl rotational levels is much less than that on the HCl levels; the agreement between calculated and observed spacings is within the experimental error in the observed values.

If future reduction in the experimental uncertainties warrant, it may be possible to improve the calculation by using an appropriate angular dependent potential in the Hamiltonian and by including interaction between the translational mode and the vibrational modes of the lattice. The latter improvement should be particularly important in argon where the mass difference between HCl and the atoms of the lattice is small; in this case the approximation of a rigid lattice is expected to be especially bad.

Induced Q Branch

The line at 2852.8 cm^{-1} in the monomer region of HCl in krypton and the corresponding lines for HCl and DCl in krypton and xenon (see Table III) are assigned to Q branch vibration-rotation

Table VI. Comparison of calculated and observed rotational spacings.

HCl

$$A = 0.13 \text{ \AA}$$

Matrix	Translational Frequency (units of B)	R(0) - P(1) (cm ⁻¹)		R(1) - P(1) (cm ⁻¹)	
		Calc.	Obs.	Calc.	Obs.
Argon	3.0	35.2	34.5	45.6	42.4
Krypton	5.5	35.4	35.3 ± 1	49.8	49.6 ± 4
Xenon	3.5	35.8	32.7 ± 2	47.5	46.5 ± 4

DCl

$$A = 0.096 \text{ \AA}$$

Matrix	Translational Frequency (units of B)	R(0) - P(1) (cm ⁻¹)		R(1) - P(1) (cm ⁻¹)	
		Calc.	Obs.	Calc.	Obs.
Argon	6.0	20.5	21	29.2	—
Krypton	11.0	19.8	20.9 ± 2	29.4	31 ± 4
Xenon	7.0	20.6	22 ± 2	29.2	28 ± 4

transitions. There is a correlation between the observed Q branch intensity relative to the R(0) line and the concentration of HCl. At 0.20% HCl in krypton the relative intensity is 0.06; at 1%, 0.09 to 0.24; and at 2%, 0.17 to 0.26.

Although it is forbidden by dipole selection rules for isolated HCl, an induced Q branch has been observed in gas phase mixtures of HCl in argon, krypton, or xenon (20, 21). The rare gas densities used were between two and five amagats. An induced Q branch has also been observed for HCl in liquid xenon (7).

In general, induced spectra arise because of distortions of the molecular structure by the surroundings. When the symmetry of the environment is low enough, these interactions result in a net system dipole moment which may depend on the rotational and vibrational coordinates of the molecule in question and give rise to Raman type ($\Delta J = 0, \pm 2$) selection rules.

Another mechanism to change the rotational selection rules becomes important if the interaction energy depends on the rotational coordinates and consequently mixes the zero-order rotational levels. It should be noted that the translation-rotation interaction discussed above cannot induce a Q branch by this mechanism because the $J = 0$ and $J = 1$ zero-order levels belong to different symmetry species (see Fig. 13). For HCl in the solid rare gases, several possibilities exist which may induce a Q branch and they will be examined in turn.

If the intermolecular separations are sufficiently small, exchange interactions can produce induced spectra. Following

Van Kranendonk and Bird (22), the system dipole moment of HCl in the solid rare gases may be expanded in terms of the vibrational coordinate of HCl

$$\underline{\mu} = \underline{\mu}_0 + \underline{\mu}'r + \dots \quad (9)$$

where

$$\underline{\mu}' = \left(\frac{\partial \underline{\mu}}{\partial r} \right)_0 \quad (10)$$

is a function of the nearest neighbor distance, R , of the lattice and the rotational coordinates, θ and ϕ , of HCl. The first term of equation 9 gives rise to pure rotational transitions; the second term is responsible for vibration-rotation transitions.

We expand $\underline{\mu}'$ in terms of spherical harmonics

$$\underline{\mu}' = \sum_{\ell, m} \underline{D}_{\ell m}(R) Y_{\ell}^m(\theta, \phi) \quad (11)$$

Because of the octahedral symmetry of the substitutional site, equation 11 becomes

$$\underline{\mu}'_Z = [D_{00} + D_{10} P_1^0(\cos \theta) + D_{20} P_2^0(\cos \theta) + \dots] \quad (12)$$

If either the first or second term of equation 12 is nonzero, $\Delta J = 0$, $\Delta M = 0$ selection rules result and a Q branch should be observed. This effect may be important for HCl in argon, but because of the size of the lattice constants of krypton and xenon, exchange interactions

are not expected to be very important for HCl at substitutional sites in these rare gases.

Another mechanism for producing changes in the rotational selection rules involves the dipole moment induced in the nearest neighbor rare gas atoms by the permanent dipole and quadrupole moments of HCl; such an induced dipole moment is given by

$$\underline{\mu}^i = \alpha \sum_N \underline{E}_N \quad (13)$$

where α is the polarizability of the rare gas and the summation is over the N nearest neighbor rare gas atoms. Including dipole and quadrupole terms in the electric field \underline{E}_N , equation 13 becomes

$$\underline{\mu}^i = \alpha \sum_N \left[\frac{-\underline{\mu}}{R^3} + \frac{3(\underline{\mu} \cdot \underline{R}_N)\underline{R}_N}{R^5} - \frac{3Q \underline{R}_N}{2 R^5} \right. \\ \left. \frac{-3Q(\underline{\mu} \cdot \underline{R}_N)\underline{\mu}}{\mu^2 R^5} + \frac{15Q(\underline{\mu} \cdot \underline{R}_N)^2 \underline{R}_N}{2\mu^2 R^7} \right] \quad (14)$$

where \underline{R}_N is the position of the N th nearest neighbor rare gas atom with respect to the substitutional site occupied by HCl (see Fig. 26), μ is the permanent dipole moment, and Q is the permanent quadrupole moment of HCl. To evaluate equation 14, it is convenient first to carry out the summation over the nearest neighbor atoms and then to expand the resulting expression in terms of the vibrational coordinate of HCl. When equation 14 is evaluated for the face-centered cubic (FCC) lattice, $\underline{\mu}^i$ is found to be zero; this of course is a direct consequence of the high symmetry of such a lattice.

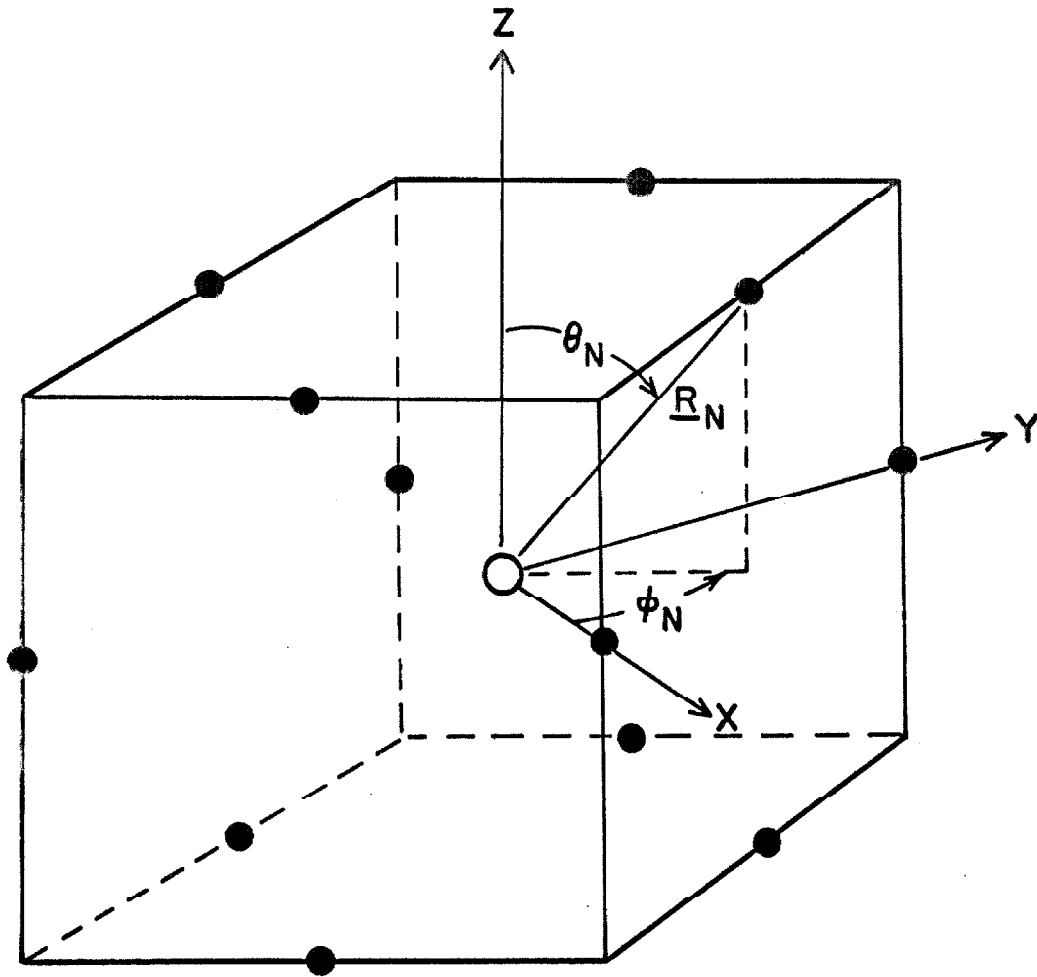


Fig. 26a. Face-centered cubic lattice.



Substitutional site



Nearest neighbor site

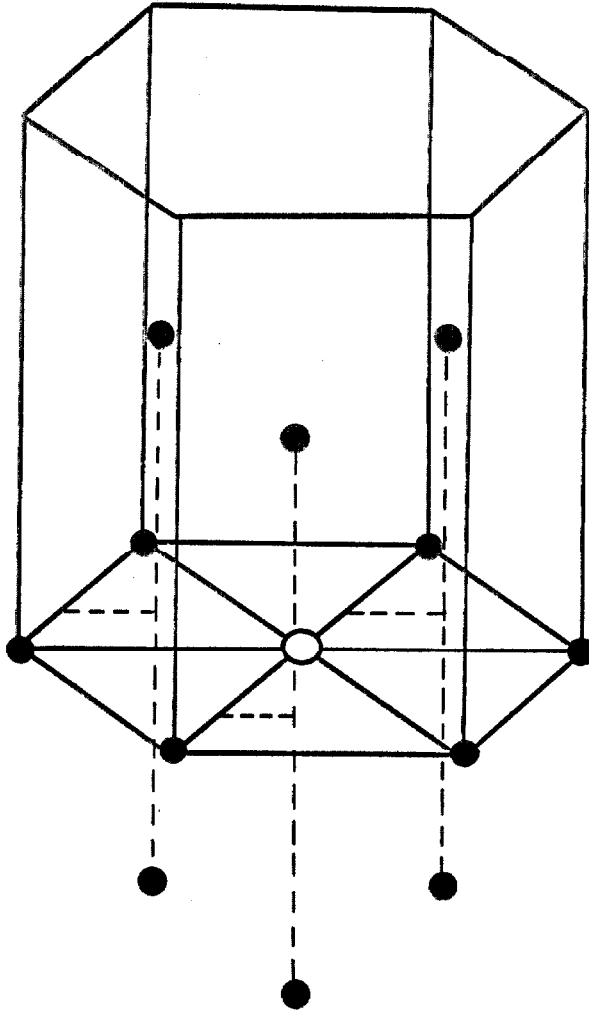


Fig. 26b. Hexagonal close-packed lattice.

- Substitutional site
- Nearest neighbor site

The possibility that HCl impurities will stabilize hexagonal close packed (HCP) structures in solid argon, krypton, and xenon, has been noted above (11). If equation 14 is evaluated for an HCP structure, $\underline{\mu}^i$ is found to be nonzero; the components are given by

$$\mu_X^i = 3.74(\alpha Q/R^4) \sin^2 \theta \cos 2\phi \quad (15a)$$

$$\mu_Y^i = -7.48(\alpha Q/R^4) \sin^2 \theta \sin \phi \cos \phi \quad (15b)$$

$$\mu_Z^i = 0.0$$

where θ and ϕ are again the rotational coordinates of HCl. Since only the quadrupole moment Q is a function of the vibrational coordinate of HCl, the expansion in terms of this coordinate is easily carried out. The angular dependent factors in equation 15 determine the rotational selection rules which are

$$\Delta J = 0, \pm 2; \quad \Delta M = \pm 2. \quad (16)$$

Thus Q, S, and O branches are allowed.

At the low temperatures of these experiments (near 10°K) most of the intensity of any induced Q branch would be due to the transition from the $J'' = 0$ level of the ground vibrational state to the $J' = 0$ level of the first excited vibrational state; such a transition requires $\Delta J = 0, \Delta M = 0$ selection rules. Because of the M selection rule in equation 16 no Q branch transition originating from the $J'' = 0$ level is made allowed by the induced dipole of equation 15.

A Q branch can be induced by another mechanism if the interaction energy of HCl with its surroundings depends on the rotational coordinates in the appropriate manner. The interaction of the HCl dipole with dipoles induced in the nearest neighbor rare gas atoms by the permanent dipole and quadrupole moments of HCl is given by

$$W = -\alpha \sum_N \left[\frac{\mu^2}{R^6} + \frac{3(\underline{\mu} \cdot \underline{R}_N)^2}{R^8} + \frac{6Q(\underline{\mu} \cdot \underline{R}_N)^3}{\mu^2 R^{10}} \right]. \quad (17)$$

In the FCC lattice, equation 17 reduces to

$$W = -24 \alpha \mu^2 / R^6. \quad (18)$$

In this case the interaction energy is independent of the orientation of HCl and cannot produce changes in the rotational selection rules.

Examining equation 17 more closely, we see that the first term is independent of the rotational coordinates and cannot give rise to induced spectra. The second term depends on the rotational coordinates to the second power; for example, one term which results when $(\underline{\mu} \cdot \underline{R}_N)^2$ is expanded is

$$\mu_X^2 \sin^2 \theta_N \cos^2 \phi_N = (\mu^2 \sin^2 \theta_N \cos^2 \phi_N) \sin^2 \theta \cos^2 \phi. \quad (19)$$

The second term thus causes the Jth rotational level to interact only with the $J \pm 2$ levels and cannot lead to Q, S, or O branches. The third term of equation 17 contains the rotational coordinates to the third power; it causes interaction between the Jth level and the $J \pm 1$ and the $J \pm 3$ levels. This term can give rise to Q, S, and O branches.

In the HCP lattice the third term of equation 17 becomes

$$W_3 = -(3 \alpha Q \mu / R^7) \sin^3 \theta \cos 3\phi . \quad (20)$$

This causes the ($J = 0, M = 0$) level to interact only with the ($J = 3, M = 3$) level and as a result cannot give rise to a Q branch transition from the $J'' = 0$ rotational level.

To summarize the discussion so far it may be said that exchange interactions can give rise to a Q branch even at a substitutional site in a FCC lattice; but they are not expected to be important because of the size of the substitutional sites especially in krypton and xenon. The net dipole moment induced in the nearest neighbors by the dipole and quadrupole moments of HCl is zero in a FCC lattice. In the HCP lattice the net induced dipole moment is nonzero but the selection rules do not allow a Q branch transition from the $J'' = 0$ rotational level. In this case a transition from the $J'' = 0$ to the $J' = 2$ rotational level is allowed. The interaction energy of the HCl dipole with dipoles induced in the surrounding rare gas atoms does not depend on the orientation of the HCl in a FCC lattice (see equation 18); thus no induced spectra can arise. In the HCP lattice the interaction energy contains a term which depends on the third power of the rotational coordinates; however, it causes the $J = 0$ level to interact only with the $J = 3$ level and thus cannot lead to a Q branch transition from the $J'' = 0$ level.

No Q branch can be induced in a FCC lattice by dipole and quadrupole interactions because of the high symmetry at the

substitutional site. The symmetry may be reduced sufficiently to induce a Q branch even in an FCC lattice if the molecule is displaced a small distance from the center of the site; to simplify the discussion we will take the displacement along the X axis (see Fig. 26a). Since we are primarily interested in transitions from the $J'' = 0$ rotational level, only those terms which give rise to $\Delta J = 0$, $\Delta M = 0$ selection rules will be considered. Expanding equation 14 we find that the only nonzero terms with these selection rules are

$$\mu_X^i = \frac{15}{2} \alpha Q \cos^2 \theta \sum_N \frac{\sin \theta_N \cos^2 \theta_N \cos \phi_N}{R_N^4} ; \quad (21a)$$

$$\mu_Y^i = \frac{15}{2} \alpha Q \cos^2 \theta \sum_N \frac{\sin \theta_N \cos^2 \theta_N \sin \phi_N}{R_N^4} ; \quad (21b)$$

where R_N , θ_N , and ϕ_N are the spherical polar coordinates of the Nth nearest neighbor rare gas atom and θ is the angular orientation of the HCl molecule with respect to some space fixed Z axis. The distance R_N must be included in the summation because it is now slightly different for each nearest neighbor. For a displacement of the central molecule a distance D along the X axis, the summations in equation 21 may be evaluated. This results in

$$\mu_X^i = 15.91 \frac{\alpha Q D}{R^5} \cos^2 \theta \quad (22a)$$

$$\mu_Y^i = -\mu_X^i \quad (22b)$$

The intensity of the induced infrared transition is proportional to

$$\begin{aligned} \left(\frac{d\mu^i}{dr}\right)^2 &= \left(\frac{d\mu_X^i}{dr}\right)^2 + \left(\frac{d\mu_Y^i}{dr}\right)^2 \\ &= 506 \left(\frac{\alpha D}{R^5}\right)^2 \left(\frac{dQ}{dr}\right)^2. \end{aligned} \quad (23)$$

For HCl equation 23 becomes

$$\left(\frac{d\mu^i}{dr}\right)^2 = 0.024 D^2 \text{ in argon;} \quad (24a)$$

$$\left(\frac{d\mu^i}{dr}\right)^2 = 0.058 D^2 \text{ in krypton;} \quad (24b)$$

$$\left(\frac{d\mu^i}{dr}\right)^2 = 0.044 D^2 \text{ in xenon.} \quad (24c)$$

The units are debyes² per angstrom²; D is in angstroms. Since D cannot be more than a few tenths of an angstrom (see Table IV), the value of $(d\mu^i/dr)^2$ can be at most about 0.006. This is to be compared to the value of about 0.8 for $(d\mu/dr)^2$ from the gas phase intensity of HCl. Unless there is an increase by a factor of five to ten in the value of (dQ/dr) in the solid, the induced dipole of equation 21 cannot be important in producing the observed Q branch.

Next the interaction potential for the displaced molecule will be considered. Expanding $(\underline{\mu} \cdot \underline{R}_N)^3$ in equation 17, the terms which cause the $J = 0$ level to interact with the $J = 1$ level are given by

$$W = - \frac{18 \alpha Q}{\mu^2} \mu_X \mu_Z^2 \sum_N \frac{\sin \theta_N \cos^2 \theta_N \cos \phi_N}{R_N^7} \quad (25)$$

Evaluating the summation in equation 25 for a displacement D along the X axis, we obtain

$$W = - \frac{76.36 \alpha Q \mu}{R^8} D \sin \theta \cos^2 \theta \cos \phi \quad (26)$$

$$\beta = \frac{76.36 \alpha Q \mu}{R^8} \quad (27)$$

is 64.9 cm⁻¹ per Å for HCl in argon, 57.3 in krypton, and 53.5 in xenon. The perturbed ground state rotational wave function which results because of the interaction expressed in equation 25 is

$$\psi^{(1)} = Y_0^0 - C_1 Y_1^1 C - C_3 Y_3^1 C \quad (28)$$

where

$$C_1 = 0.410 \beta D/2B$$

$$C_3 = 0.146 \beta D/2B .$$

The zero-order rotational wave functions are

$$Y_J^{MS} = N_J^M P_J^M (\cos \theta) \sin M \phi \quad (29a)$$

$$Y_J^{MC} = N_J^M P_J^M (\cos \theta) \cos M \phi . \quad (29b)$$

where

$$N_J^M = \left[\frac{(2J+1)}{2\pi} \cdot \frac{(J - |M|)!}{(J + |M|)!} \right]^{\frac{1}{2}} \quad \text{if } M \neq 0$$

$$N_J^0 = \left[\frac{(2J+1)}{4\pi} \right]^{\frac{1}{2}} \quad \text{if } M = 0.$$

The rotational line strength of the Q(0) transition calculated from the wave function of equation 28 using only terms with $J = 0$ and $J = 1$ is

$$S_0^Q = 4C_1^2/3. \quad (30)$$

For a displacement of 0.15 Å from the center of the substitutional site in krypton, C_1 is 0.169; the Q(0) line strength is then 0.038 compared to 1.0 for the gas phase R(0) line. This accounts for most of the Q branch intensity observed at low concentrations of HCl in krypton, and suggests that the interaction expressed in equation 25 is responsible for the Q branch at these concentrations. Its concentration dependence indicates that part of the Q branch intensity may be induced at crystal imperfections; if the symmetry at an imperfection is low enough, any one or a combination of the mechanisms discussed above may be responsible for the induced transition.

The same mechanisms which induce the Q branch can induce S branch vibration-rotation transitions ($\Delta J = +2$). The S(0) transition should lie on the high frequency side of the R(0) transition; however, the absorption peaks which occur in this region at 2917 cm^{-1} for HCl

in krypton and at 2885 cm^{-1} in xenon cannot be assigned with confidence to S(0) transitions. The frequency of the S(0) transition calculated from the observed frequencies of the Q(0), R(1), and P(1) transitions by means of the relation, $S(0) = Q(0) + R(1) - P(1)$, is 2902 and 2884 cm^{-1} in krypton and xenon respectively. The 15 cm^{-1} difference between the calculated and observed positions of the S(0) transition in krypton is far outside the maximum experimental error of $\pm 4\text{ cm}^{-1}$; furthermore, these high frequency lines do not decrease in intensity when the sample is warmed (see Fig. 10) as would be expected if they were due to S(0) transitions. Thus these high frequency lines cannot be assigned to S(0) transitions. A possible interpretation of the 2917 and 2885 cm^{-1} lines is to assign them to monomeric HCl at interstitial sites in krypton and xenon; however, this assignment is only tentative.

Polymers

The absorption features on the low frequency side of the spectrum appear only at high concentrations of HCl and increase in intensity when the sample is warmed and recooled (see Figs. 8, 9, and 27). They are assigned to dimers and polymers of HCl and DCl. These spectra will be discussed in terms of a model similar to that used by Hornig and Hiebert (23) to interpret the infrared spectra of crystalline HCl and HCl-DCl mixtures. These workers have shown that in its low temperature crystalline phase HCl is arranged in linear zigzag chains and that the only important interactions are between nearest neighbors in the same chain. Using this model we have

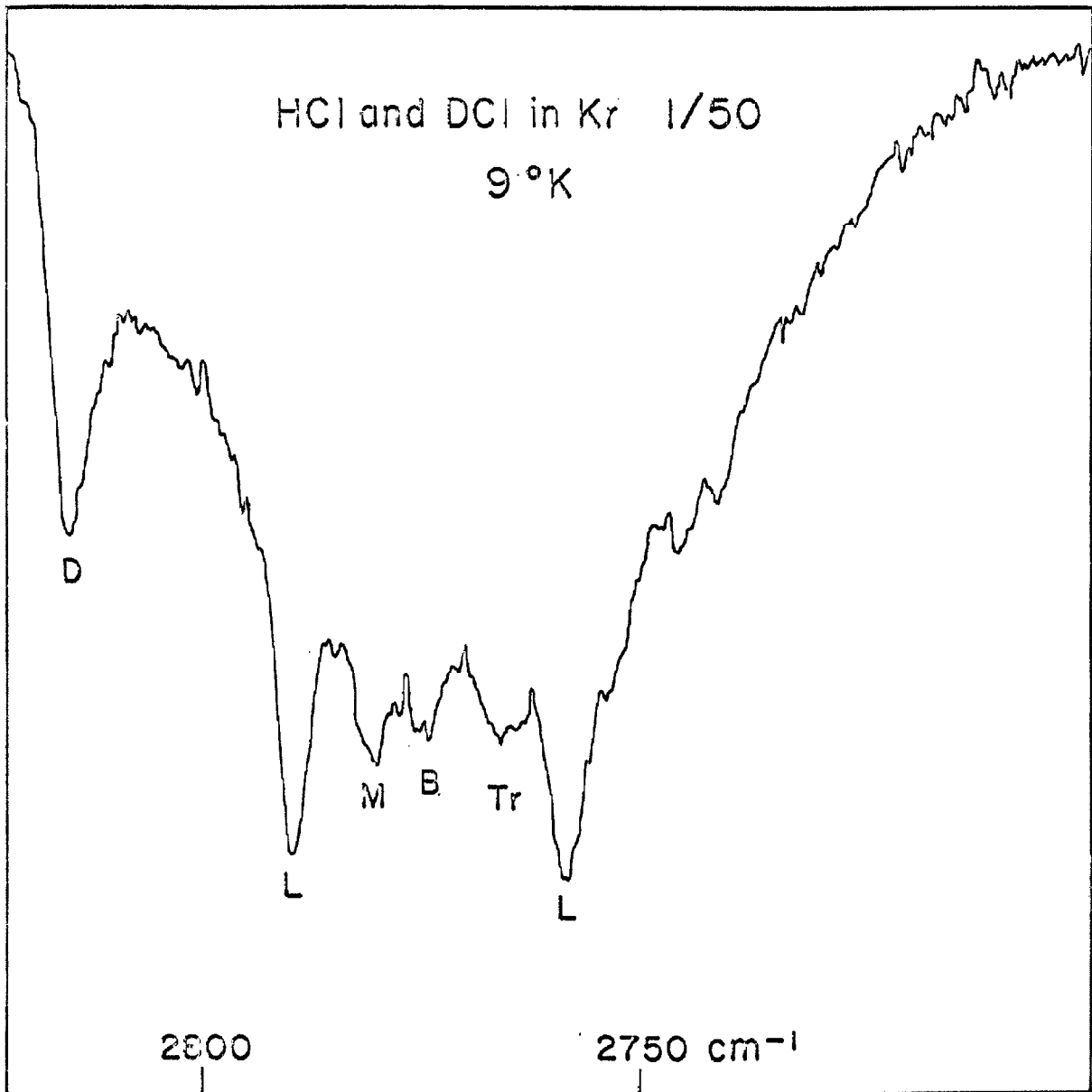


Fig. 27. Polymer absorption of HCl and DCl in krypton after annealing at 44°K. D, L, B, and Tr correspond to the dimer and trimer species listed in Table VII. M identifies the HCl-DCl mixed trimer.

calculated the normal frequencies and relative intensities for various dimeric and trimeric chains possible in a face centered cubic lattice. These are shown in Table VII.

The line at 2815 cm^{-1} for HCl in krypton appears at lower concentrations than the other polymer lines and it decreases in intensity as the lower frequency polymer lines grow. This line and the weak absorption at 2795 cm^{-1} are assigned to nearest neighbor dimers of HCl. The separation of these lines gives a value for the interaction force constant of ± 0.0324 millidynes per Å, which agrees with the value ± 0.035 obtained by Hornig and Hiebert. The relative intensity of the lines indicates that the molecules are nearly aligned in the dimer. A broad unresolved absorption appears in the region between these two lines when DCl is present in the sample. This is evidently due to the HCl-DCl mixed dimer (see Table VII).

In order to calculate the absorption frequencies of the trimer species, we have assigned the central line at 2774.5 cm^{-1} to the zero-order frequency λ_T of trimeric HCl in krypton; the line at 2009.5 cm^{-1} has been similarly assigned to trimeric DCl. From Table VII it will be noted that only the "bent" trimeric species has an active mode at the unshifted, zero-order frequency. If the positive value of the interaction force constant is used, it is possible to make the assignments shown in Table VIII.

Whenever DCl is present in the sample, only one additional line is observed at 2780.2 cm^{-1} in the HCl region of the spectrum (see Fig. 27). Examination of Table VII reveals that this is just what one

Table VII. Polymer frequencies and intensities.



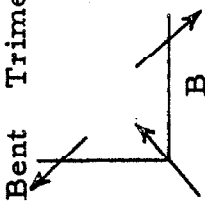
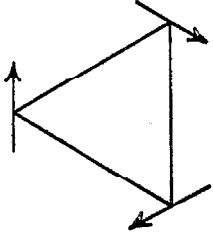

Polymer type	Molecules	Normal frequencies ^a	Relative intensities
Dimer D 	HCl-HCl	$\lambda_1 = \lambda_D + \lambda'$ $\lambda_2 = \lambda_D - \lambda'$	$2 \cos 2\theta$ $2 \sin 2\theta$
	HCl-DCI	$\lambda_1 = \lambda_D$ $\lambda_2 = \lambda_D/\rho$	1 $1/\rho$
Linear Trimer 	HCl-HCl-HCl	$\lambda_1 = \lambda_T$ $\lambda_2 = \lambda_T + 2\frac{1}{2}\lambda'$ $\lambda_3 = \lambda_T - 2\frac{1}{2}\lambda'$	0 $(5.83 \cos 2\theta + 0.17 \sin 2\theta)/2$ $(0.17 \cos 2\theta + 5.83 \sin 2\theta)/2$
	HCl-HCl-DCI	$\lambda_1 = \lambda_T + \lambda'$ $\lambda_2 = \lambda_T - \lambda'$ $\lambda_3 = \lambda_T/\rho$	$2 \cos 2\theta$ $2 \sin 2\theta$ $1/\rho$
	HCl-DCI-HCl	$\lambda_1 = \lambda_T$ $\lambda_2 = \lambda_T$ $\lambda_3 = \lambda_T/\rho$	1 1 $1/\rho$

Table VII (continued)

Polymer type	Molecules	Normal frequencies ^a	Relative intensities
Bent Trimer 	HCl-HCl-HCl	$\lambda_1 = \lambda_T$	2
		$\lambda_2 = \lambda_T + 2\frac{1}{2}\lambda'$	1/2
		$\lambda_3 = \lambda_T - 2\frac{1}{2}\lambda'$	1/2
Triangular Trimer 	HCl-HCl-HCl	$\lambda_1 = \lambda_T - \lambda'$	3/2
		$\lambda_2 = \lambda_T - \lambda'$	3/2
		$\lambda_3 = \lambda_T + 2\lambda'$	0
Tr 	HCl-HCl-DCI	$\lambda_1 = \lambda_T + \lambda'$	1/2
		$\lambda_2 = \lambda_T - \lambda'$	3/2
		$\lambda_3 = \lambda_T/\rho$	1/p

^a Frequency $\nu = \lambda^2/2\pi$, λ_D and λ_T are zero order HCl dimer and trimer frequencies respectively; λ' is interaction constant; ρ is ratio of DCI reduced mass to that of HCl, $\rho = 1.944$. For mixed HCl-DCI trimers, normal frequencies of B are same as those of L.

Table VIII. Trimer frequencies.

HCl in krypton		DCI in krypton		Assignment
ν_{obs} (cm^{-1})	ν_{calc} (cm^{-1})	ν_{obs} (cm^{-1})	ν_{calc} (cm^{-1})	
2788.8	2789	2020.4	2020	$(\lambda_{\text{T}} + 2\frac{1}{2}\lambda')$ L
2780.2 ^a	2784	2017	2017	$(\lambda_{\text{T}} + \lambda')$ M
2774.5	b	2009.5	b	λ_{T} B
2764	2764	2003	2002	$(\lambda_{\text{T}} - \lambda')$ Tr
2759	2760	1998	1999	$(\lambda_{\text{T}} - 2\frac{1}{2}\lambda')$ L

^aObserved only if DCI is present in sample.

^bThis value used to determine λ_{T} .

would expect from HCl-DCI mixed trimers in which there are two nearest neighbor HCl molecules. Such trimers have normal frequencies at $\lambda_T \pm \lambda'$; the frequency at $\lambda_T - \lambda'$ is the same as the active mode of the "triangular" trimer, but the frequency at $\lambda_T + \lambda'$ is unique to the mixed species.

In the calculation of normal frequencies discussed above and summarized in Tables VII and VIII, equal zero-order frequencies for the HCl molecules of the trimer were assumed. Except for the "triangular" species, this is not strictly true. Due to environmental effects, the central HCl is expected to have a somewhat lower zero-order frequency than the end molecules of the "linear" and "bent" species. It can be shown, however, that essentially the same results as those shown in Tables VII and VIII are obtained if the frequencies of the end and central molecules differ by as much as 4 or 5 cm^{-1} ; the model still predicts only one new line in the HCl frequency region for HCl-DCI mixed trimers.

The HCl low frequency lines have been interpreted as arising from nearest neighbor dimers and three distinct trimeric species. This model correctly predicts the low frequency spectrum of HCl and DCI in krypton and the one new line observed in mixed HCl-DCI samples in krypton.

Finally, when the sample is warmed to 50°K and recooled, two broad (20 cm^{-1}) maxima are observed at 2709 and 2754 cm^{-1} ; only traces remain of the higher frequency dimer and trimer lines. The two broad maxima compare closely to the spectrum of pure crystalline HCl which absorbs at 2706 and 2747 cm^{-1} (23).

APPENDIX I. Derivation of the Hamiltonian operator for the interaction of translational and rotational motions.

The classical kinetic energy of a rigid, translating, rotating molecule is

$$2T = \dot{\underline{R}}^2 \sum_i m_i + \sum_i m_i (\underline{\omega} \times \underline{r}_i) \cdot (\underline{\omega} \times \underline{r}_i) + 2\dot{\underline{R}} \cdot \underline{\omega} \times \sum_i m_i \underline{r}_i \quad (\text{A-1})$$

where \underline{R} is the position of the center of interaction with respect to the space fixed reference system; \underline{r}_i is the position of the i^{th} atom with respect to the center of interaction. The orientations of the angular velocities are shown in Fig. A. For a linear molecule

$$\underline{\omega} = \dot{\underline{\theta}} + \dot{\underline{\phi}} = -\dot{\theta} \sin \phi \underline{e}_{X'} + \dot{\theta} \cos \phi \underline{e}_{Y'} + \dot{\phi} \underline{e}_{Z'} \quad (\text{A-2})$$

$$\underline{r}_i = z_i \cos \theta \underline{e}_{Z'} + z_i \sin \theta \cos \phi \underline{e}_{X'} + z_i \sin \theta \sin \phi \underline{e}_{Y'} \quad (\text{A-3})$$

Evaluating the vector products, equation A-1 becomes

$$2T = \dot{\underline{R}}^2 \sum_i m_i + (\dot{\theta}^2 + \dot{\phi}^2 \sin^2 \theta) \left(\sum_i m_i z_i^2 \right) + 2[\dot{X}(\dot{\theta} \cos \phi \cos \theta - \dot{\phi} \sin \theta \sin \phi) + \dot{Y}(\dot{\phi} \sin \theta \cos \phi + \dot{\theta} \cos \theta \sin \phi) - \dot{Z} \dot{\theta} \sin \theta] \left(\sum_i m_i z_i \right) \quad (\text{A-4})$$

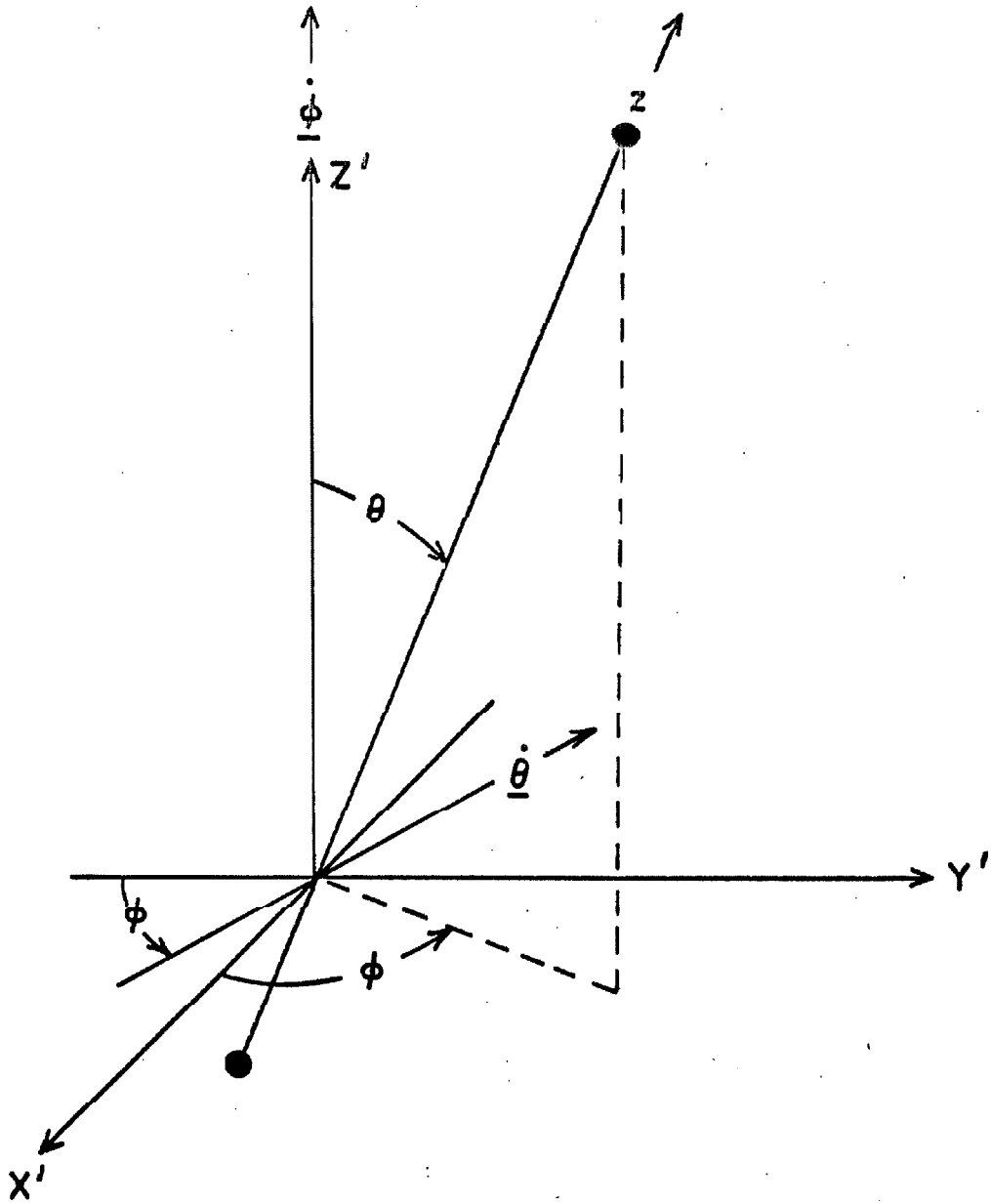


Fig. A. Orientation of the angular velocities.

This can be simplified somewhat by using the relation between the center of mass coordinates and the center of interaction coordinates;

$$z_i = z_i^G + A . \quad (\text{A-5})$$

Then

$$\sum_i m_i z_i = \sum_i m_i (z_i^G + A) = MA ; \quad (\text{A-6})$$

where

$$M = \sum_i m_i$$

$$\sum_i m_i z_i^2 = \sum_i m_i [(z_i^G)^2 + 2z_i^G A + A^2] = I + MA^2 ; \quad (\text{A-7})$$

where $I = \sum_i m_i (z_i^G)^2$ is the moment of inertia with respect to the center of mass.

Substituting (A-6) and (A-7) into (A-4), the classical kinetic energy becomes

$$\begin{aligned} ZT = & MR^2 + (\dot{\theta}^2 + \dot{\phi}^2 \sin^2 \theta) (1 + MA^2) \\ & + 2MA[\dot{X}(\dot{\theta} \cos \theta \cos \phi - \dot{\phi} \sin \theta \sin \phi) \\ & + \dot{Y}(\dot{\theta} \cos \theta \sin \phi + \dot{\phi} \sin \theta \cos \phi) - \dot{Z} \dot{\theta} \sin \theta] . \end{aligned} \quad (\text{A-8})$$

The momenta conjugate to X, Y, Z, θ , and ϕ are found by differentiating T with respect to the respective velocities. The resulting equations are then solved for the velocities in terms of the momenta;

substituting these expressions for the velocities in equation A-8 and retaining terms up to A^2 , results in

$$\begin{aligned}
2T = & \frac{P_X^2}{M} + \frac{P_Y^2}{M} + \frac{P_Z^2}{M} + \frac{P_\theta^2}{I} + \frac{P_\phi^2}{I \sin^2 \theta} \\
& + \frac{2A}{I} \left[\sin \theta P_Z P_\theta - \cos \theta \cos \phi P_X P_\theta + \frac{\sin \phi}{\sin \theta} P_X P_\phi \right. \\
& \left. - \cos \theta \sin \phi P_Y P_\theta - \frac{\cos \phi}{\sin \theta} P_Y P_\phi \right] \\
& + \frac{A^2}{I} [(1 - \sin^2 \theta \cos^2 \phi) P_X^2 + (1 - \sin^2 \theta \sin^2 \phi) P_Y^2 \\
& + \sin^2 \theta P_Z^2 - 2 \sin^2 \theta \sin \phi \cos \phi P_X P_Y \\
& - 2 \sin \theta \cos \theta \cos \phi P_X P_Z - 2 \sin \theta \cos \theta \sin \phi P_Y P_Z]
\end{aligned} \tag{A-9}$$

Since the kinetic energy expressed in equation A-9 is not exclusively in terms of momenta conjugate to Cartesian coordinates, the transformation to the quantum mechanical kinetic energy operator is not straightforward. The general problem of transformation of coordinates will be discussed first and the results then will be applied to the problem at hand.

Consider a classical kinetic energy function written in terms of mass weighted Cartesian coordinates ζ_m

$$2T = \sum_m \dot{\zeta}_m^2 \tag{A-10a}$$

$$2T = \sum_m P_m^2, \quad (\text{A-10b})$$

where P_m is the momentum conjugate to ζ_m . If one now carries out a transformation to a generalized set of coordinates q_1, q_2, \dots

$$\zeta_m = \zeta_m(q_1, q_2, \dots) = \sum_i \left(\frac{\partial \zeta_m}{\partial q_i} \right)_0 q_i + \dots \quad (\text{A-11})$$

If the function $\zeta_m(q_1, q_2, \dots)$ is approximated by terms linear in q_i ,

$$2T = \sum_m \sum_{i,j} \left(\frac{\partial \zeta_m}{\partial q_i} \right)_0 \left(\frac{\partial \zeta_m}{\partial q_j} \right)_0 \dot{q}_i \dot{q}_j \quad (\text{A-12a})$$

$$2T = \sum_{i,j} g_{ij} \dot{q}_i \dot{q}_j \quad (\text{A-12b})$$

where

$$g_{ij} = \sum_m \left(\frac{\partial \zeta_m}{\partial q_i} \right)_0 \left(\frac{\partial \zeta_m}{\partial q_j} \right)_0 \quad (\text{A-13})$$

The kinetic energy may be written in terms of the momenta p_i conjugate to the q_i

$$2T = \sum_{i,j} g^{ij} p_i p_j; \quad (\text{A-14})$$

where g^{ij} is the inverse matrix of g_{ij} .

$$g^{ij} = \sum_m \left(\frac{\partial q_i}{\partial \zeta_m} \right)_0 \left(\frac{\partial q_j}{\partial \zeta_m} \right)_0 . \quad (\text{A-15})$$

The quantum mechanical kinetic energy operator in the original system of Cartesian coordinates is

$$2\hat{T} = -\hbar^2 \sum_m \frac{\partial^2}{\partial \zeta_m^2} . \quad (\text{A-16})$$

Under the transformation to generalized coordinates this becomes

$$2\hat{T} = -\hbar^2 g^{-\frac{1}{2}} \sum_i \frac{\partial}{\partial q_i} \left(g^{\frac{1}{2}} \sum_k g^{ik} \frac{\partial}{\partial q_k} \right) , \quad (\text{A-17})$$

where g is the determinant of the g_{ij} matrix.

The Schrödinger equation in the generalized q coordinate system is

$$\hat{H}\psi = -\frac{\hbar^2}{2} g^{-\frac{1}{2}} \sum_i \frac{\partial}{\partial q_i} \left(g^{\frac{1}{2}} \sum_k g^{ik} \frac{\partial}{\partial q_k} \right) \psi + V\psi = E\psi . \quad (\text{A-18})$$

The normalization integral for ψ in q space is of the form

$$\int |\psi|^* \psi g^{\frac{1}{2}} dq_1 dq_2 \dots dq_N .$$

The factor $g^{\frac{1}{2}}$ is the Jacobian of the original Cartesian coordinates with respect to the q coordinates; $g^{\frac{1}{2}}$ is sometimes called the density factor in q space.

Returning to the translation-rotation problem, the g_{ij} matrix is given by equation A-19. The determinant of (g_{ij}) , out to terms second order in A , is

$$g = \det(g_{ij}) = M^3 I^2 \sin^2 \theta . \quad (\text{A-20})$$

Using this value for g , equation A-18 becomes

$$H\psi = \frac{-\hbar^2}{2 \sin \theta} \sum_i \frac{\partial}{\partial q_i} \left(\sin \theta \sum_k g^{ik} \frac{\partial}{\partial q_k} \right) \psi + V\psi = E\psi \quad (\text{A-21})$$

The g^{ik} quantities can be obtained from equation A-9; substitution of these in equation A-21 results in the Hamiltonian operator given in equation 3.

APPENDIX II. Symmetry properties of the translation-rotation Hamiltonian.

The Hamiltonian of equation 3 is invariant under the symmetry operations of the D_{2h} group if they are carried out simultaneously in the space fixed XYZ and the translating X'Y'Z' coordinate systems (see Fig. 12).

Inversion of the XYZ system transforms X into -X, Y into -Y, and Z into -Z. Inversion of the X'Y'Z' system transforms X' into -X', Y' into -Y', Z' into -Z', θ into $\pi - \theta$, and ϕ into $\pi + \phi$. The transformations of the operators which appear in the Hamiltonian then can be readily obtained:

$$\frac{\partial}{\partial X} \rightarrow -\frac{\partial}{\partial X} ; \frac{\partial}{\partial Y} \rightarrow -\frac{\partial}{\partial Y} ; \frac{\partial}{\partial Z} \rightarrow -\frac{\partial}{\partial Z}$$

$$\frac{\partial}{\partial \theta} \rightarrow -\frac{\partial}{\partial \theta} ; \frac{\partial}{\partial \phi} \rightarrow \frac{\partial}{\partial \phi}$$

$$\sin \theta \rightarrow \sin \theta ; \cos \theta \rightarrow -\cos \theta$$

$$\sin \phi \rightarrow -\sin \phi ; \cos \phi \rightarrow -\cos \phi .$$

Substitution of the transformed operators into the Hamiltonian shows that it is invariant with respect to simultaneous inversion in the XYZ and X'Y'Z' systems.

The same argument may be followed for the other symmetry operations of the D_{2h} group. Reflection in the XY and X'Y' planes transforms

$$\begin{array}{lll}
 X \rightarrow X & X' \rightarrow X' & \theta \rightarrow \pi - \theta \\
 Y \rightarrow Y & Y' \rightarrow Y' & \phi \rightarrow \phi . \\
 Z \rightarrow -Z & Z' \rightarrow -Z' &
 \end{array}$$

Reflection in the XZ and the X'Z' planes transforms

$$\begin{array}{lll}
 X \rightarrow X & X' \rightarrow X' & \theta \rightarrow \theta \\
 Y \rightarrow -Y & Y' \rightarrow -Y' & \phi \rightarrow 2\pi - \phi . \\
 Z \rightarrow Z & Z' \rightarrow Z' &
 \end{array}$$

Reflection in the YZ and the Y'Z' planes transforms

$$\begin{array}{lll}
 X \rightarrow -X & X' \rightarrow -X' & \theta \rightarrow \theta \\
 Y \rightarrow Y & Y' \rightarrow Y' & \phi \rightarrow \pi - \phi . \\
 Z \rightarrow Z & Z' \rightarrow Z' &
 \end{array}$$

REFERENCES

1. H. P. Gush, W. F. J. Hare, E. J. Allin, and H. L. Welsh, *Canad. J. Phys.*, 38, 176 (1960).
2. R. L. Redington and D. E. Milligan, *J. Chem. Phys.*, 37, 2162 (1962).
3. A. Cabana, G. B. Savitsky, and D. F. Hornig, *J. Chem. Phys.*, 39, 2942 (1963).
4. D. E. Milligan, R. M. Hexter, and K. Dressler, *J. Chem. Phys.*, 34, 1009 (1961).
5. L. J. Schoen, D. E. Mann, C. Knobler, and D. White, *J. Chem. Phys.*, 37, 1146 (1962).
D. E. Mann, L. J. Schoen, C. Knobler, and D. White, *Proceedings International Symposium on Molecular Structure and Spectroscopy, Tokyo, 1962*, p. A209.
6. G. W. Robinson and M. McCarty, Jr., *J. Chem. Phys.*, 30, 999 (1959).
7. J. Kwok and G. W. Robinson, *J. Chem. Phys.*, 36, 3137 (1962).
8. R. E. Behringer, *J. Chem. Phys.*, 29, 537 (1958).
9. D. H. Rank, D. P. Eastman, B. S. Rao, and T. A. Wiggins, *J. Opt. Soc. Am.*, 52, 1 (1962).
10. W. H. Flygare, *J. Chem. Phys.*, 39, 2263 (1963).
11. An hexagonal form of argon is known to be stabilized by impurities such as N_2 , O_2 , or CO (12); it is possible that HCl impurities will also stabilize an hexagonal close-packed (HCP) structure in solid argon, krypton, and xenon. Since the symmetry (D_{3h}) of a substitutional site in an HCP crystal is much lower than the octahedral (O_h) symmetry of such a site in face-centered cubic crystals, lower order terms will contribute to the potential energy expansion in spherical harmonics and the rotational perturbations could be considerably different. As will be seen in the discussion below, however, a serious difficulty with the hindered rotator model arises because, contrary to what is observed, it predicts that the DCl rotational levels should be perturbed more than those of HCl. Because this difficulty is also expected to appear for a D_{3h} potential field, the problem of hindered rotation in an HCP crystal will not be considered further in this discussion.

12. C. S. Barrett and L. Meyer, *J. Chem. Phys.*, 41, 1078 (1964).
13. A. F. Devonshire, *Proc. Roy. Soc. (London)*, A153, 601 (1936).
14. R. M. Hexter and D. A. Dows, *J. Chem. Phys.*, 25, 504 (1956);
R. M. Hexter, *J. Mol. Spect.*, 3, 67 (1959).
15. G. Ewing, *J. Chem. Phys.*, 37, 2250 (1962).
16. H. Friedmann and S. Kimel, *J. Chem. Phys.*, 41, 2552 (1964).
17. E. B. Wilson, Jr., J. C. Decius, and P. C. Cross, *Molecular Vibrations* (McGraw-Hill Book Company, Inc., New York, 1955),
p. 274.
18. A. Babloyantz, *Mol. Phys.*, 2, 39 (1959).
19. H. Friedmann, *Adv. Chem. Phys.*, 4, 225 (1962).
20. D. H. Rank, B. S. Rao, and T. A. Wiggins, *J. Chem. Phys.*,
37, 2511 (1962).
21. R. D. Sharma and G. C. Turrell, *J. Chem. Phys.*, 39, 2638
(1963).
22. J. Van Kranendonk and R. B. Bird, *Physica*, 17, 953 (1951).
23. D. F. Hornig and G. L. Hiebert, *J. Chem. Phys.*, 27, 752
(1957).

PART II

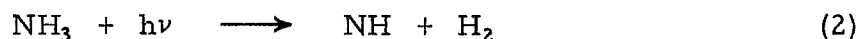
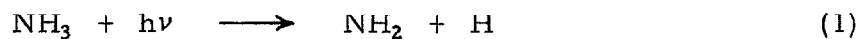
INFRARED SPECTRA OF NH_2 AND ND_2 PRODUCED BY
PHOTOLYSIS AND X-RADIOLYSIS OF AMMONIA IN SOLID KRYPTON

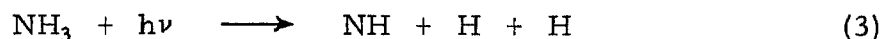
INTRODUCTION

Recently much work has been done on the electronic absorption spectrum of the amidogen (NH_2) radical in the gas phase (1) and trapped in rare gas matrices (2). Dressler and Ramsay have determined the geometry of the radical and two of its vibrational frequencies in the excited electronic state. The vibrational frequencies of the ground state of NH_2 , however, have not been definitely established. The stretching frequencies have only been tentatively assigned and the bending frequency has never been observed. A knowledge of the ground vibrational frequencies would be a valuable aid in unravelling the complicated emission spectrum of NH_2 which often appears in cometary spectra.

Studies of the photolysis of gaseous ammonia and of ammonia in solid argon indicated that NH_2 and NH could be formed and trapped in one of the rare gases. Some control over which radical is produced may be had by varying the wavelength of the photolyzing radiation. Since the electronic absorption spectra of NH_2 and NH are well known, they may be used to determine the presence of the radicals and to give a rough measure of their concentrations. In this way the infrared spectra may be correlated with the radicals known to be present in the sample.

Recent studies of the gas phase photolysis of ammonia (3, 4) have established that the important primary steps are





By using ethylene as a scavenger for hydrogen atoms, it was shown (3) that under 1849 Å radiation, reaction 1 accounts for 96% of the primary dissociation; under 1236 Å radiation about 14% of the primary process goes by reaction 2, 86% by reaction 1 plus 3.

Photolysis of 0.3 mole percent mixtures of ammonia in solid argon also produces NH_2 and NH (5); the radicals were identified in the solid by their electronic absorption spectra. Photolysis with the 1849 Å mercury line produces NH_2 but no NH . This result is in agreement with the gas phase work. Both NH and NH_2 are formed upon irradiation with wavelengths shorter than 1550 Å.

The electronic absorption spectrum of gaseous NH_2 has been analyzed by Dressler and Ramsay (1) in the wavelength range, 3900–8300 Å. They find that the ground state ($^2\text{B}_1$) of NH_2 is bent with a bond angle of $103^\circ 23'$. Two of the vibrational frequencies of the linear upper state ($^2\text{A}_1\Pi_u$) have been found. The symmetric hydrogen stretching mode occurs at 3325 cm^{-1} , while the bending mode occurs at 622 cm^{-1} .

Amidogen has been identified in cometary spectra (6) and as the carrier of the α flame bands of ammonia (7). The emission spectrum is very complex, and a vibrational and rotational analysis has not been accomplished as yet. It has not been possible to obtain the ground state vibrational frequencies of NH_2 from its electronic absorption or emission spectrum.

Tanner and King (8) have observed the infrared spectra of transient species which appear after the flash photolysis of hydrazine in the gas phase. One absorption feature appears at $3.125 \pm 0.01\mu$ ($3200 \pm 10 \text{ cm}^{-1}$); its intensity decreases as that of ammonia at 3.00μ (3330 cm^{-1}) grows. The half life of the species absorbing at 3200 cm^{-1} is approximately one millisecond. Another transient peak at 3.049μ (3280 cm^{-1}) may be present as a broad absorption between the 3.125μ peak and the 3.0μ ammonia peak. The 3200 cm^{-1} absorption frequency is tentatively assigned to the symmetrical stretching mode of NH_2 , the 3280 cm^{-1} peak to the unsymmetrical stretching mode of NH_2 . The lower frequency region of the bending mode was not investigated.

The electronic spectrum of NH in the gas phase has been studied by Dixon (9); his analysis established that the ground state ($^3\Sigma^-$) vibrational frequency of NH lies at 3125.6 cm^{-1} . Recently Milligan and Jacox (10) have directly observed the fundamental vibration frequency of NH at $3133 \pm 2 \text{ cm}^{-1}$ in solid nitrogen and argon.

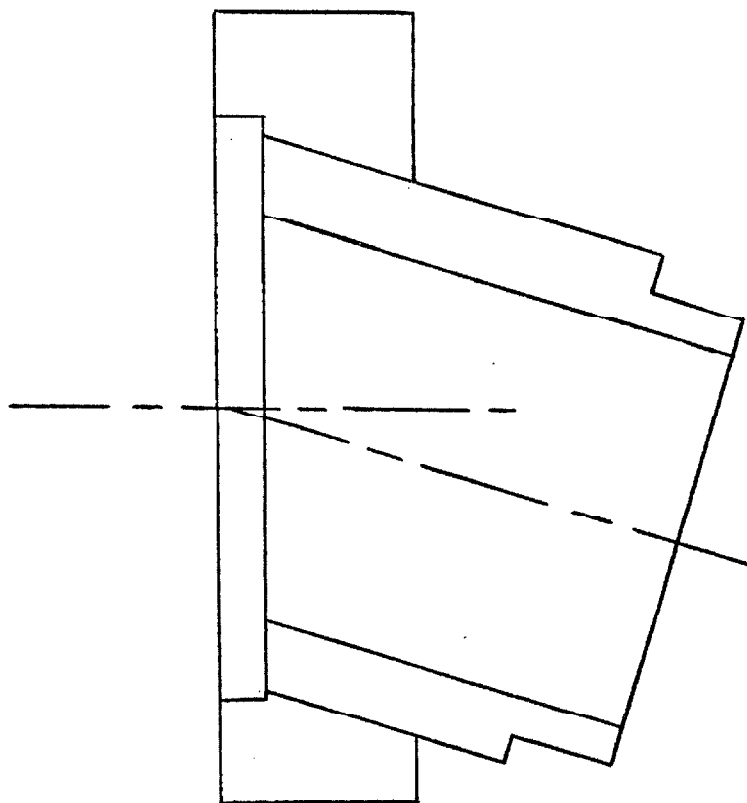
EXPERIMENTAL

These experiments were carried out with the variable temperature infrared cell described in Part I. Barium fluoride windows were used in the middle heat shield and in the housing. The ammonia and krypton were mixed in the gas phase prior to deposition on a helium cooled cesium bromide window. The concentration of ammonia in krypton was approximately 0.5 mole percent; a total of 50 to 100μ moles of ammonia was deposited in each experiment. The temperature

of the cold window during deposition was kept around 10°K. Deposition rates were approximately 1 to 2 cc STP per minute.

One set of photolysis experiments was carried out with a low pressure mercury vapor lamp manufactured by Engelhard Hanovia, Inc. The output of the lamp at 1849 Å was about the same as its output at 2537 Å. It was operated at 650 volts, 10 watts; and because of the long photolysis times (6 hours) required, the lamp was cooled in a stream of dry nitrogen. During photolysis the lamp was set approximately two to three cm from the barium fluoride window of the infrared cell; a stream of dry nitrogen between the lamp and the window minimized atmospheric absorption of the 1849 Å radiation. The temperature of the sample during photolysis was about 7°K.

The photolysis was also carried out by means of X radiation. The X-ray source was a General Electric XRD-5 unit operated at 50 Kev and 45 milliamp. For these experiments the infrared cell was modified by adding a port in the housing between the inlet tube and one of the window openings (see Fig. 2 of Part I). A 1.44 inch diameter by 0.029 inch thick beryllium window with an O-ring seal provided for admission of the X radiation. The brass adapter shown in Figure 1 fit the General Electric X-ray tube outlet and minimized stray radiation. Lead sheeting around the adapter and the base of the infrared cell further reduced stray radiation below background levels at all times. A one inch diameter hole was cut into the middle heat shield so that by properly aligning the heat shielding and the cold window with respect to the X-ray port, the entire sample could be exposed to the X



X-RAY ADAPTER

SCALE: 2/1

FIGURE 1

radiation. The temperature of the cold window during the X-ray photolysis was about 6°K.

The electronic absorption spectra were taken on a 0.5 meter Jarrell-Ash f/6.3 plane grating spectrograph. The plate factor was about 20 Å per mm in the second order. The infrared spectra were recorded on a Beckman IR-7 spectrophotometer. The resolution of this instrument is 1 to 2 cm^{-1} with an accuracy of 0.5 to 1 cm^{-1} . The spectrum was scanned between 800 cm^{-1} (740 cm^{-1} for deuterated ammonia) and 1700 cm^{-1} , and between 2800 cm^{-1} and 3500 cm^{-1} .

The ammonia supplied by Matheson Co. had a stated minimum purity of 99.99%. The krypton was MSC grade from the Linde Co. The deuterated ammonia was supplied by Merck, Sharp, and Dohme; the stated minimum isotopic purity was 98%. The gases were used without further purification.

RESULTS

Infrared Spectrum of Ammonia in Solid Krypton

The infrared spectrum of ammonia in solid krypton is shown in Figures 2, 3, and 4. The frequencies of the absorption maxima in the 3μ region are listed in Table I.

The fine structure observed in the vibrational spectra of ammonia in solid nitrogen and solid argon has been variously interpreted as being due to the rotation of ammonia (11) or to dimeric and polymeric species (12). Both of these interpretations agree, however, in assigning the intense line near 975 cm^{-1} to the monomer $R(0)$ frequency which also appears as the most intense line in our samples. The concentration and temperature were not varied enough in our experiments to decide between these two interpretations for ammonia in krypton; however, one temperature variation experiment was performed and the resulting spectra are shown in Figures 5 and 6.

Photolysis of Ammonia with 1849 \AA Radiation

In this experiment 55μ moles of ammonia at a concentration of 0.5 percent in krypton were deposited on a cesium bromide window cooled to 7°K . The sample was then photolyzed with the low pressure mercury lamp for 5.5 hours. After the photolysis, strong absorption lines due to the ($A\ ^2A_1\Pi_u \leftarrow X\ ^2B_1$) transition of NH_2 were observed in the visible region of the spectrum. The most intense lines appeared at 5161.9 , 5207.4 , 5638.1 , 5696.5 , and 6288.8 \AA in krypton (13);

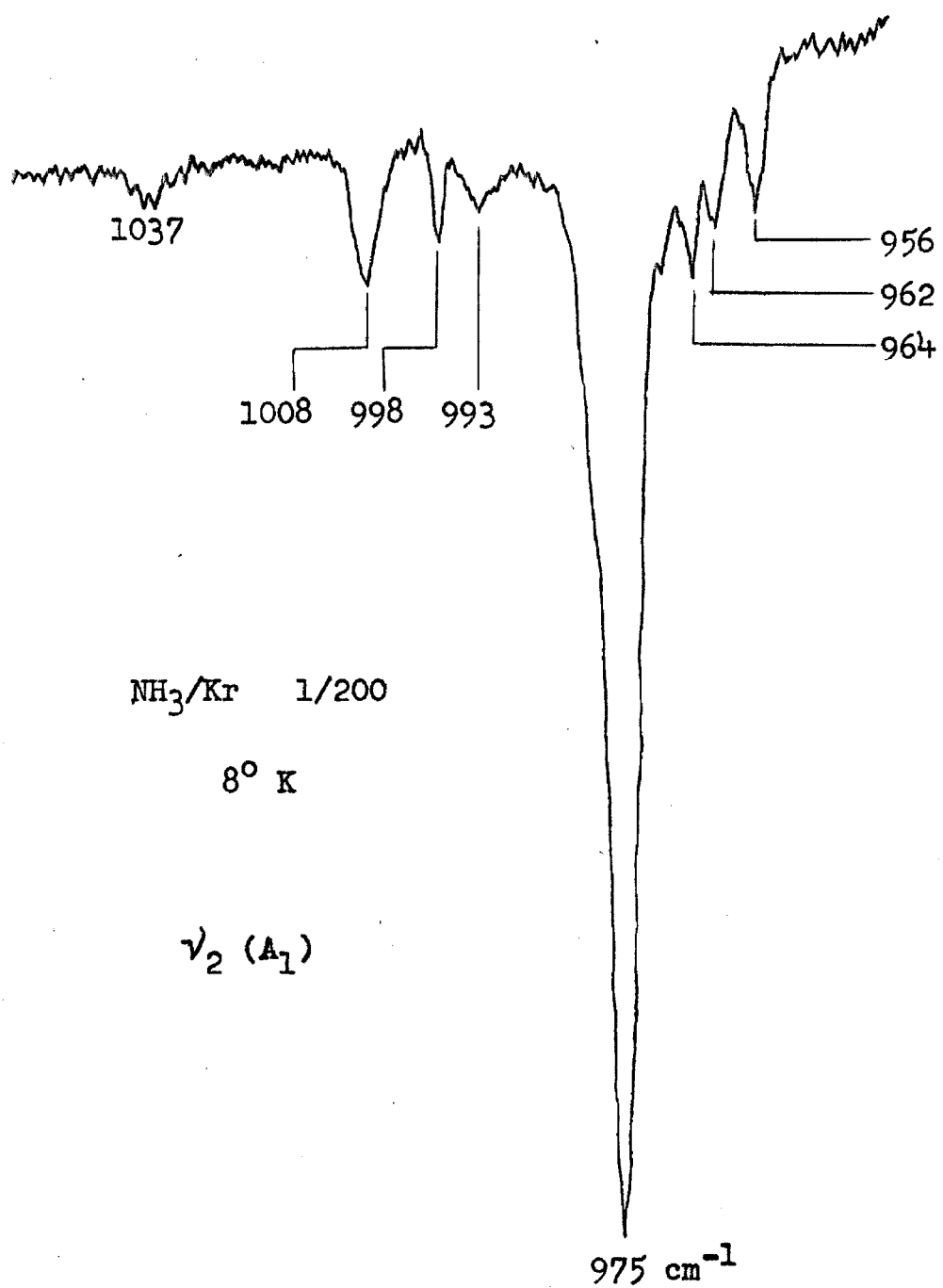


FIGURE 2

NH_3/Kr 1/150 9 °K ν_4 (E)

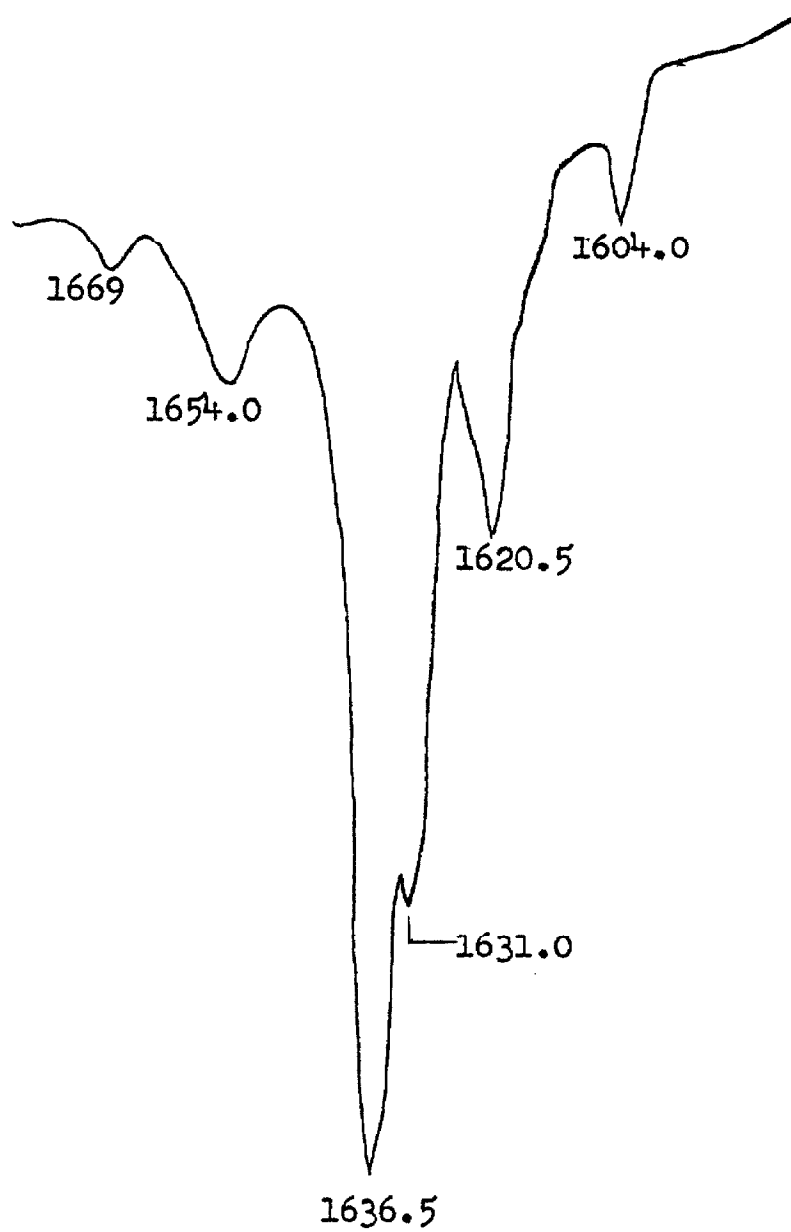


FIGURE 3

NH_3/Kr 1/150 16 °K

3 μ region

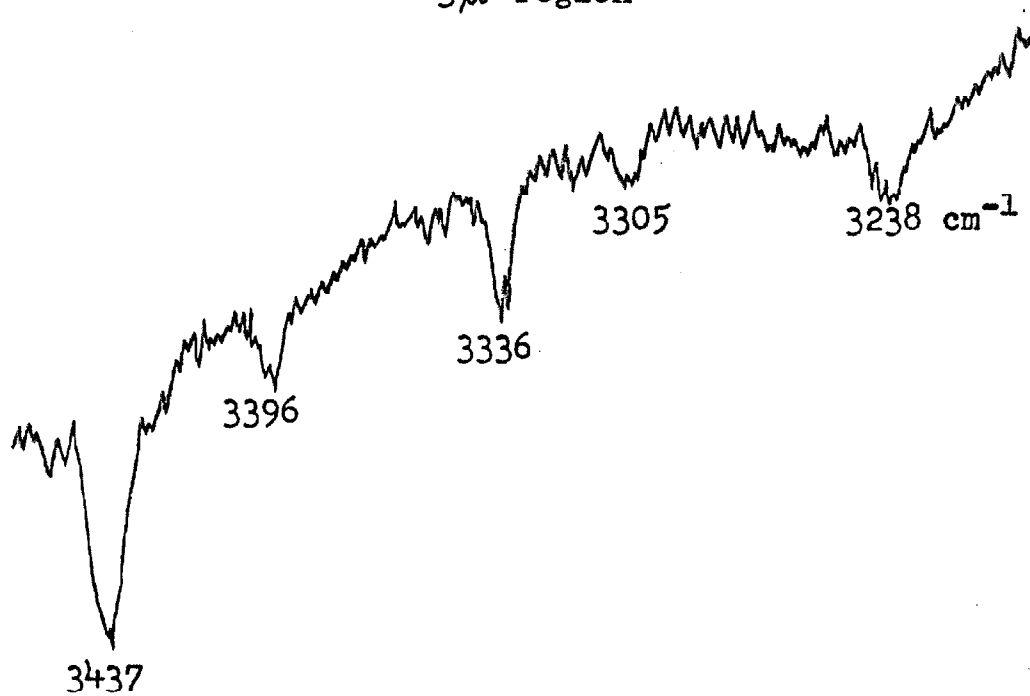


FIGURE 4

Table I. Absorption maxima of ammonia in krypton; 3μ region.

ν_{obs} (cm^{-1}) $\pm 5 \text{ cm}^{-1}$	Relative Intensity	Assignment
3238	3	$2\nu_4$
3305	2	
3336	5	$\nu_1 (A_1)$
3396	2	
3437	10	$\nu_3 (E)$

Figure 5. Ammonia in krypton absorption spectrum near 10μ ; temperature is 14°K . Spectrum of same sample at 8°K is shown in Figure 2.

Figure 6. Absorption of same sample after recooling from 20°K to 9°K . Elapsed time between the spectra shown in Figures 5 and 6 is about 0.75 hours.

NH_3/Kr 1/200 14 °K

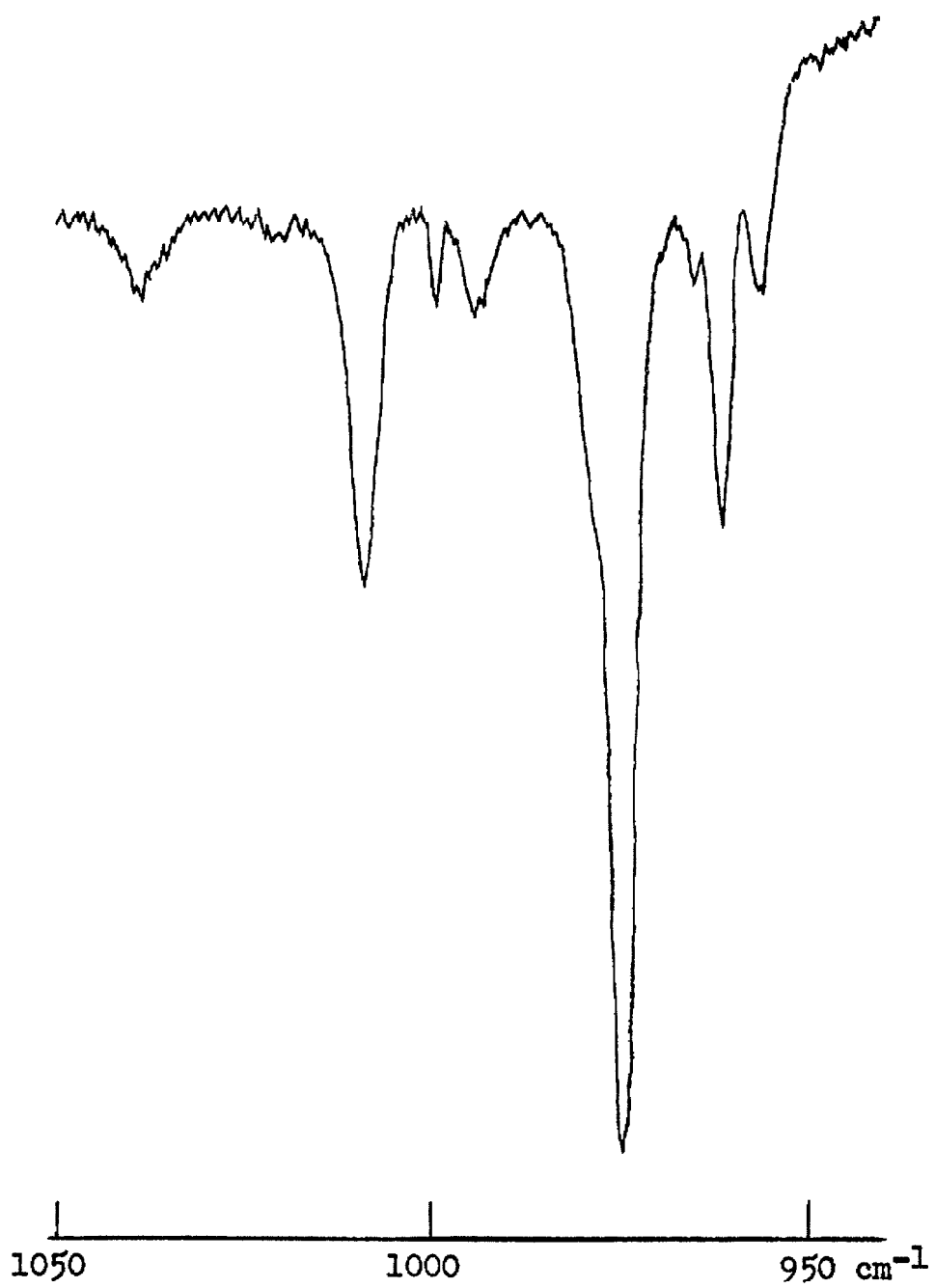


FIGURE 5

NH_3/Kr 1/200 9 °K

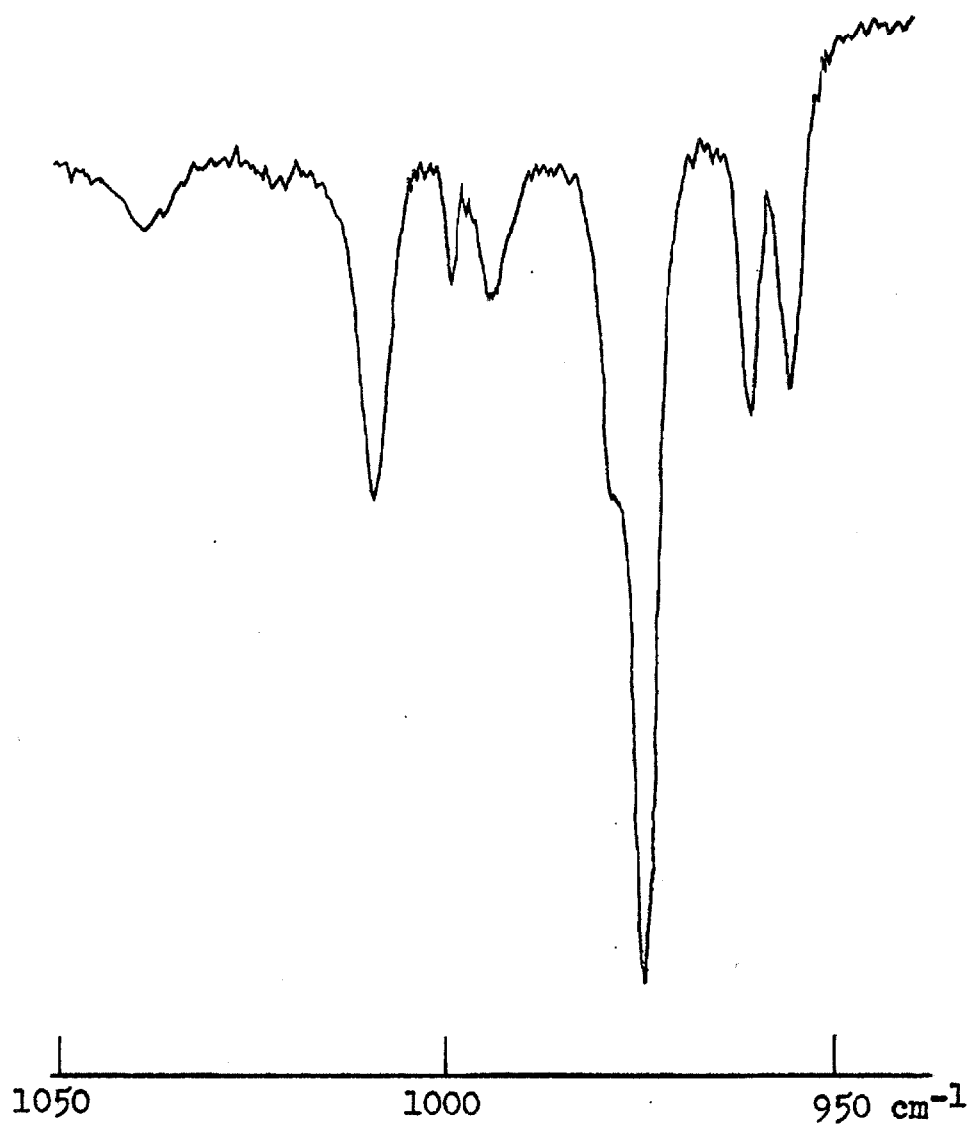


FIGURE 6

many other weaker absorption features also attributable to NH_2 were observed in this spectral region. The visible spectrum demonstrates that NH_2 is present in the photolyzed sample in considerable amounts.

The (0-0) and (1-0) bands of the ($A \ ^3\Pi_1 \leftarrow X \ ^3\Sigma^-$) transition of NH appeared weakly in absorption after photolysis. In krypton these bands occur at 3389 and 3081 Å respectively.

In the infrared, new absorption features appeared at 1289, 1521, and 1613 cm^{-1} . No new spectra were observed between 3000 and 3500 cm^{-1} . The spectral regions in which the 1289 and the 1521 cm^{-1} lines occurred are shown before and after photolysis in Figures 7 and 8.

X-Ray Photolysis of Ammonia

In several experiments, X rays were used as the photolyzing radiation. Approximately 100 μ moles of ammonia at a concentration of 0.7 percent in krypton were deposited on the cold window. After 2.75 hours of X-irradiation at 6°K, the optical spectrum indicated the presence of both NH_2 and NH in considerable amounts. Visual estimates of the relative intensities, made directly from the photographic plates, showed that the amount of NH_2 present after 2.75 hours of X-irradiation was about the same as after 5.5 hours of photolysis with the mercury lamp. The amount of NH present after 2.75 hours of X-irradiation was estimated to be ten times that present after 5.5 hours of photolysis with the mercury lamp. After an additional 2.75 hours of X-irradiation of the same sample, the intensities of NH_2 and NH as

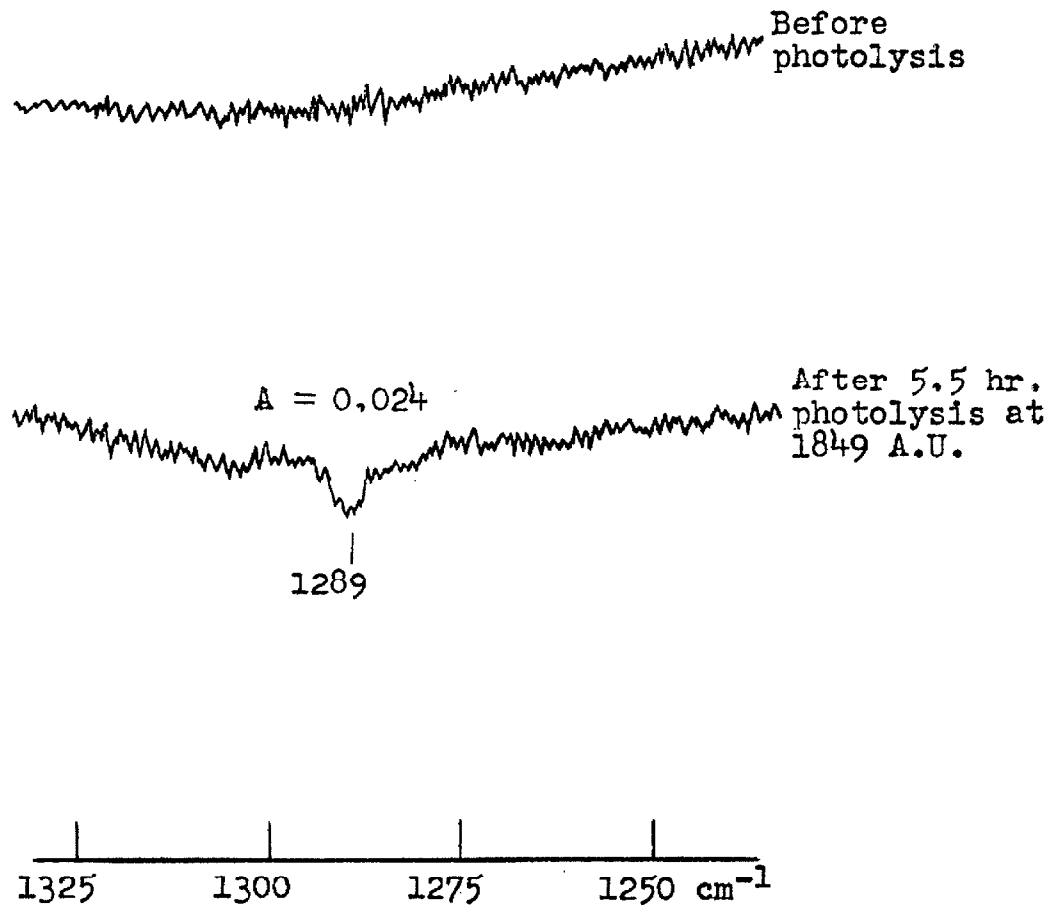
NH_3/Kr 1/200

FIGURE 7

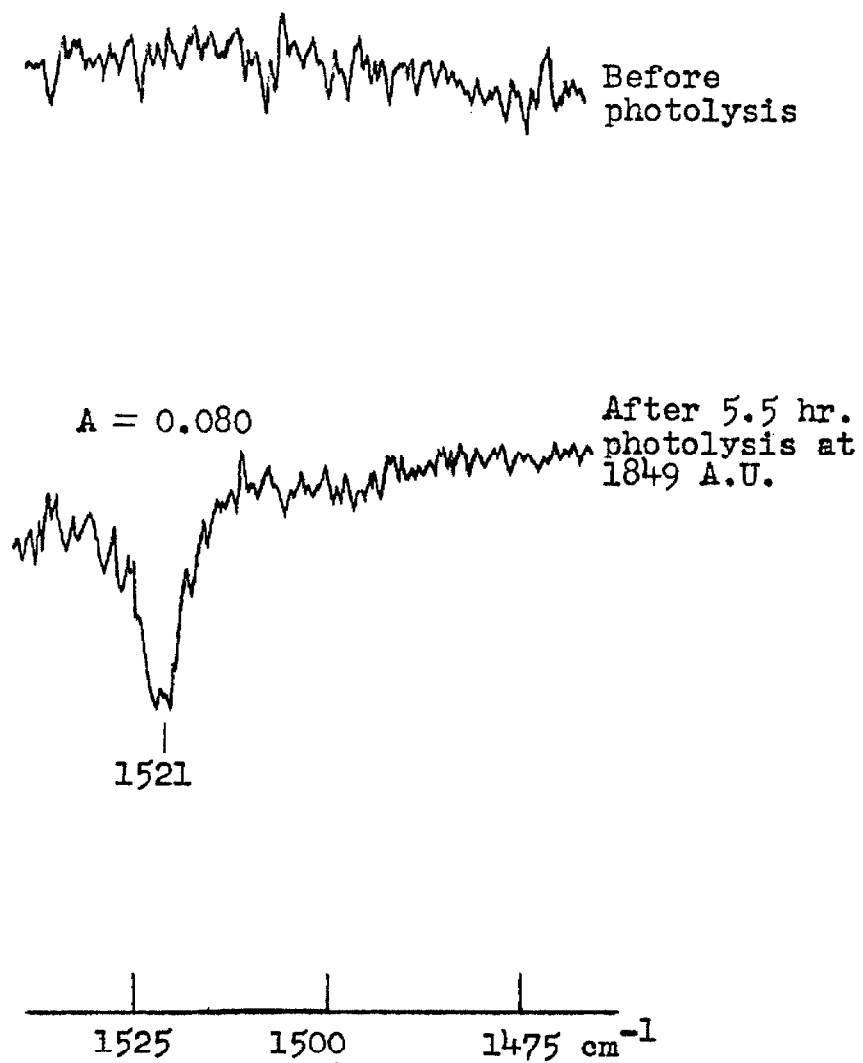
NH_3/Kr 1/200

FIGURE 8

seen in the optical spectrum did not change noticeably.

In the infrared region, new absorption features appeared at 1114, 1280, and 1521 cm^{-1} ; a weak feature also appeared at 1017.5 cm^{-1} as a shoulder on the parental ammonia absorption in this region. Spectra recorded in the regions near 1114, 1280, and 1521 cm^{-1} before and after X-irradiation are shown in Figures 9 and 10.

The decrease in the $\nu_2(\text{E})$ ammonia line at 1636 cm^{-1} and the concurrent growth of the new infrared absorption features upon X-irradiation are shown at the left in Figure 11. The effect of warming and recooling the sample on the intensities of the new absorption features is shown at the right in Figure 11. The optical spectrum taken after the sample had been warmed to 20°K and re-cooled shows no noticeable decrease in the intensity of the NH_2 or NH absorption bands.

Infrared Spectrum of Deuterated Ammonia in Solid Krypton

The infrared spectrum of a sample containing about 100 μ moles of deuterated ammonia at 0.8 percent in krypton are shown in Figures 12, 13, and 14. The observed frequencies in the ν_4 region and their assignments to the isotopic species of ammonia are given in Table II.

X-Ray Photolysis of Deuterated Ammonia

After the sample had been irradiated for 5.5 hours with 50 Kev X rays, the electronic absorption spectrum showed that ND_2 was present in considerable amounts. The most intense absorption lines observed in the visible region are listed in Table III along with their

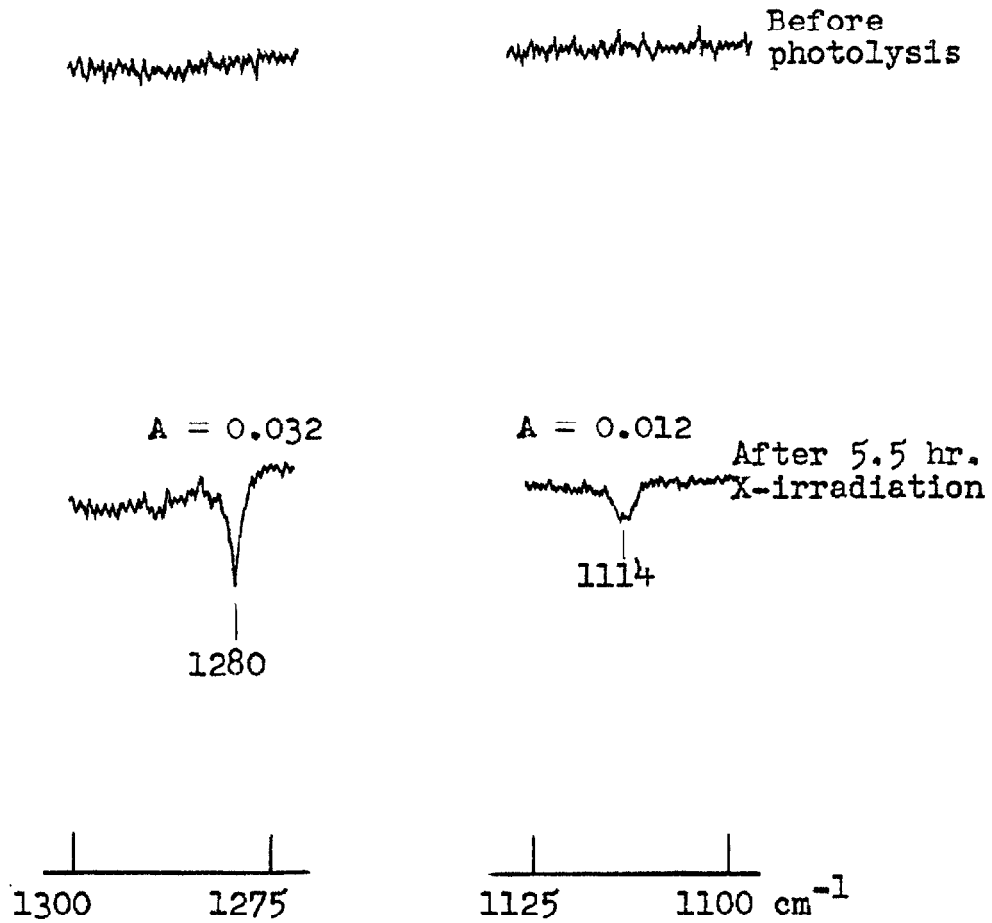
NH_3/Kr 1/150

FIGURE 9

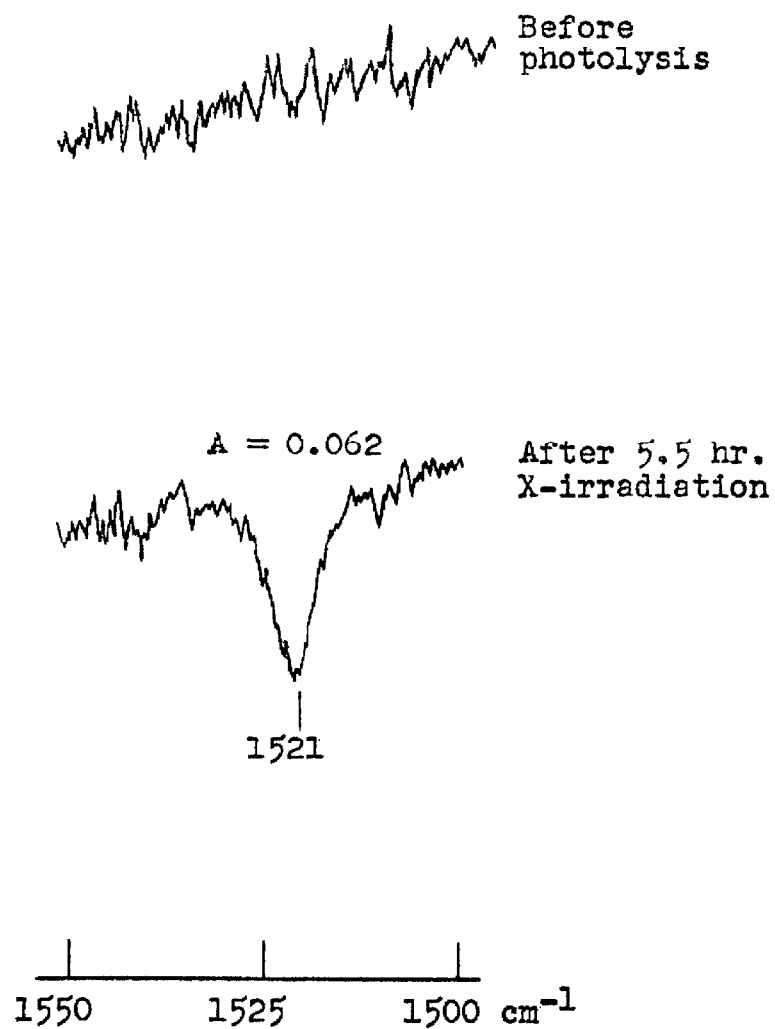
NH_3/Kr 1/150

FIGURE 10

Figure 11. Absorbancy, $A = \log_{10}(I_0/I)$, vs. photolysis time and annealing temperature. Absorbancy of the 1636 cm^{-1} NH_3 line is ten times the value shown in the figure.

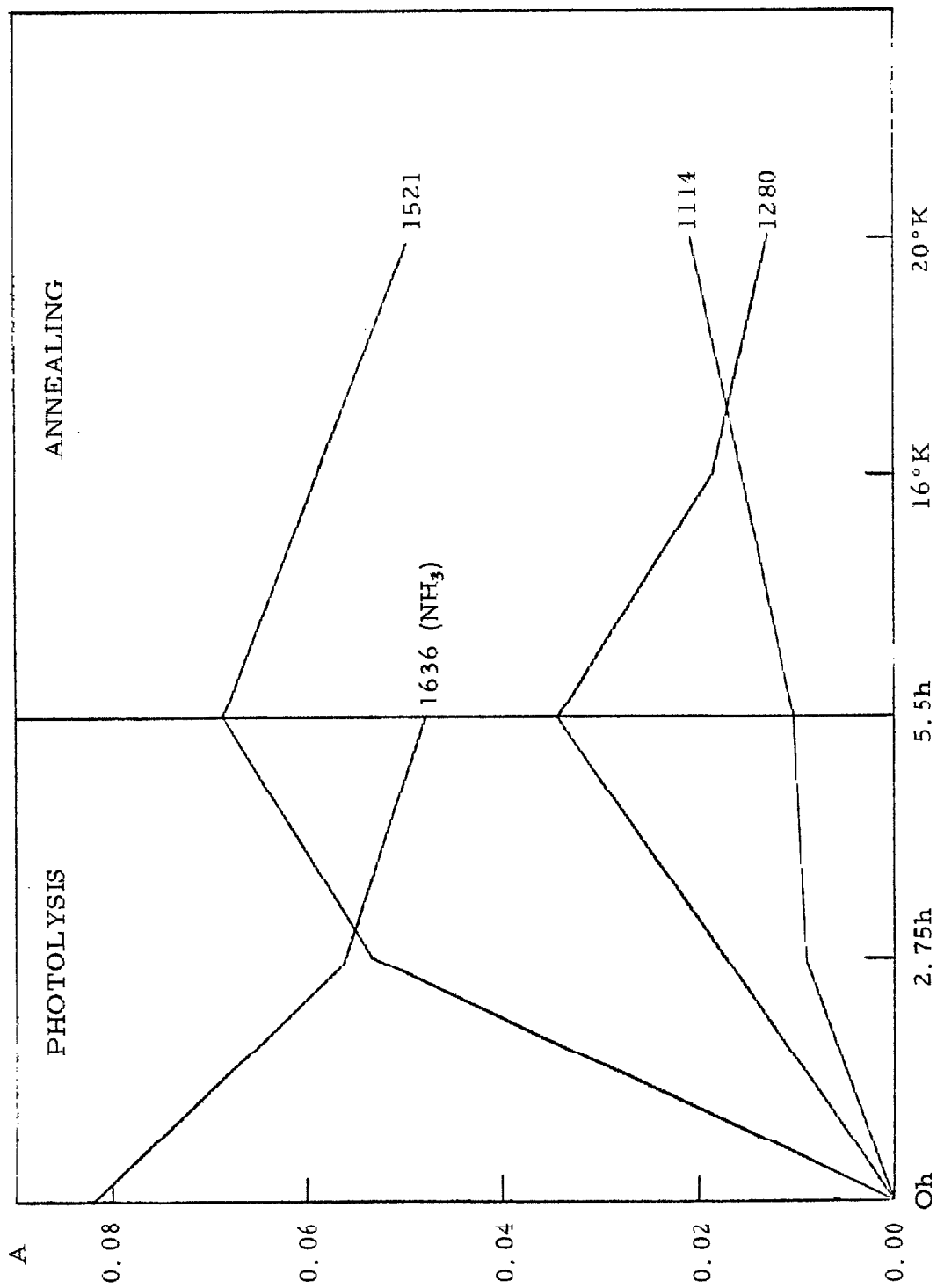


FIGURE 11

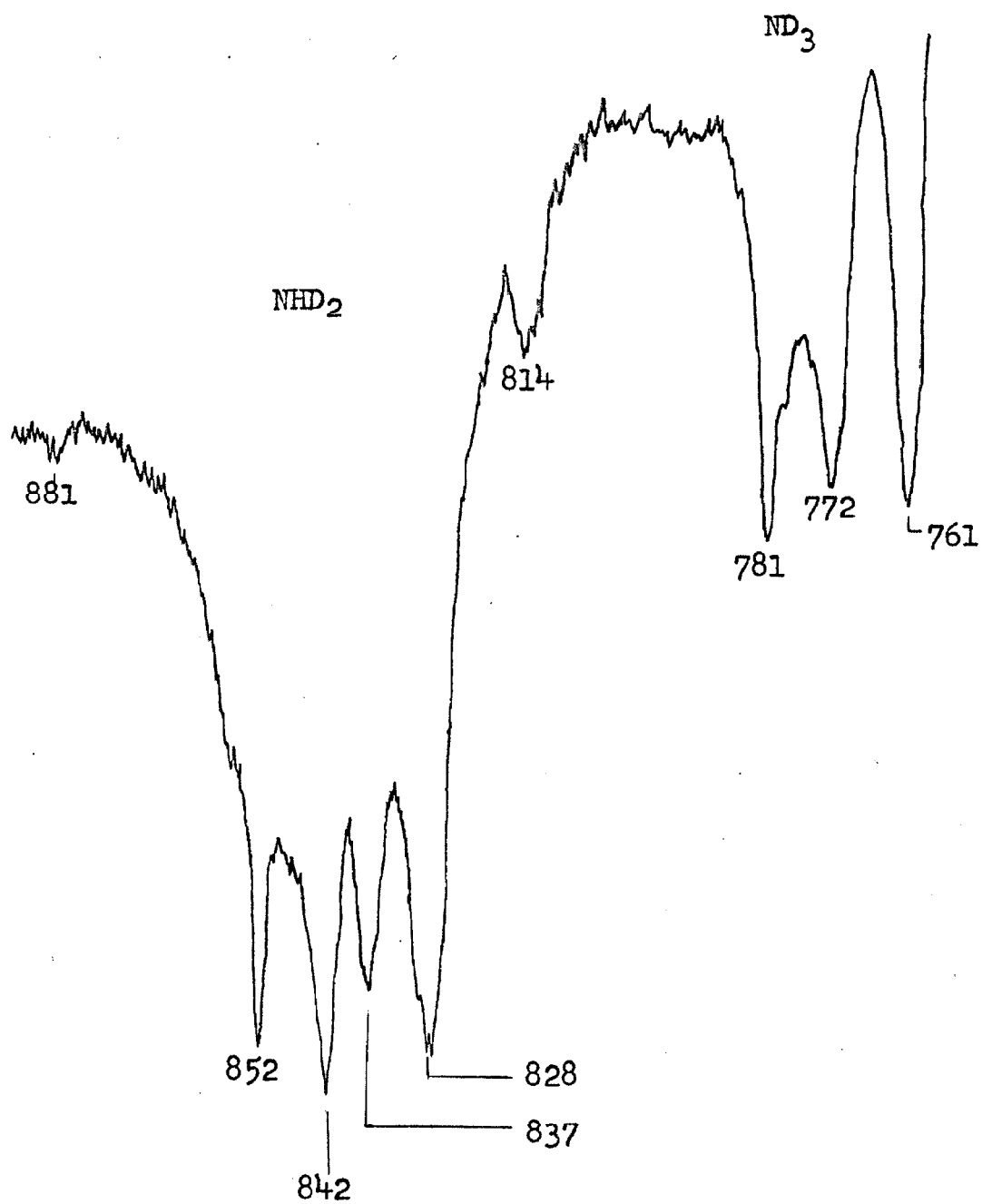


FIGURE 12

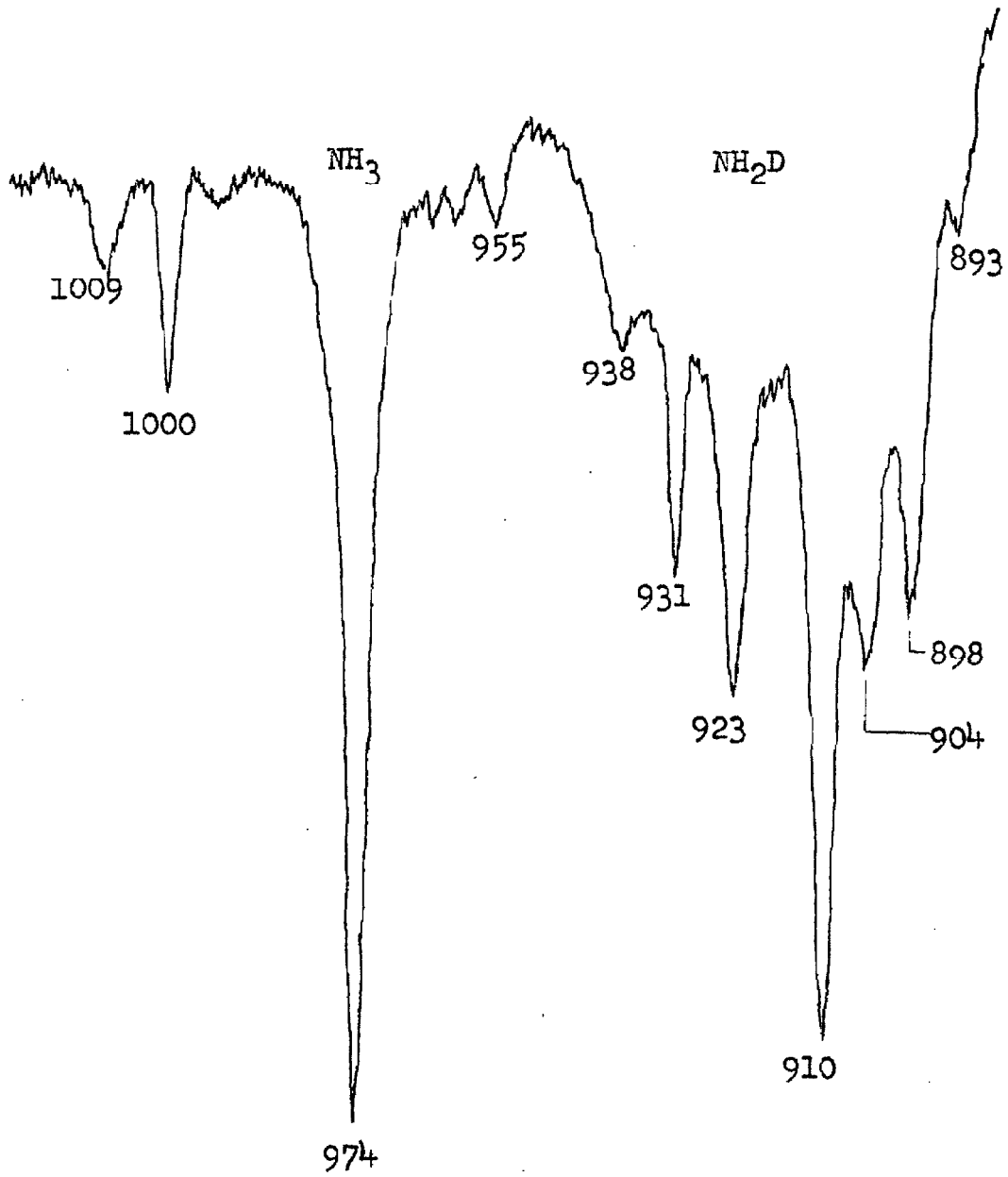


FIGURE 13

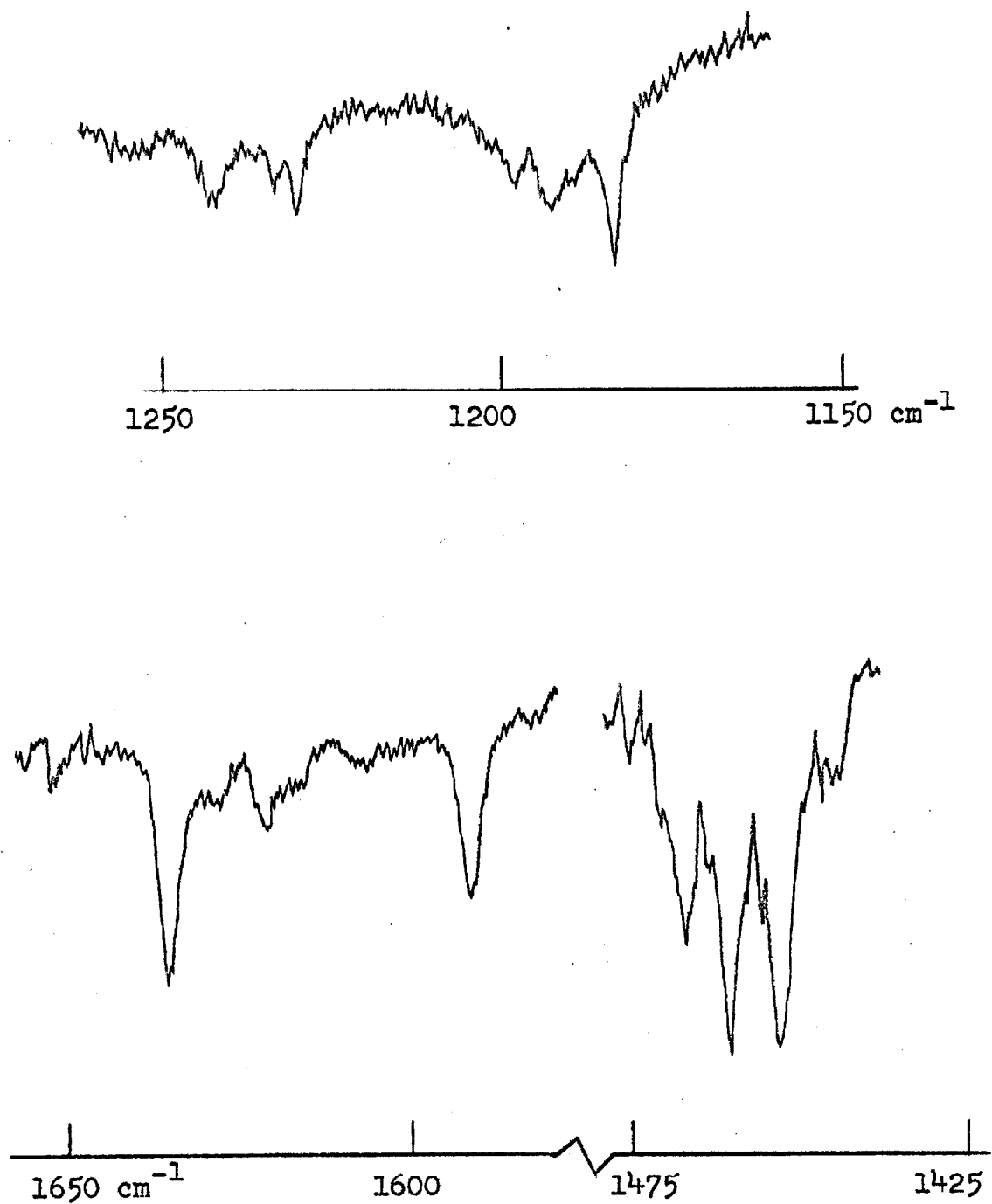


FIGURE 14

Table II. Absorption maxima of deuterated ammonia in krypton; ν_4 modes.

ν_{obs} (cm ⁻¹)	Assignment
1185	ν_4 ND ₃
1194	"
1199	"
1232	ν_4' ND ₂ H
1234	"
1244	"
1447	ν_4'' ND ₂ H
1454	"
1462	"
1473	"
1592	ν_4' NH ₂ D
1607	—
1617	—
1621	ν_4 NH ₃
1628	"
1636	"

Table III. Strongest absorption lines observed in visible region after X-ray photolysis of deuterated ammonia in krypton.

λ (Å)	ν (cm ⁻¹)	Assignment ^a	
		$\nu_1' \nu_2' \nu_3'$	$N_{T'} - N_{T''}$
6041	16,554	ND ₂ (0, 12, 0) II	1 ₀ - 1 ₋₁
6017	16,620	ND ₂ (0, 12, 0) II	$\left\{ \begin{array}{l} 1_1 - 0_0 \\ 2_0 - 1_{-1} \end{array} \right.$
5696	17,556	NH ₂ (0, 10, 0) II	1 ₁ - 0 ₀
5616	17,806	NHD (?)	
5576	17,934	ND ₂ (0, 14, 0) II	1 ₁ - 0 ₀
5572	17,947	ND ₂ (0, 14, 0) II	2 ₀ - 1 ₋₁
5542	18,044	NHD (?)	
5191	19,264	NHD (?)	
5162	19,372	NH ₂ (0, 12, 0) II	1 ₁ - 0 ₀
5111	19,566	NHD (?)	
5081	19,681	NHD (?)	

^a(ν_1' , ν_2' , ν_3') denote symmetric stretching, bending, and anti-symmetric stretching vibrations in upper electronic state; II refers to upper state vibronic symmetry. N is the rotational quantum number and τ is the asymmetric rotor index. The assignments are based on the work of Dressler and Ramsay, Reference 1.

assignments to ND_2 or NH_2 transitions. The unassigned lines are presumably due to NHD since they cannot be assigned to either NH_2 or ND_2 .

As indicated by their absorption bands in the ultraviolet, the NH and ND radicals are also present after X -irradiation. The (0-0) bands of NH and ND overlap near 3389 Å; the (1-0) bands were observed at 3081 and 3148 Å in solid krypton.

After X -irradiation new absorption lines appeared at 794, 865, 948, and 1106 cm^{-1} in the infrared region. The 794 and 948 cm^{-1} peaks increased in intensity after the sample was warmed and recooled, while the 865 cm^{-1} peak remained the same. Their temperature behavior shows that they are due to secondary reaction products or to polymeric species of the deuterated ammonia. The line at 1106 cm^{-1} disappeared after the sample was warmed to 25°K and recooled.

DISCUSSION

After photolysis or X -irradiation of the ammonia in krypton samples, six new absorption maxima appear in the infrared region. The frequencies and maximum absorbancies of these new lines are given in Table IV. In this series of experiments the 1613 cm^{-1} line appeared only once and will not be considered further in the discussion which follows.

Table IV. Absorption maxima which appear after photolysis of NH_3 in krypton.

Mercury Lamp (1849 Å)		X Radiation	
ν (cm^{-1})	Absorbancy	ν (cm^{-1})	Absorbancy
—	—	1017.5	shoulder
—	—	1114	0.012
—	—	1280	0.032
1289	0.024	—	—
1521	0.080	1521	0.070
1613	0.039	—	—

The 1114 cm^{-1} Line

Figure 11 shows the intensity increase in the 1114 cm^{-1} line when the sample is warmed and re-cooled; in contrast, the other absorption peaks decrease in intensity following the same operation. The 1114 cm^{-1} peak is evidently not related to the other absorption maxima and, therefore, must be given a separate interpretation.

Absorption peaks have been observed previously in the 1100 cm^{-1} region following photolysis of hydrazoic acid (HN_3) in solid nitrogen and argon (10, 14). They have been assigned to hydroxylamine, which absorbs strongly at 1120 cm^{-1} in the gas phase (15) and at 1191 cm^{-1} in the solid (16).

Hydroxylamine presumably forms by the reaction of an NH radical with water present in the sample as an impurity. No absorption bands due to water have been detected in our samples; it is not possible, however, to rule out the presence of trace quantities of water because it absorbs (17) in the same region as the ammonia band near 1600 cm^{-1} . Nevertheless, the absence of detectable amounts of water makes the assignment of the 1114 cm^{-1} peak to hydroxylamine uncertain.

Another possible interpretation of the 1114 cm^{-1} line is to assign it to hydrazine which absorbs strongly at 1087 cm^{-1} in solid nitrogen (18). The presence of hydrazine is not unexpected because it should readily form by the combination of two NH_2 radicals which are known to be present in the sample. There should also be a strong absorption maximum due to hydrazine near 982 cm^{-1} in the absorption

region of parental ammonia. Possibly the shoulder at 1017.5 cm^{-1} corresponds to this hydrazine frequency in krypton; but most likely it would be obscured by the ammonia bands.

The species responsible for the absorption at 1114 cm^{-1} is a secondary reaction product; this is demonstrated by its increase in intensity when the sample is warmed and re-cooled (see Fig. 11). Both of the above assignments to hydroxylamine or to hydrazine are consistent with this behavior, but hydrazine seems to be the more likely alternative.

The 1280 and the 1289 cm^{-1} Lines

Since the accuracy of the spectrometer in the 1300 cm^{-1} region is estimated to be better than $\pm 2\text{ cm}^{-1}$, the two new absorption maxima which appear in this region are distinct. Both the 1521 cm^{-1} line and the two lines in the 1300 cm^{-1} region decrease in intensity when the sample is warmed and re-cooled. The question naturally arises whether these features are due to the same photolysis product or to separate species. It is not possible, however, to make reasonable assignments of the 1521 cm^{-1} line and the 1300 cm^{-1} lines to known vibrational frequencies of likely products such as hydroxylamine, hydrazine, or diimide (N_2H_2). A further indication that these lines are not due to the same species is that the 1521 cm^{-1} line appears after both 1849 \AA photolysis and X-irradiation; however, the 1289 cm^{-1} line appears only after 1849 \AA photolysis while the 1280 cm^{-1} line appears only after X-irradiation.

Absorption maxima appear in the 1300 cm^{-1} region following photolysis of hydrazoic acid in solid nitrogen or argon; they have been assigned to various species including NH_2 , NH_2N_3 , and N_2H_2 (10, 14). Rosengren and Pimentel (19) have recently identified absorption features at 1286 and 1279 cm^{-1} with trans and cis forms of diimide (N_2H_2) respectively. It is possible that the 1289 and 1280 cm^{-1} peaks observed in our experiments are also due to diimide. The electronic absorption spectrum shows that NH is present, and the presence of its dimer is, therefore, quite possible. It is not clear, however, why 1849 \AA photolysis should exclusively form the trans isomer and X-ray photolysis the cis isomer.

The 1521 cm^{-1} Line

The 1521 cm^{-1} absorption maximum is assigned to the bending mode of the NH_2 radical for the following reasons. First, it is in the expected frequency region for HNH bending modes of amines and hydrazines which occur between 1550 and 1650 cm^{-1} in the gas phase. Secondly, it is the only absorption feature appearing after photolysis which correlates consistently with the NH_2 concentration in the sample. Whenever the electronic absorption spectrum indicates that a considerable amount of NH_2 is present in the sample, the line at 1521 cm^{-1} is observed; moreover, whenever the electronic absorption of NH_2 is weak, the 1521 cm^{-1} line is not observed (the 1280 , 1289 , 1114 , and 1613 cm^{-1} lines do not show this correlation). Thirdly, it decreases in intensity when the sample is warmed and recooled (see

Figure 11); this is consistent with the behavior of a reactive species such as NH_2 . This assignment is further supported by the isotopic substitution experiment discussed below.

Isotopic Substitution

After X-irradiation of deuterated ammonia in krypton, an absorption feature at 1106 cm^{-1} appears. This is a distinct line not related to the absorption line at 1114 cm^{-1} which appears after X-irradiation of ammonia- h_3 in krypton. The frequency difference between 1106 and 1114 cm^{-1} is outside the estimated maximum error of $\pm 2 \text{ cm}^{-1}$ in this region of the spectrum. The line at 1106 cm^{-1} disappears when the sample is warmed and recooled; in contrast, the 1114 cm^{-1} line increases in intensity following the same operation.

The effect of isotopic substitution on the normal frequencies of NH_2 may be calculated if an approximation to the vibrational force field is made. If valence forces are assumed, the two symmetric frequencies of NH_2 are given by

$$\lambda_1 + \lambda_2 = F_1(\mu_{\text{H}} + 2\mu_{\text{N}} \cos^2 \beta) + \frac{2F_3}{r^2} (\mu_{\text{H}} + 2\mu_{\text{N}} \sin^2 \beta) \quad (4a)$$

$$\lambda_1 \lambda_2 = 2\mu_{\text{H}}(\mu_{\text{H}} + 2\mu_{\text{N}}) \frac{F_1 F_3}{r^2} \quad (4b)$$

where λ_1 and λ_2 are the angular frequencies squared; F_1 and F_3/r^2 are the stretching and bending valence force constants respectively; r is the NH bond distance; 2β is the HNH bond angle; μ_{H} and μ_{N} are the reciprocal masses of the H atom and the N atom.

If the symmetric frequencies of NH_2 are known, equation 4 may be used to determine the force constants. These may then be used in turn to calculate the symmetric frequencies of ND_2 , assuming that the geometry and force constants do not change appreciably in the heavy isotopic molecule.

Strictly speaking the zero order frequencies and not the observed frequencies should be used in equation 4 to determine the quadratic force constants, F_1 and F_3/r^2 . Since the anharmonicity constants of NH_2 are not available, the observed frequencies at 3200 and 1521 cm^{-1} have been used in the calculation. As a check on the accuracy to be expected, a parallel calculation for H_2O and D_2O has been done using the observed symmetric frequencies of H_2O . The molecular constants used in the calculation and its results are summarized in Table V. Considering the approximate nature of the force field, the agreement between the observed and calculated frequencies of D_2O is good. The calculated frequencies for ND_2 should also be reasonably close to the true values if 3200 and 1521 cm^{-1} are the correct symmetric frequencies of NH_2 .

The absorption maximum at 1106 cm^{-1} can now be assigned to the bending mode of ND_2 . The assignment is consistent with the temperature behavior of the 1106 cm^{-1} line and with the fact that considerable amounts of ND_2 are known to be present in the sample.

Conclusion

The photolysis of ammonia in solid krypton with 1849 \AA light or with X radiation gives rise to new absorption maxima at 1521, 1114,

Table V. Comparison of observed and calculated frequencies.

Molecule	ν_1 (cm ⁻¹)		ν_2 (cm ⁻¹)	
	calc.	obs.	calc.	obs.
NH ₂	—	3200 ^a	—	1521 ^b
ND ₂	2326	c	1111	1106 ^b
H ₂ O	—	3656.6 ^d	—	1594.6 ^d
D ₂ O	2646	2671.5 ^d	1162	1178.3 ^d

	r (Å)	β	F_1 (mdyne/Å)	F_3/r^2 (mdyne/Å)
NH ₂ (ND ₂)	1.024 ^e	51°42' ^e	5.76	0.635
H ₂ O(D ₂ O)	0.9572 ^d	52°16' ^d	7.57	0.703

^aReference 8.^bThis work.^cNot observed.^dReference 20.^eReference 1.

1289, and 1280 cm^{-1} in the infrared; no new absorption features were observed in the hydrogen stretching region, 2800 to 3500 cm^{-1} . The line at 1521 cm^{-1} is assigned to the previously unobserved bending mode of the NH_2 radical. Experiments with isotopic ammonia show that the bending mode of ND_2 occurs at 1106 cm^{-1} in solid krypton. This is in agreement with a calculated value of 1111 cm^{-1} which is obtained by assuming valence forces and using 1521 cm^{-1} for the bending frequency of NH_2 . The line at 1114 cm^{-1} which appears only after the photolysis of ammonia- h_3 is tentatively assigned to hydrazine. The lines at 1280 and 1289 cm^{-1} may correspond to cis and trans isomers of diimide.

REFERENCES

1. K. Dressler and D. A. Ramsay, *Phil. Trans. Roy. Soc. (London)*, A251, 553 (1959).
2. G. W. Robinson and M. McCarty, Jr., *J. Chem. Phys.*, 30, 999 (1959).
3. J. R. McNesby, I. Tanaka, and H. Okabe, *J. Chem. Phys.*, 36, 605 (1962).
4. K. D. Bayes, K. H. Becker, and K. H. Welge, *Z. für Naturforschung*, 17A, 676 (1962).
5. O. Schnepf and K. Dressler, *J. Chem. Phys.*, 32, 1682 (1960).
6. P. Swings, A. McKellar, and R. Minkowski, *Astrophys. J.*, 98, 142 (1943).
7. G. Herzberg and D. A. Ramsay, *J. Chem. Phys.*, 20, 347 (1952).
8. K. N. Tanner and R. L. King, *Nature*, 181, 963 (1958).
9. R. N. Dixon, *Canad. J. Phys.*, 37, 1171 (1959).
10. D. E. Milligan and M. E. Jacox, *J. Chem. Phys.*, 41, 2838 (1964).
11. D. E. Milligan, R. M. Hexter, and K. Dressler, *J. Chem. Phys.*, 34, 1009 (1961).
12. G. C. Pimentel, M. O. Bulanin, and M. Van Thiel, *J. Chem. Phys.*, 36, 500 (1962).
13. M. McCarty, Jr., Ph.D. thesis, The Johns Hopkins University, Baltimore, Maryland, 1960.
14. M. Van Thiel and G. C. Pimentel, *J. Chem. Phys.*, 32, 133 (1960).
15. P. A. Giguère and I. D. Liu, *Canad. J. Chem.*, 30, 948 (1952).
16. R. E. Nightingale and E. L. Wagner, *J. Chem. Phys.*, 22, 203 (1954).
17. R. L. Redington and D. E. Milligan, *J. Chem. Phys.*, 39, 1276 (1963).

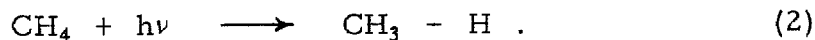
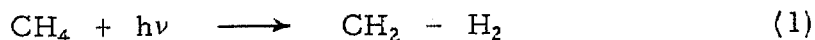
18. E. Catalano, R. H. Sanborn, and J. W. Frazer, *J. Chem. Phys.*, 38, 2265 (1963).
19. K. Rosengren, private communication.
20. W. S. Benedict, N. Gailar, and E. K. Plyler, *J. Chem. Phys.*, 24, 1139 (1956).

PART III

ULTRAVIOLET SPECTRA OF CH PRODUCED BY X-RADIOLYSIS
OF METHANE IN SOLID ARGON

INTRODUCTION

Previous experiments showed that the amidogen (NH_2) radical could be produced easily by X-radiolysis of ammonia in solid krypton (see Part II). This suggested that under similar conditions methylene (CH_2) and methyl (CH_3) might be obtained by X-radiolysis of methane. Methyl radicals have been produced by γ -irradiation of methane in solid argon and krypton (1), in solid xenon (2), and in solid methane (3); electron spin resonance was used to detect the radicals. Previous studies (4, 5, 6) of the gas and solid phase photolysis of methane have indicated that reactions 1 and 2 are important primary steps



Another possible product of methane photolysis is the methyldyne (CH) radical.

The electronic spectra of CH , CH_2 , and CH_3 have been observed previously. Three well known transitions of CH occur near 4315, 3890, and 3140 Å in the gas phase (7). Two transitions of CH_2 are known (8). The absorption in the vacuum ultraviolet near 1400 Å is interpreted as a ${}^3\Sigma_u^- \leftarrow {}^3\Sigma_g^-$ transition in which CH_2 is linear in both states. The three red bands of CH_2 at 8190, 7315, and 6531 Å are assigned to transitions between a bent ground state ($\theta = 103.2^\circ$) and a linear excited state. It is not known whether the true ground state of CH_2 is bent or linear; however, indirect evidence suggests that the lowest energy state of CH_2 is the linear ground state of the

1400 Å transition. If this is also true for CH₂ in a solid rare gas environment, one would not expect to observe the red bands because of depopulation of their initial state. The most intense transitions of methyl occur near 2160, 1500, and 1380 Å (8). They are assigned to transitions between electronic states in which CH₃ is planar or nearly so.

In the spectral region covered by these experiments (2100 to 9000 Å), it is possible to observe the three known transitions of CH, the red bands of CH₂, and the 2160 Å transition of CH₃. In addition, the transition from the $\cdots (e')^4 (a_2'')^{---2}A_2''$ ground state of CH₃ to the first excited configuration $\cdots (e')^3 (a_2'')^2 \text{---}^2E'$ is expected to lie in this region. This transition is forbidden if methyl is strictly planar (D_{3h} symmetry) but becomes allowed if it is pyramidal (C_{3v} symmetry).

EXPERIMENTAL

The experimental arrangement was essentially the same as that described above for the X-ray photolysis of ammonia. In order to observe the emission spectrum during X-irradiation, all the heat shields except the inner one in the liquid helium dewar were removed. The concentration of methane in the rare gas was typically 0.8 percent. The temperature of the cold window was 12°K while the sample was being deposited; during X-irradiation the temperature was 9°K or lower. The methane supplied by Matheson was C. P. grade (99% minimum purity).

The absorption spectra were taken with a 0.5 meter Jarrell-Ash f/6.3 plane grating spectrograph. The plate factor was about 20 Å per mm in the second order. The emission spectra were observed on the Jarrell-Ash spectrograph and on a 2 meter plane grating f/11 spectrograph. The plate factor of the 2 meter instrument was 4 Å per mm in the second order. Exposure times necessary to observe the emission spectra were generally one half hour with a 50 μ slit width on the Jarrell-Ash; two hour exposures with a 200 μ slit width were used on the 2 meter instrument.

A 100 watt tungsten lamp was used as a source in the 3500 to 9000 Å region; a 150 watt high pressure xenon lamp (Hanovia No. 510CI) was used as a source in the region from 2000 to 4000 Å.

RESULTS

The observed spectra are listed in Table I. The emission spectra were excited by X-irradiation of the methane in argon or krypton samples. Most of the lines observed have been assigned either to CH or to N₂ and O₂ present as impurities. The Vegard-Kaplan bands of nitrogen have previously been observed in solid argon by Broida and Peyron (9); in addition to the bands observed by them in the (0, v'') progression, we have observed the (0, 4) and the (0, 3) bands. The (0, 6), (0, 7), and (0, 8) Herzberg bands of oxygen appear weakly in solid argon; these bands and others of the (0, v'') progression have been observed in solid nitrogen by Broida and Peyron (9). The frequencies of the bands are approximately 75 cm⁻¹ lower in solid argon than in solid nitrogen. Fine structure appears in three of the CH bands, densitometer tracings of which are shown in Figures 1 to 3. Emission from a vibrationally excited upper state occurs in the B²Σ⁻ → X²Π transition of CH and in the Vegard-Kaplan bands of nitrogen.

The results in krypton were mostly negative. Except for the two weak absorption features reported, no spectra were observed between 2400 and 9000 Å after four hours of X-irradiation. The rate of production of CH in solid krypton relative to the rate in solid argon is less than 0.1. This value was obtained by comparing absorption intensities of CH in argon and krypton after equal times of X-irradiation.

Table I. Spectra observed after X-irradiation of methane in solid argon and krypton.

Absorption in Argon

λ_{air}^a (Å)	ν_{vac}^b (cm ⁻¹)	$\Delta\nu_{1/2}$ (cm ⁻¹)	Relative Intensity ^b	Assignment
3149.9	31,738 ± 5	70	20	CH C ² Σ ⁺ ← ² Π
3152.7	31,710 ± 5	10	2	"
3156.7	31,670 ± 5	10	2	"
3658.2	27,328 ± 3	120	5	CH B ² Σ ⁻ ← X ² Π(1,0)
3909.5	25,572 ± 3	25	10	CH B ² Σ ⁻ ← X ² Π(0,0)
3921.0	25,496 ± 3	25	10	"
4285	23,331 ± 5	shoulder		CH A ² Δ ← X ² Π
4296	23,271 ± 5	shoulder	30	"
4305.9	23,217 ± 3	50		"

Absorption in Krypton

3169.8	31,539	-	weak	CH C ² Σ ⁺ ← X ² Π
5224.8	19,134	-	weak	?

Table I (continued)

Emission in Argon

λ_{air}^a (Å)	ν_{vac} (cm ⁻¹)	$\Delta\nu_{1/2}$ (cm ⁻¹)	Relative Intensity ^b	Assignment
3157.3	31,664 ± 3	65	8	CH C ² Σ ⁺ → X ² Π
3172.6	31,511 ± 3	40	2	"
3659.6	27,318 ± 3	100	10	CH B ² Σ ⁻ → X ² Π(1, 0)
3921.2	25,495 ± 3	15	15	CH B ² Σ ⁻ → X ² Π(0, 0)
3925.1	25,470 ± 6	shoulder	2	"
3932.9	25,419 ± 6	shoulder	4	"
4308.9	23,201 ± 3	shoulder	20	CH A ² Δ → X ² Π
4320	23,138 ± 6	80	20	"
4329	23,082 ± 6	shoulder	20	"

Table I (continued)

Emission in Argon

λ_{air}^a (Å)	ν_{vac} (cm ⁻¹)	Relative Intensity ^c	Assignment
2340.5	42,713	3	N ₂ (Vegard-Kaplan) (0, 3)
2469.9	40,476	3	(0, 4)
2612.8	38,261	3	(0, 5)
2770.9	36,079	3	(0, 6)
2946.7	33,926	7	(0, 7)
3143.6	31,802	7	(0, 8)
3211.2	31,132	2	(1, 9)
3365.7	29,703	7	(0, 9)
3617.5	27,636	3	(0, 10)
			O ₂ (Herzberg)
3974.2	25,155	2	(0, 6)
4210.6	23,743	2	(0, 7)
4473	22,351	2	(0, 8)
3960.0	25,246	2	?
4067.8	24,577	2	?

^aFor broad bands the measurement was made at the low frequency edge in absorption, at the high frequency edge in emission. ^bEstimated from densitometer tracings. ^cEstimated directly from plates using a scale of 10.

Figures 1, 2, and 3. Fine structure in the CH bands; the positions of the emission and absorption features are given in Å.

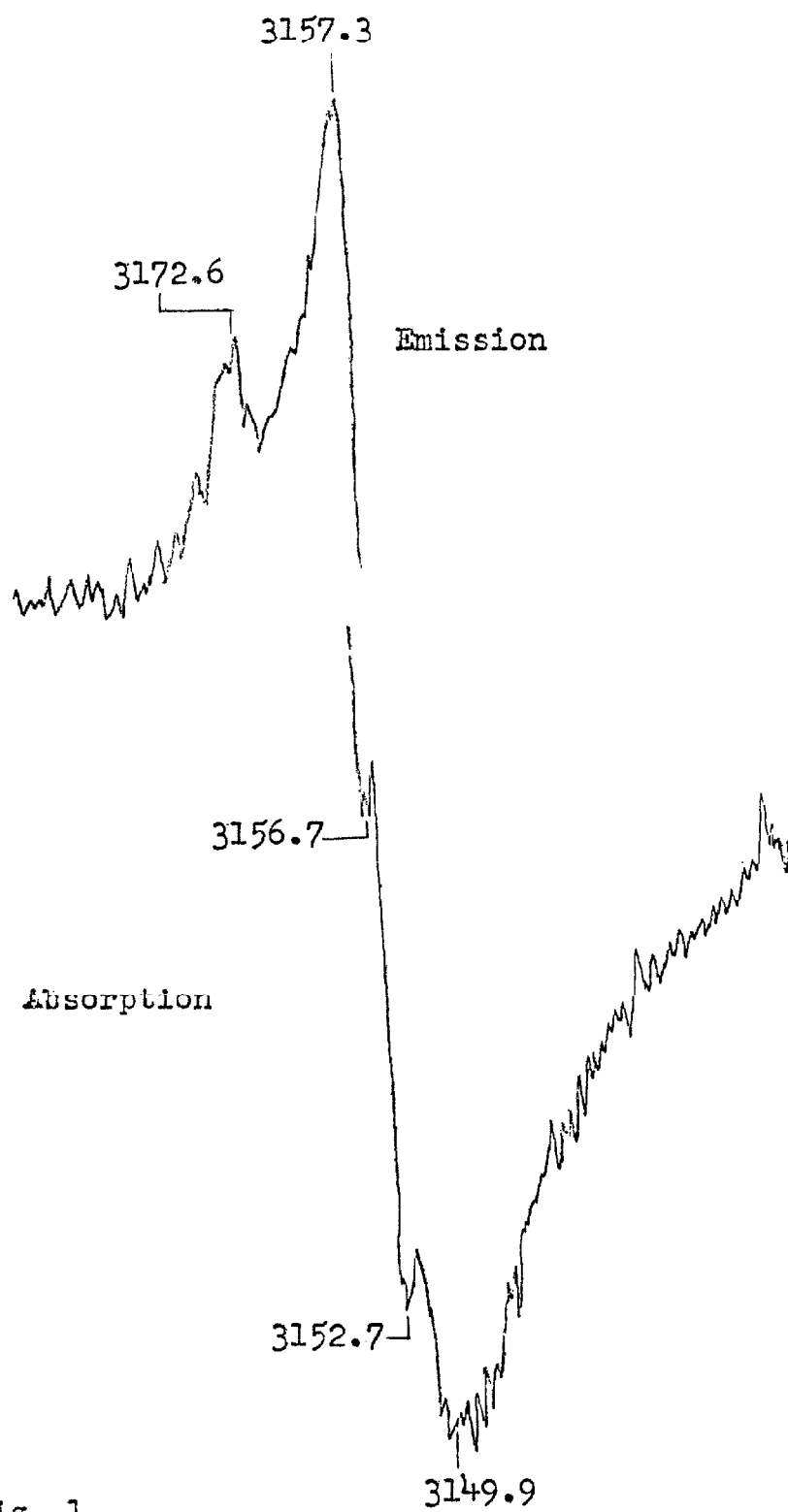


Fig. 1.

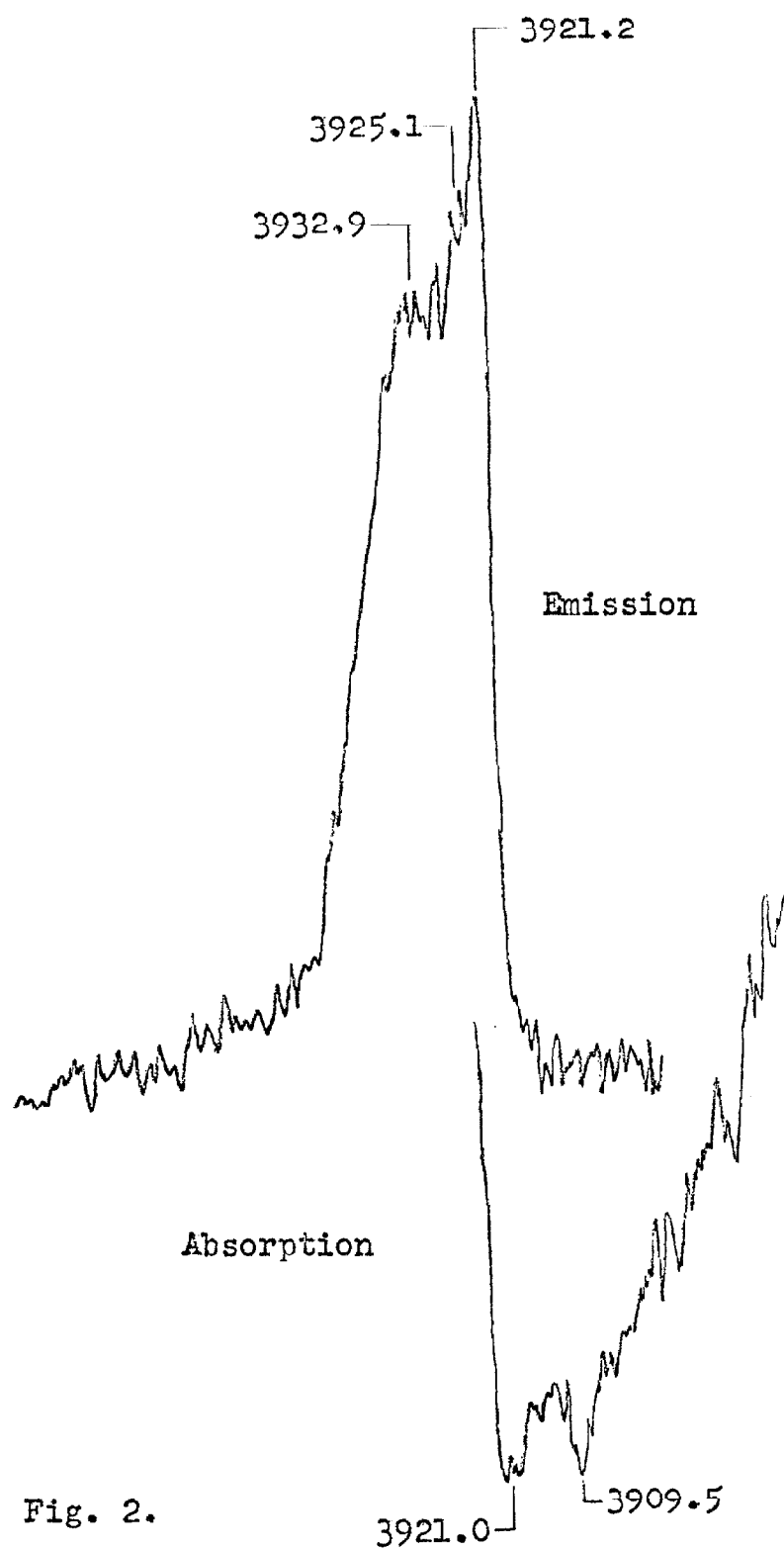


Fig. 2.

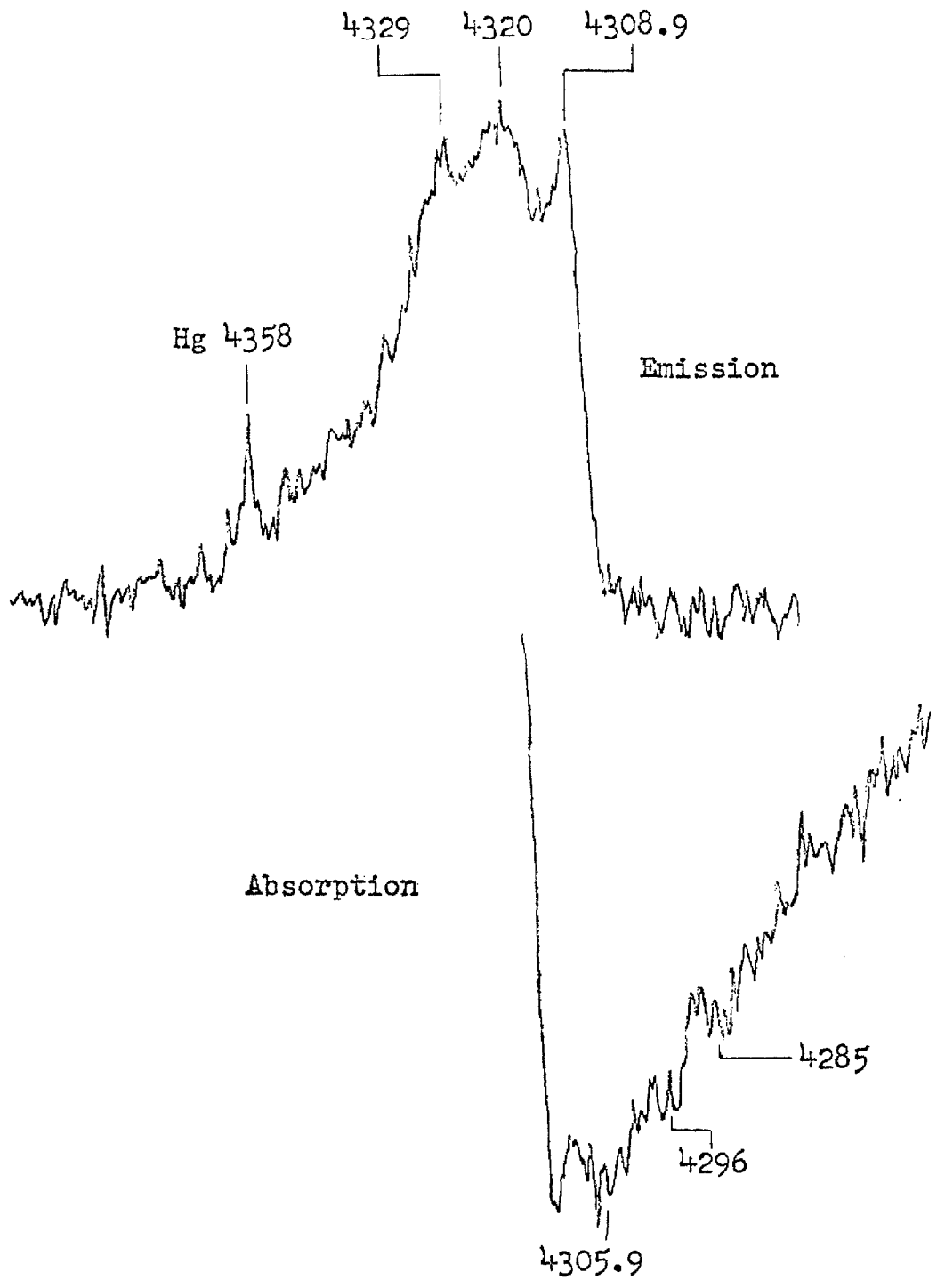


Fig. 3.

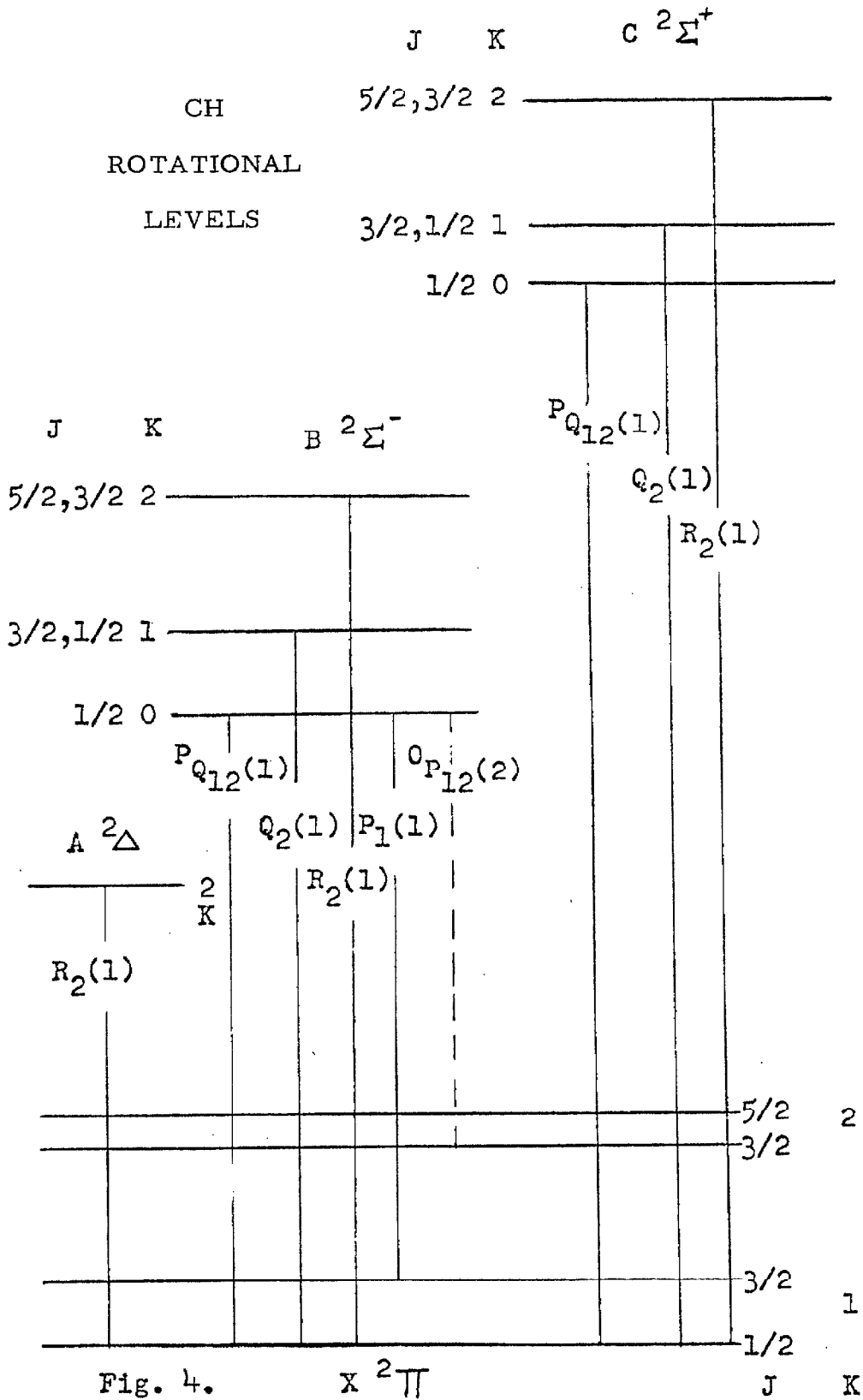
The relative amounts of methane present before and after the X-irradiation was determined by its infrared absorption near 1303 cm^{-1} in solid argon. The peak absorbancy, $\log_{10}(I_0/I)$, before photolysis in a typical experiment was 2.67; after 9 hours of X-irradiation, the absorbancy was reduced to 2.45. Approximately 8% of the methane was decomposed by 9 hours of X-ray photolysis in solid argon.

DISCUSSION

The CH Bands

The fine structure of the CH bands (see Figs. 1 to 3) could be produced by several mechanisms among which are rotation in the solid, combinations with lattice vibrations, and multiple trapping sites. The last of these can be ruled out; because if multiple sites were the cause, one would expect the emission and absorption frequencies to coincide.

Although there are some difficulties pointed out below, rotation of CH in solid argon is a possible explanation for part of the fine structure. The lowest rotational levels of the four known electronic states of CH are shown in Figure 4. Transitions which are drawn with solid lines are allowed by case b selection rules ($\Delta J = 0, \pm 1$; $\Delta \Lambda = 0, \pm 1$; $\Delta K = 0, \pm 1$; $+\leftrightarrow -$); the transition drawn with the dashed line is forbidden in strict case b coupling but is allowed in case a and intermediate cases. In case a the K selection rule is replaced by $\Delta \Omega = 0, \pm 1$ ($\Omega = \Lambda + \Sigma$). For a discussion of Hund's coupling cases and spectroscopic notation, see Herzberg (10). The



rotational assignments are given in Table II where the frequencies observed in solid argon are compared with the gas phase values.

The frequency shifts of the ${}^P Q_{12}(1)$ and $Q_2(1)$ lines of the 3150 Å band agree within experimental error. The $R_2(1)$ line is shifted about 20 cm^{-1} lower; however, this line is rather broad (see Table I) and the measurement was made near its low frequency side so that the 20 cm^{-1} shift may or may not be real. The observed relative intensities of the rotational lines do not agree with the calculated values. The emission which occurs on the low frequency side of the absorption band evidently distorts the observed intensities. Only the ${}^P Q_{12}(1)$ line of the 3150 Å band is seen in emission. The other emission line at $31,511 \text{ cm}^{-1}$ is tentatively assigned to CH since it appears at the same time as the CH bands; however, it cannot be assigned to a rotational transition.

The assignments given for the 3900 Å band indicate the apparent absence of the $Q_2(1)$ line which should appear with an intensity comparable to that of the ${}^P Q_{12}(1)$ line. The absorption features are broad and it is possible that the peak interpreted as the ${}^P Q_{12}(1)$ line may really be the unresolved ${}^P Q_{12}(1)$ and $Q_2(1)$ lines. Three rotational lines are seen in emission with nearly equal frequency shifts of about 210 cm^{-1} . The ${}^P Q_{12}(1)$ line is observed in both absorption and emission in the 3650 Å band.

The fine structure of the 4300 Å band cannot be assigned to rotation. Only one rotational transition from the ground ${}^2\Pi$ state is allowed by the $\Delta J = 0, \pm 1$ selection rule, but three absorption maxima are seen.

Table II. Rotational assignments for CH in solid argon.

$\nu_{\text{argon}} (\text{cm}^{-1})$	Emission	Assignment	$\nu_{\text{gas}}^a (\text{cm}^{-1})$	$\nu_{\text{argon}} - \nu_{\text{gas}} (\text{cm}^{-1})$
		$C^2\Sigma^+ - X^2\pi$ (3150 Å band)		
31, 738		$R_2(1)$	31, 863 (5)	-125
31, 710		$Q_2(1)$	31, 806 (10)	-96
31, 670	31, 664	$P_{Q_{12}}(1)$	31, 777 (10)	-107
		$B^2\Sigma^- - X^2\pi$ (3650 Å band)		
27, 328	27, 318	$P_{Q_{12}}(1)$	27, 493	-165
		$B^2\Sigma^- - X^2\pi$ (3900 Å band)		
25, 572		$R_2(1)$	25, 774 (5)	-202
—		$Q_2(1)$	25, 723 (10)	—
25, 496	25, 495	$P_{Q_{12}}(1)$	25, 698 (10)	-202
	25, 470	$F_1(1)$	25, 680 (10)	-210
	25, 419	$OP_{12}(2)$	25, 632 (10)	-214

^aThe gas phase frequencies were taken from the analysis by Gerö (11) for the 3900 and 3650 Å bands. The gas phase frequencies for the 3150 Å band were calculated from the data given by Heimer (12) and from the known ground state rotational spacings. The numbers in parentheses are the relative intensities for pure case b coupling (13).

Since rotation cannot completely explain the observed fine structure, it may at least be partly due to combinations with the lattice vibrations. The Debye temperature of argon is 80°K (14); this is equivalent to a lattice frequency of 56 cm⁻¹ which is in the same range as the observed fine structure spacings.

CH₃ and CH₂

Although both methyl and methylene are expected to be produced by the photolysis of methane (1-6), neither radical was observed in these experiments. The 2100 Å region of the CH₃ absorption was difficult to observe because of light scattering in the polycrystalline solids used. On one occasion after four hours of X-irradiation in solid argon, the spectrum could be taken down to the 2100 Å region; however, no absorption features were observed. The red bands of CH₂ are in a readily accessible region, but no sign of CH₂ could be detected in any of these experiments. The fact that CH₂ production is an important primary step in the photolysis (4-6) suggests that it should be present in relatively large amounts after the X-irradiation. The failure to observe the CH₂ red bands is in agreement with the evidence given by Herzberg (8) that the true ground state of CH₂ is not the lower state of the red bands.

Photolysis Mechanism

The X-rays incident on the sample can be absorbed by the rare gas atoms or directly by the impurities (methane or ammonia, for example) themselves. The most important mechanism of X-ray

absorption for energies below 50 Kev is the photoelectric effect. The attenuation of the X rays by the sample can be related to the mass absorption coefficient by

$$I/I_0 = \exp[-(\mu/\rho)\rho X] ,$$

where (I/I_0) is the fraction of incident intensity that is transmitted by the sample, ρ is the density of the sample, and X is the sample thickness. The mass absorption coefficients for methane, ammonia and the rare gases are given in Table III.

Photolysis of methane and ammonia occurs when the molecules are excited to a dissociative state. This can be effected either by direct absorption of the X rays or by an energy transfer mechanism in the solid. The X-ray absorption coefficients and concentrations of methane and ammonia are very small compared to those of the surrounding rare gas atoms (see Table III). Thus direct absorption by the impurity molecules accounts for only a small fraction of the total X-ray absorption. Furthermore, if direct absorption of the X rays were important in the photolysis mechanism, one would expect that the decomposition rate of methane would be independent of the rare gas matrix. The experiments indicate, however, that the decomposition rate is lower by an order of magnitude in krypton than it is in argon.

The alternative photolysis mechanism involves X-ray excitation of the rare gas atoms in the solid and the subsequent transfer of this energy to the trapped impurity molecule. Experiments by Boulden,

Table III. Mass absorption coefficients, μ/ρ (cm^2/g).

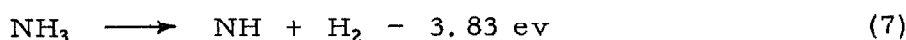
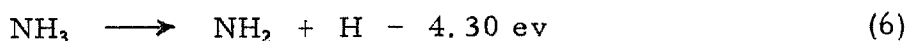
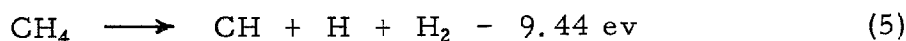
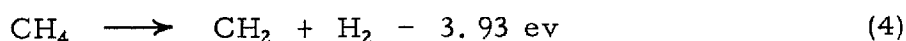
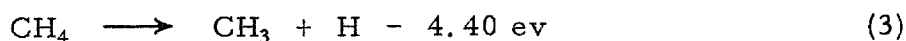
X-ray Energy (Kev)	CH_4^{a}	NH_3^{a}	Ar^{a}	Kr^{b}
10	1.91	3.34	61.6	
20	0.252	0.392	8.05	
25				32.5
30	0.134	0.157	2.41	

^aReference 15.

^bReference 16.

Patten, and Gordy (1) indicate that energy transfer of this type is at least partially responsible for the decomposition of methane during γ -irradiation in solid argon and krypton.

The approximate energies needed for the dissociation of methane and ammonia can be obtained from the bond dissociation energies given in Table IV. Possible dissociation paths are shown in equations 3 to 7.



The bond dissociation energy of the N-H bond in NH_2 has been taken to be 4 ev. If molecular hydrogen is not produced, -4.48 ev must be added to the energies needed in reactions 4, 5, and 7.

The electronic absorption spectra of the rare gas solids and the ionization potentials of the rare gases may be used to estimate the amount of energy available for transfer to the impurity molecule. Schnepf and Dressler (18) have observed the absorption spectrum of solid xenon and krypton. In xenon absorption bands occur at 1508, 1485, 1360, and 1305 Å. They assign the 1485 and 1305 Å absorptions to the allowed transition between the ground state and the two $J' = 1$ states of the $5p^56s$ configuration. These correspond to the gas phase resonance doublet of xenon. The 1508 Å band is assigned to the gas

Table IV. Bond dissociation energies.^a

Bond	Dissociation Energy		
	ev	kcal/mole	cm ⁻¹
H ₃ C-H	4.4	101	35,500
H ₂ C-H	<4	92	<32,300
HC-H	~5.5	~127	~44,400
C-H	3.47	80	28,000
H ₂ N-H	4.3	100	34,700
N-H	3.7	85	29,800
H-H	4.476	103.2	36,110

^aReference 17.

phase forbidden transition between the ground state and the $J' = 2$ state of the $5p^56s$ configuration. In krypton they observe bands at 1244 and 1222 Å, which are assigned to transitions between the ground state and the $J' = 2$ and the $J' = 1$ states respectively of the $4p^55s$ configuration. Baldini (19) has reported the absorption spectrum of solid xenon, krypton, and argon. The resonance doublet of xenon was observed at 1453 and 1289 Å, the krypton doublet was observed at 1216 and 1139, the argon doublet at 1033 and 1008 Å. Because of their longer lifetimes, the lowest excited states of the rare gas solids are expected to be the most important states in the transfer of energy to impurity molecules. The energy available per excited atom in solid xenon is 8.22 eV, in solid krypton 9.96 eV, and in solid argon 12.0 eV.

The absorption spectra of ammonia and methane locate the important molecular states available for energy transfer. Two continuous absorption regions of methane are known, one lies between 1100 and 1450 Å with a maximum absorption at 1250 Å or 9.92 eV (20). The second region lies between 374 and 1300 Å with a maximum at 1000 Å or 12.4 eV. Five electronic transitions of ammonia are known. The band origins of the first four transitions are at 2168 Å (5.72 eV), 1665 Å (7.44 eV), 1434 Å (8.64 eV), and 1330 Å (9.32 eV). The origin of the fifth transition is unknown but bands occur in the region of 1268 Å. The bands of the 2168 Å progression in ν_2' (out of plane bending) are all predissociated, the predissociation being very strong for $\nu_2' \geq 3$ (21).

The photolysis mechanism must account for the order of magnitude difference in the CH formation rate in argon and krypton. In argon the crystal excitation energy may be transferred to both absorption continua of methane, but in krypton only the lower methane continuum is available. This difference makes the slower rate in krypton understandable if CH is formed directly from methane by reaction 5. The energy available in argon is about 2.5 ev in excess of that required by reaction 5, in krypton the excess is only about 0.5 ev. The additional energy in argon is most likely important in allowing the free radicals to escape the immediate locale in which they are formed.

The fact that the ionization potentials (see Table V) of krypton and argon are both at least 5 ev greater than the energy needed to produce CH from methane via reaction 5 suggests that the rate of CH formation in these matrices should be similar. An ionic mechanism thus is probably not important. Also a path involving CH_3 or CH_2 as intermediates cannot account for the rate difference, since from energy considerations, CH_3 and CH_2 should be formed as readily in krypton as in argon.

The ease of ammonia decomposition in krypton is understandable because the krypton excitation can transfer more than enough energy to dissociate ammonia into NH or NH_2 via reactions 6 or 7.

Table V. Ionization potentials (ev).

NH_3^{a}	CH_4^{b}	Ar^{c}	Kr^{c}	Xe^{c}
10.2	13.2	15.7	14.0	12.1

^aReference 22.

^bReference 23.

^cReference 24.

REFERENCES

1. W. V. Boulden, R. A. Patten, and W. Gordy, *Phys. Rev. Letters*, 9, 98 (1962).
2. R. E. Florin, D. W. Brown, and L. A. Wall, *J. Phys. Chem.*, 66, 2672 (1962).
3. D. W. Brown, R. E. Florin, and L. A. Wall, *J. Phys. Chem.*, 66, 2602 (1962).
4. B. H. Mahan and R. Mandal, *J. Chem. Phys.*, 37, 207 (1962).
5. J. E. Manton and A. W. Tickner, *Canad. J. Chem.*, 38, 858 (1960).
6. P. Ausloos, R. E. Rebert, and S. G. Lias, *J. Chem. Phys.*, 42, 540 (1965).
7. R. W. B. Pearse and A. G. Gaydon, *The Identification of Molecular Spectra* (Wiley & Sons, Inc., New York, 1963), p. 101.
8. G. Herzberg, *Proc. Roy. Soc. (London)*, A262, 291 (1961).
9. H. P. Broida and M. Peyron, *J. Chem. Phys.*, 32, 1068 (1960).
10. G. Herzberg, *Spectra of Diatomic Molecules* (Van Nostrand, Inc., New York, 1950), p. 218 f.
11. L. Gero, *Z. für Physik*, 118, 27 (1941-42).
12. T. Heimer, *Z. für Physik*, 78, 771 (1932).
13. R. Mulliken, *Rev. Mod. Physics*, 3, 125 (1931).
14. G. A. Cook, Ed., *Argon, Helium, and the Rare Gases* (Interscience, New York, 1961), Vol. I, p. 340.
15. R. T. Berger, *Rad. Res.*, 15, 1 (1961).
16. G. L. Clark, *Applied X-Rays* (McGraw-Hill Book Co., Inc., New York, 1955), p. 164.
17. T. L. Cottrell, *The Strength of Chemical Bonds* (Butterworths Scientific Pub., London, 1958), p. 173 f.

18. O. Schnepf and K. Dressler, *J. Chem. Phys.*, 33, 49 (1960).
19. G. Baldini, *Phys. Rev.*, 128, 1562 (1962).
20. P. G. Wilkinson, *J. Mol. Spect.*, 6, 29 (1961).
21. A. D. Walsh and P. A. Warsop, *Trans. Faraday Soc.*, 57, 345 (1961).
22. K. Watanabe, *J. Chem. Phys.*, 22, 1564 (1954).
23. F. H. Field and J. L. Franklin, *Electron Impact Phenomena* (Academic Press, New York, 1957).
24. C. E. Moore, *Atomic Energy Levels*, U. S. National Bureau of Standards, Circular No. 467 (1949).

PROPOSITION I

It is proposed that the infrared spectrum of hydroxylamine be observed at various concentrations in rare gas solids to study the effects of hydrogen bonding on the vibrational frequencies of dimeric and polymeric species of hydroxylamine.

The infrared spectra of gaseous and solid hydroxylamine have been studied by Giguère and Liu (1). Nightingale and Wagner (2) have also observed the vibrational spectrum of the solid. The solid samples used in these two independent investigations were prepared differently. Giguère and Liu (GL) used a paraffin oil (Nujol) mull prepared at room temperature and subsequently placed between NaCl plates in a low temperature absorption cell. Nightingale and Wagner (NW) sublimed a film of hydroxylamine onto a NaCl window cooled to 77°K. The spectra reported for the gas phase and for the two solid phase preparations are given in Table I along with assignments to the normal modes of hydroxylamine.

Comparison of the two reported solid phase spectra reveals several inconsistencies, the most obvious of which involves the intense band observed at 2867 cm^{-1} in the solid film of NW but not reported by GL. The failure of GL to observe this band may be due to the proximity of a strong absorption at 2941 cm^{-1} due to the paraffin oil used to disperse their sample. If this is the case and the 2867 cm^{-1} band is indeed due to the OH stretching mode of hydroxylamine as

Table I. Vibrational frequencies of hydroxylamine.

Gas Phase ^a		Solid Mull ^a	Sublimed Solid ^b		Normal Mode
ν (cm ⁻¹)	Int.	ν (cm ⁻¹) ^c	ν (cm ⁻¹) ^d	Int.	
3656	S	3331	2867	VS	ν_1 (a') OH stretch
3350	W	3268	3302	S	ν_7 (a'') NH stretch
3297	M	3207	3173	S	ν_2 (a') NH stretch
1605	M	1657	1515	M	ν_3 (a') NH ₂ bend
1357	S	1502	1191	S	ν_4 (a') OH bend
1120	VS	1187	950	M	ν_5 (a') NF ₂ wag
895	M	926	912	M	ν_6 (a') NO stretch
765	W	845	867	W	ν_8 (a'') NF ₂ rock
430	VW	490 (?)	--	--	ν_9 (a'') torsion

^aReference 1 (GL).^bReference 2 (NW).^cAnother moderately intense band not assigned to a fundamental was observed at 3088 cm⁻¹.^dOther moderately intense bands not assigned to fundamentals were observed at 3065, 2787, 2675, 1697, and 1675 cm⁻¹.

assigned by NW, the large shift (-800 cm^{-1}) from the corresponding gas phase frequency at 3656 cm^{-1} indicates that strong hydrogen bonding occurs in the solid. The observed intensity increase of the high frequency stretching modes in the solid (see Table I) is also consistent with strong hydrogen bonding in solid hydroxylamine.

Other inconsistencies in the solid phase spectra involve differences in assignments; an obvious case is the OH bending mode which GL assign to the 1357 cm^{-1} band in the gas phase. This assignment seems reasonable when compared with the OH bending modes of hydrogen peroxide which occur at 1266 and 1380 cm^{-1} in the gas phase (3). In the solid the OH bending mode is assigned to the 1502 cm^{-1} band by GL; the frequency increase in the solid is expected for bending modes when hydrogen bonding occurs. However, NW have assigned the OH bending mode to the 1191 cm^{-1} band observed in their solid sample; this assignment is not consistent with the expected frequency increase for this normal mode in the solid.

The discussion above has pointed out some inconsistencies in the observed frequencies and assignments of the infrared spectra of solid hydroxylamine. An assignment which is consistent with strong hydrogen bonding in the solid is suggested in Table II.

The matrix isolation technique may be used to check on the assignments in Table II. Briefly, the technique involves the suspension of a reactive species such as hydroxylamine in an inert solid such as nitrogen or the rare gases at low temperatures. At sufficiently low concentrations (usually less than 0.5%), the hydroxylamine will

Table II. Assignment of vibrational frequencies of solid hydroxylamine consistent with strong hydrogen bonding.

Gas Phase ^a	Solid ^b	Assignment
ν (cm ⁻¹)	ν (cm ⁻¹)	
3656	2867	OH stretch
3350	3302	NH stretch
3297	3173	NH stretch
1605	1675 or 1697	NH ₂ bend
1357	1515	OH bend
1120	1191	NH ₂ wag
895	912 or 950	NO stretch
765	867	NH ₂ rock
430	—	torsion

^aReference 1.

^bReference 2.

be surrounded only by inert matrix atoms and its spectrum should closely resemble that of the gas phase. At higher concentrations or at temperatures high enough to allow diffusion in the solid, dimers and higher polymers of hydroxylamine will form. The frequency shifts characteristic of hydrogen bonded dimers and trimers are intermediate between the gas phase frequencies and those of the pure solid. Therefore, if the assignment of Table II is correct, one should be able to detect new absorption maxima between 3656 and 2867 cm^{-1} due to the OH stretching modes of dimeric and trimeric aggregates of hydroxylamine. One should also see new absorption maxima between the gas and solid phase frequencies corresponding to the other normal modes; for example, new absorption features should appear between 1357 and 1515 cm^{-1} , between 1120 and 1191 cm^{-1} , and between 1605 and 1675 cm^{-1} if the assignments in Table II are correct.

Giguère and Liu observed a doubling (5 to 6 cm^{-1} splittings) in the gas phase vibration-rotation bands of hydroxylamine near 1120 and 765 cm^{-1} ; they suggest that the doubling is due to cis and trans isomers of hydroxylamine. At the low temperatures used in the matrix isolation technique (below 20°K), the vibrational lines should be sharp with little or no rotational structure; thus it may be possible to observe the two isomeric species of hydroxylamine if they can both be isolated in sufficient concentration in the matrix.

References

1. P. A. Giguère and I. D. Liu, *Canad. J. Chem.*, 30, 948 (1952).
2. R. E. Nightingale and E. L. Wagner, *J. Chem. Phys.*, 22, 204 (1954).
3. E. Catalano and R. H. Sanborn, *J. Chem. Phys.*, 38, 2273 (1963).

PROPOSITION II

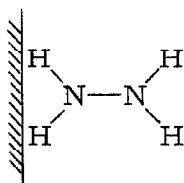
A strong absorption maximum at 1587 cm^{-1} , previously assigned to a fundamental vibration of gaseous hydrazine, may be due instead to hydrazine adsorbed on an alkali halide surface. An experiment is proposed to check this interpretation of the 1587 cm^{-1} line.

The vibrational spectrum of hydrazine vapor exhibits a strong absorption maximum at 1587 cm^{-1} (1). This band has been assigned to the ν_{10} (B) HNH fundamental bending mode which by analogy with methylamine is expected to occur in this region.

Recently Catalano, Sanborn, and Frazer (2) have observed that the 1587 cm^{-1} band remained after the hydrazine in their absorption cell had been condensed in a side arm maintained at liquid nitrogen temperature (77°K). They observed this behavior in several absorption cells which had alkali halide or Kodak Irtran ABC II windows. The same experiment with methylhydrazine and the two dimethylhydrazines, which also have HNH bending modes near 1600 cm^{-1} , showed no unusual behavior; i. e., the entire spectrum of these substituted hydrazines disappeared when they were condensed at 77°K .

An obvious interpretation of the above behavior is that hydrazine has been adsorbed on the cell windows; and, therefore, the 1587 cm^{-1} absorption maximum does not correspond to a fundamental of gaseous hydrazine. The frequency of this band is close to the value

expected for HNH bending modes which occur at 1605 cm^{-1} in hydroxylamine (3) and at 1593 cm^{-1} in 1, 1-dimethylhydrazine (4). This suggests that if the 1587 cm^{-1} band is due to adsorbed hydrazine, one of the two NH_2 groups of the molecule is relatively free in its vibrational motion. A possible configuration of the adsorbed molecule on the surface is shown below.



To check on this possible interpretation of the 1587 cm^{-1} peak of hydrazine, it is proposed that a study be made of the infrared spectra of hydrazine and the deuterated hydrazines adsorbed on salt windows. If adsorption indeed occurs as suggested above, absorption maxima should remain after removal of gaseous hydrazine from the absorption cell. One should of course observe the 1587 cm^{-1} peak due to a free NH_2 group; and, depending on the completeness of the deuterium substitution, one should also observe a peak near 1200 cm^{-1} due to a free ND_2 group and a peak near 1400 cm^{-1} due to a free NHD group of the adsorbed hydrazine.

References

1. P. A. Giguère and I. D. Liu, *J. Chem. Phys.*, 20, 136 (1952).
2. E. Catalano, R. H. Sanborn, and J. W. Frazer, *J. Chem. Phys.*, 38, 2265 (1963).
3. P. A. Giguère and I. D. Liu, *Canad. J. Chem.*, 30, 948 (1952).
4. E. R. Shull, J. L. Wood, J. G. Aston, and D. H. Rank, *J. Chem. Phys.*, 22, 1191 (1954).

PROPOSITION III

A study of the infrared spectra of monomeric HBr, HI, and HCN in the solid rare gases is proposed to determine if interaction between rotation and localized translation occurs in these molecules.

The infrared spectra of HCl and DCl have recently been observed in solid argon (1), krypton, and xenon (2). On the basis of concentration and temperature variation experiments, the spectra can be assigned to monomeric and polymeric species of HCl and DCl.

Absorption maxima of the monomeric species have been assigned to perturbed vibration-rotation transitions of HCl and DCl in the solid rare gases. When the spacings between the components of the vibration-rotation bands in the rare gas crystal are compared with the corresponding spacings in the gas phase spectra, it is found that the rotational levels of HCl are perturbed by about 5 to 10 cm^{-1} in the rare gas crystal; the DCl rotational levels are perturbed by only 1 to 3 cm^{-1} .

The perturbations on the rotational levels of HCl and DCl in the solid rare gases have been interpreted in terms of interaction between the rotational motion and the localized translational motion of HCl and DCl at substitutional sites in the rare gas crystals (2). The strength of this interaction may be expressed in terms of a molecular parameter A, which is defined as the distance between the center of

mass and the center of electrical symmetry in the molecule. In HCl the experimentally determined value of A is 0.13 \AA , in DCl A is 0.096 \AA ; the difference between these two values is just the shift in the center of mass between HCl and DCl.

Up to the present time, the interaction between rotation and localized translation in the solid has been examined in detail solely in the vibration-rotation spectra of HCl and DCl in the solid rare gases. The occurrence of this type of interaction should be expected in similar molecules isolated in the solid rare gases. It would be of interest to observe this interaction in a series of molecules with different values of the interaction parameter A . It is proposed that the infrared spectra of monomeric HBr, HI, and HCN in the solid rare gases be studied for the purpose of detecting possible interaction between rotation and localized translation in these molecules.

Another aspect of the proposed study is an investigation of the infrared spectra of polymeric species of HBr, HI, and HCN. This investigation could be carried out even in the event that these molecules do not rotate in the solid rare gases.

The spectra of polymeric HCl and DCl in krypton were discussed (2) in terms of dimers and three distinct trimeric species which included "linear," "bent," and "triangular" forms. It may be possible to interpret the absorption spectra of polymeric HBr, HI, and HCN in terms of dimers and trimers such as those used to interpret the polymer spectra of HCl and DCl.

References

1. L. J. Schoen, D. E. Mann, C. Knobler, and D. White, *J. Chem. Phys.*, 37, 1146 (1962).
D. E. Mann, L. J. Schoen, C. Knobler, and D. White, *Proceedings International Symposium on Molecular Structure and Spectroscopy*, Tokyo, 1962, p. A209.
2. L. F. Keyser, J. Kwok, and G. W. Robinson, to be published.

PROPOSITION IV

A study of the N^{14} quadrupole resonance in cis and trans difluorodiazine and tetrafluorohydrazine is proposed.

There are very little data available on the nuclear quadrupole resonance (NQR) of N^{14} bonded to atoms other than hydrogen. In particular the NQR of N^{14} bonded to fluorine has been observed only recently in one compound, nitrogen trifluoride (1). It is proposed that the NQR of N^{14} be studied in other nitrogen-fluorine compounds such as cis and trans difluorodiazine (N_2F_2) and tetrafluorohydrazine (N_2F_4).

Difluorodiazine can be prepared by the electrolysis of ammonium bifluoride; the resulting mixture of cis and trans isomers of N_2F_2 can be separated by chromatography and low temperature distillation (2). The trans isomer melts at $101^\circ K$ and boils at $162^\circ K$; the cis isomer melts below $78^\circ K$ and boils at $167^\circ K$. Electron diffraction studies (3) on gaseous N_2F_2 indicate that the N-F and N-N bond distances are 1.44 and 1.25 Å respectively; the FNN bond angle is 115° . Tetrafluorohydrazine is available commercially (Stauffer Chemical Co.). The microwave spectrum (4) of N_2F_4 indicates that its molecular structure is the same as that of hydrazine (C_2 symmetry).

Nuclear quadrupole resonance spectra correspond to transitions between energy levels which arise from the interaction of the

electric quadrupole moment of the nucleus in question with the electric field gradient at the nucleus. The nuclear spin quantum number of N^{14} is unity; therefore, the quadrupole Hamiltonian can be written (5):

$$H_Q = e^2qQ \left[\frac{1}{2} I_X^2 - \frac{(1-\eta)}{4} I_Y^2 - \frac{(1+\eta)}{4} I_Z^2 \right]$$

where eQ is the nuclear quadrupole moment, eq is the maximum electric field gradient

$$eq = V_{ZZ} ,$$

and η is the asymmetry parameter of the electric field gradient tensor in the principal axis system

$$\eta = \frac{V_{XX} - V_{YY}}{V_{ZZ}} .$$

The components of the nuclear spin operator are denoted by I_X , I_Y , and I_Z . Eigenvalues of H_Q are given by

$$E_0 = -e^2qQ/2$$

$$E_{\pm 1} = \frac{e^2qQ(1 \pm \eta)}{4}$$

Transitions between the E_0 and the $E_{\pm 1}$ quadrupole levels can be induced by radio frequency magnetic fields; these transitions give rise to resonance frequencies at

$$\nu_{\pm} = \frac{3}{4} \frac{e^2qQ(1 \pm \eta/3)}{h} .$$

The two resonance frequencies ν_{\pm} give enough information to obtain e^2qQ and η from zero magnetic field NQR measurements alone.

The quadrupole resonance frequency ν_0

$$\nu_0 = \frac{3}{4} \frac{e^2qQ}{h}$$

of N^{14} in solid nitrogen trifluoride is 5,3012 Mc; the asymmetry parameter is 0.00112 (1). If NF_3 had the same pyramidal (C_{3v}) symmetry in the solid as it has in the gas phase, the X and Y directions would be equivalent and the asymmetry parameter should be zero. The small nonzero asymmetry parameter observed in solid NF_3 may be due to slight distortions of the molecule in the solid or to nonequivalent X and Y crystal directions. Because of the lower symmetry of the electronic environment of N^{14} in N_2F_2 and N_2F_4 , the asymmetry parameter η is expected to be considerably larger in these compounds than it is in NF_3 ; thus a much larger splitting is anticipated in the NQR frequencies of N_2F_2 and N_2F_4 .

References

1. G. A. Matzkanin, T. A. Scott, and P. J. Haigh, *J. Chem. Phys.*, 42, 1646 (1965).
2. C. B. Colburn, F. A. Johnson, A. Kennedy, K. McCallum, L. C. Metzger, and C. O. Parker, *J. Am. Chem. Soc.*, 81, 6397 (1959).
3. S. H. Bauer, *J. Am. Chem. Soc.*, 69, 3104 (1947).
4. D. R. Lide and D. E. Mann, *J. Chem. Phys.*, 31, 1129 (1959).
5. T. P. Das and E. L. Hahn, Nuclear Quadrupole Resonance Spectroscopy (Academic Press, Inc., New York, 1958), p. 17.

PROPOSITION V

Photolysis of OF_2 isolated in solid argon or krypton is proposed as a possible method to produce the previously unobserved OF radical.

The OF radical apparently has never been definitely observed. It has been postulated as a primary product in the photolysis of OF_2 (1) and it may be an intermediate in the thermal decomposition of O_2F_2 into F_2 and O_2 (2).

Oxygen difluoride (OF_2) is the only known fluoride of oxygen that is relatively stable; it is a colorless gas at room temperature and may be purified by fractional distillation from the liquid (b. p. -144.8°C). OF_2 does not react with glass when cold but does attack metal surfaces readily.

Electron diffraction studies (3) of the gas indicate that OF_2 is a nonlinear molecule; the O-F bond distance is $1.41 \pm 0.05 \text{ \AA}$ and the bond angle is $100 \pm 3^\circ$. The infrared spectrum of OF_2 is well known (4, 5); the fundamental OF stretching modes occur at 928 and 831 cm^{-1} , the bending mode occurs at 461 cm^{-1} .

The electronic absorption spectrum (1) of OF_2 is continuous from 5400 \AA to the limit of the observation at 2100 \AA . The continuous nature of the absorption suggests that the upper electronic states of OF_2 are dissociative; in fact, Glissmann and Schumacher (1) found that OF_2 decomposes to F_2 and O_2 upon irradiation with a quartz mercury arc.

It may be possible to form and stabilize the OF radical by the photolysis of OF_2 isolated in rare gas solids at low temperatures. In particular, an experiment is proposed in which 0.5% mixtures of OF_2 in solid argon or krypton are irradiated with light of wavelength 4000 Å or less. Since the infrared spectrum of OF_2 is well known, infrared spectra of the solid sample before and after irradiation seem to be the most likely means to detect the presence of the OF radical.

If OF can be produced by the photolysis of OF_2 , additional experiments could be carried out by raising the temperature of the irradiated sample to allow diffusion of OF to occur in the solid. In this way it may be possible to form and observe the infrared spectrum of another interesting unstable fluoride of oxygen, O_2F_2 .

References

1. A. Glissmann and H. J. Schumacher, Z. physik. Chem., 24B, 328 (1934).
2. H. J. Schumacher and P. Frisch, Z. physik. Chem., 37B, 1 (1937).
3. L. R. Maxwell, J. Opt. Soc. Am., 30, 374 (1940).
4. H. J. Bernstein and J. Powling, J. Chem. Phys., 18, 685 (1950).
5. E. A. Jones, J. S. Kirby-Smith, P. J. H. Woltz, and A. H. Nielsen, J. Chem. Phys., 19, 337 (1951).